

# SRM Drives for Electric Traction

edited by Pere Andrada



UNIVERSITAT POLITÈCNICA  
DE CATALUNYA  
BARCELONATECH



# SRM Drives for Electric Traction

---

edited by Pere Andrada



UNIVERSITAT POLITÈCNICA  
DE CATALUNYA  
BARCELONATECH

First Edition: December 2019

© The Authors, 2019

© Iniciativa Digital Politècnica, 2019

Oficina de Publicacions Acadèmiques Digitals de la UPC

Jordi Girona 1-3,

Edifici K2M - Planta S1, 08034 Barcelona

Tel.: 934 015 885

[www.upc.edu/idp](http://www.upc.edu/idp)

E-mail: [info.idp@upc.edu](mailto:info.idp@upc.edu)

Printed on: QPPrint

Miquel Torelló i Pagès, 4-6

08750 Molins de Rei, Barcelona

DL: B 29167-2019

ISBN: 978-84-9880-817-9

This work is subject to copyright. All rights are reserved by the Publisher to reproduction, distribution, public communication or transformation.



# Contents

- 7 Preface**
- 9 Contributors**
- 13 Chapter 1. Trends in switched reluctance drives for electric traction**  
Pere Andrada. GAECE, DEE EPSEVG UPC, Spain.
- 29 Chapter 2. Soft Magnetic materials for switched reluctance machine**  
Pere Andrada. GAECE, DEE EPSEVG UPC, Spain.
- 41 Chapter 3. PM to RSM rotor replacement study on traction machines.**  
Avo Reinap. Industrial Electrical Engineering and Automation. Lund University, Sweden.
- 57 Chapter 4. Variable reluctance motors for automotive applications. The modular construction approach**  
Loránd Szabó. Technical University of Cluj Napoca. Romania
- 87 Chapter 5. Double-stator switched reluctance motors**  
H. Torkaman and Majid Asgar. Shahid Beheshti University. Iran.
- 107 Chapter 6. Definition of a strategy for an axial flux switched reluctance machine torque control**  
A. Egea, G. Ugalde, J. Poza. Machines and Automatics Mondragon University-Faculty of Engineering Arrasate-Mondragon, Spain.
- 123 Chapter 7. Novel in-wheel double rotor axial-flux SRM drive for light electric traction**  
Pere Andrada, Balduí Blanqué, Eusebi Martínez, José I. Perat, José A. Sánchez, Marcel Torrent. GAECE, DEE EPSEVG UPC, Spain.
- 143 Chapter 8. Axial-flux twin-rotor segmented-stator high-speed SRM for high-performance traction applications**  
Francisco J. Márquez-Fernández. Div. Industrial Electrical Engineering and Automation, LTH Faculty of Engineering, Lund University, Lund, Sweden. Johannes H. J. Potgieter, Dyson Ltd, Malmesbury, UK. Malcolm D. McCulloch. Energy and Power Group, Dept. of Engineering Science, University of Oxford, Oxford, UK. Alexander G. Fraser. McLaren Automotive Ltd, Woking, UK.



## Preface

Current environmental concerns are driving the international community into forcing the development of low-emission (hybrid electric) or zero-emission (battery electric) vehicles that will replace conventional internal combustion engine vehicles, which now constitute one of the main causes of urban pollution. Although the number of battery electric and hybrid electric vehicles has maintained an upward growth in recent years, important technological advances are necessary for improving the performance of these vehicles. This is true not only for developing batteries that guarantee greater autonomy, but also electric powertrains that demand higher torque, power densities, and efficiency. Nowadays, most powertrains use permanent magnet synchronous motors (PMSM), but automakers are intensifying their research into finding alternatives with less mass of permanent magnets or even without them.

This book presents a compilation of works carried out by a group of researchers who believe that switched reluctance motor (SRM) drives can serve as a viable alternative to PMSM drives. Its main goal is to disseminate knowledge about a number of new contributions that reinforce the suitability of SRM drives for E-Traction.

The book is organized in following order. Chapter 1 briefly explains the basics of SRM drives and describes their developments and achievements in electric traction. Chapter 2 provides a survey of the trends in soft magnetic materials for SRM with a particular emphasis on their applications for traction motors in electrical vehicles. Chapter 3 evaluates and compares two electrical machines when replacing a permanent magnet rotor of a PMSM for a rotor of a SRM. Chapter 4 provides a survey of the main modular variable reluctance motors. The investigation focuses especially on the machines proposed for diverse automotive applications, including traction drives and auxiliaries. Chapter 5 is devoted to

double-stator SRM drives and presents the motor structure, geometry, design, electromagnetic characteristics and experimental tests. This work demonstrates that double-stator SRMs can produce more torque and power density with less radial force, vibration and acoustic noise. Chapter 6 presents the torque control strategy for an axial-flux SRM with a Labak configuration. Chapter 7 presents a summary of the work developed on axial-flux SRM drives using a particular distribution of stator and rotor poles that results in short flux paths without flux reversal. In addition, it also describes an SRM controller developed especially for the propulsion of light electric vehicles. Chapter 8 summarizes the work done on a novel SRM concept, featuring a 2-phase axial flux topology with a segmented stator and twin segmented rotors. The proposed topology is designed for high-speed operations that aim for power density values within the range of 7 kW/kg.

This work would not be possible without the efforts and generosity of all who have contributed to its development.

Finally, we would like to extend our gratitude to Ana Latorre and Jordi Prats of the Iniciativa Digital Politècnica for their contributions in editing this book.

Pere Andrada  
May 2020

This book is supported by Spanish Ministry of Economy and Competitiveness  
(DPI 2014-57086-R)



## Contributors

**Pere Andrada** was born in Barcelona (Spain) in 1957. He received the M.Sc. and the Ph.D. degrees in Industrial Engineering from the Universitat Politècnica de Catalunya (UPC), Barcelona, Spain, in 1980 and 1990 respectively. In 1980 he joined the Department of Electrical Engineering, Universitat Politècnica de Catalunya UPC, where he is currently University School full professor in the Escola Politècnica Superior d'Enginyeria de Vilanova i la Geltrú (EPSVG). He is member of the Electronically Commutated Drive Group (GAECE). His teaching activities and research interests include design, modelling and control of electrical machines and drives.

**Majid Asgar** is currently an Assistant Professor at Technical and Vocational University, Tehran, Iran. He has authored over 50 technical papers, and holds three issued patents. He has co-authored three books. His main research interests include power electronics, electrical machines, and renewable energies.

**Balduí Blanqué** was born in Reus (Tarragona, Spain) in 1970. He received the B.S. degree in Telecommunications, the M.S. degree in Telecommunications, and the Ph.D. degree from the Universitat Politècnica de Catalunya (UPC), in Barcelona, Spain, in 1996, 1999, and 2007, respectively. Since 1996, he has been with the Department of Electrical Engineering, Universitat Politècnica de Catalunya (UPC), where he is currently Associate Professor in the Escola Politècnica Superior d'Enginyeria de Vilanova i la Geltrú (EPSVG). He is member of the Electronically Commutated Drives Group (GAECE). His teaching activities cover digital design and electronics applications and his research interests include modelling, simulation and control of electrical machines and drives.

**Aritz Egea** received the degree in electrical engineering from the University of Mondragon, Mondragon, Spain, in 2009 and the Ph.D. degree in electrical engi-

neering in 2012. Currently he is an Associated Professor in the Faculty of Engineering, University of Mondragon. His current research interests include electrical machine design and control and electromagnetic actuators.

**Alexander G. Fraser** graduated with a B.Eng. degree in Automotive Engineering in 2006 and has since specialized in the field of transportation electrification. Between 2007 and 2014 he was employed by Protean Electric Ltd fulfilling a variety of mechanical design, research and business development roles. Since 2014 Alexander has been employed with McLaren Automotive Ltd where he is currently principal research engineer, responsible for delivering motor research projects and systems/vehicle integration activities related to traction e-machines.

**Malcom D. McCulloch** received the B.Sc.(Eng.) and Ph.D. degrees in electrical engineering from the University of Witwatersrand, Johannesburg, South Africa, in 1986 and 1990, respectively. In 1993, he moved to the University of Oxford to head up the Energy and Power Group, where he is currently an associate professor at the Department of Engineering Science. He is active in the areas of electrical machines, transport, and smart grids. His work addresses transforming existing power networks, designing new power networks for the developing world, developing new technology for electric vehicles and developing approaches to integrated mobility. He is the Founder of three spin-out companies arising out of his research activity. He has more than 100 journal and refereed conference papers, and has been an Invited Speaker at the World Forum in Tianjin, China, 2010, and the Hindustan Leadership Conference, Delhi, India, in 2013.

**Francisco J. Márquez-Fernández** was born in Huelva (Spain) in 1982. In 2006 he graduated as a M.Sc. on Industrial Engineering with a major in Industrial Electronics from the University of Seville (Spain). He received his Ph.D. in Electrical Engineering in 2014 Lund University in Sweden. Between 2014 and 2016 he was appointed as Post-doctoral Research Assistant at the Energy and Power Group, University of Oxford, UK. Since 2016 he is a Post-doctoral Researcher at the Industrial Electrical Engineering Group, Lund University, and the Swedish Electromobility Centre. His research interests are design and control of new topologies of electrical machines and power electronic drives, applied to either renewable energy systems or electric vehicles, electrical machine characterization methods, energy management in EVs and HEVs and their interaction with the power grid.

**Eusebi Martínez-Piera** was born in Barcelona (Spain) in 1960. He received the Engineer degree in Industrial Engineering from Universitat Politècnica de Catalunya in 1984. He is currently an Assistant Professor, in the Department of Electrical Engineering, Universitat Politècnica de Catalunya, in the Escola Politècnica Superior d'Enginyeria de Vilanova i la Geltrú (EPSVG). He is member of the Electronically Commutated Drives Group (GAECE). His teaching activities and research interests include design and finite element analysis of electrical machines.

**José Ignacio Perat** was born in Tamarite de Litera (Huesca, Spain), in 1965. He received the B.Sc., M.Sc. and Ph.D. degrees in Industrial Engineering from the Universitat Politècnica de Catalunya (UPC), in 1989, 1998 and 2006 respectively. He is currently an Associate Professor in the Department of Electrical Engineering, Universitat Politècnica de Catalunya, in the Escola Politècnica Superior d'Enginyeria de Vilanova i la Geltrú (EPSVG). He is member of the Electronically Commutated Drives Group (GAECE). His teaching activities and research interests include power electronics and control of electric machines and drives.

**Johannes H. J. Potgieter** received the B.Eng. degree in electrical and electronic engineering in 2008 and the M.Sc. (Eng.) and the Ph.D. (Eng.) degrees in electrical engineering from the University of Stellenbosch, Stellenbosch, South Africa in 2011 and 2014 respectively. Between May 2014 and May 2016, he was employed as a Post-doctoral Research Assistant at the University of Oxford, United Kingdom. Currently, he is appointed as advanced motor drives engineer at Dyson UK. His research interests include wind power generation technologies, hybrid-electrical automotive drive train solutions and the design and optimization of permanent magnet and switched reluctance electrical machines.

**Javier Poza** was born in Bergara, Spain, in June 1975. He received the degree in electrical engineering from the University of Mondragon, Mondragon, Spain, in 1999, and the Ph.D. degree in electrical engineering from the Institut National Polytechnique de Grenoble, Grenoble, France. In 2002 he joined the Department of Electronics, Faculty of Engineering, University of Mondragon, where he is currently an Associate Professor.

**Avo Reinap** was born in Estonia in 1973. He received the Diploma degree in engineering and the M.Sc. degree in power engineering from Tallinn University of Technology, Tallinn, Estonia, in 1998 and 2000, respectively. He received the Ph.D. degree in technology from Lund University, Lund, Sweden, in 2005. From 2005 to 2010, he was an Associate Professor in the Department of Electrical drives and Power Electronics, Tallinn University of Technology and from 2007 to 2011 a Postdoctoral Fellow and since 2012 Associate Professor in the Division of Industrial Electrical Engineering and Automation, Faculty of Engineering, Lund University.

**José Antonio Sánchez** was born in Vilanova i la Geltrú (Barcelona, Spain), in 1953. He received the B.Sc., M.Sc. degrees in Industrial Engineering from the Universitat Politècnica de Catalunya (UPC), in 1976 and 1998 respectively. He is currently an Assistant Professor in the Department of Electrical Engineering, Universitat Politècnica de Catalunya, in the Escola Politècnica Superior d'Enginyeria de Vilanova i la Geltrú (EPSVG). He is member of the Electronically Commutated Drives Group (GAECE). His teaching activities and research interests include industrial automation and fault diagnostic techniques for electric machines and drives.

**Loránd Szabó** was born in Oradea, Romania, in 1960. He received the B.Sc. and Ph.D. degree from Technical University of Cluj-Napoca (Romania) in electrical engineering in 1985 and 1995, respectively. He joined in 1990 the Technical University of Cluj-Napoca (Romania) as a research & design engineer. Since 1999 he is with the Department of Electrical Machines and Drives, where he was a lecturer, associate professor, and by now is full professor. He is also director of Centre of Applied Researches in Electrical Engineering and Sustainable Development (CAREESD) in the frame of the same university. Prof. Szabó's current research interests include linear electrical machines, variable reluctance machines, fault tolerant designs, fault detection and condition monitoring of electrical machines, etc. He published more than 260 papers. He received the 2015 Premium Award for Best Paper in IET Electric Power Applications. He is member of IEEE since 2005, and in 2017 he was elevated to Senior member. Prof. Szabó's home page is: [http://memm.utcluj.ro/szabo\\_lorand.htm](http://memm.utcluj.ro/szabo_lorand.htm).

**Hossein Torkaman** is currently an Associate Professor of electrical engineering at the Faculty of Electrical Engineering, Shahid Beheshti University, A.C., Tehran, Iran. He has authored over 130 technical papers, and holds three issued patents. He has co-authored four books. He has been distinguished with numerous awards from university and organizations. He was elected as a senior member of IEEE. His main research interests include electrical machines, power electronics, and renewable energies.

**Marcel Torrent** was born in Menàrguens (Lleida, Spain) in 1965. He received the B.Sc., M.Sc. and Ph.D. degrees in Industrial Engineering from the Universitat Politècnica de Catalunya (UPC), in 1988, 1997 and 2004 respectively. He is currently an Associate Professor in the Department of Electrical Engineering, Universitat Politècnica de Catalunya, in the Escola Politècnica Superior d'Enginyeria de Vilanova i la Geltrú (EPSVG). He is member of the Electronically Commutated Drives Group (GAECE). His teaching activities and research interests include design, modelling and testing of electric machines and drives.

**Gaizka Ugalde** received the B.S. and the Ph.D. degrees in electrical engineering from the University of Mondragón, Mondragón, Spain, in 2006 and 2009, respectively. Since 2009, he has been with the Department of Electronics, Faculty of Engineering, University of Mondragón, where he is currently an Associate Professor. His current research interests include permanent-magnet machine design, modeling, and control. He has participated in various research projects in the fields of lift drives and railway traction.



# Trends in Switched Reluctance Motor Drives for Electric Traction

Pere Andrada

## 1.1. Introduction

The electrification of road vehicles is one of the most consistent initiatives for achieving a clean, environmentally friendly and efficient transport system. Nowadays, the worldwide stock of electric passenger vehicles, plug-in hybrid electric vehicles (PHEVs) and battery electric vehicles (BEVs) exceeds 5.1 million, 45% of the vehicles in China followed by the EU and USA. So far, Norway represents the country in which electric cars have the highest market share [1]. Several scenarios exist in regard to the expected growth of electric vehicles: the most moderate foresees global electric vehicle sales reaching 23 million and a stock of over 130 million vehicles by 2030; the more optimistic view of the EV30@30 campaign hopes that the market share will reach 30% by this same date (excluding two- and three-wheel vehicles), with 43 million in sales and a stock of more than 250 million vehicles.

In order to further boost this growth, technological improvements and cost reductions must be made not only to electric storage systems (mainly the batteries), but also to electric propulsion systems or traction drives. Currently, most traction drives for HEVs and BEVs are permanent magnet synchronous motor (PMSM) drives, which are more common due to their high power, torque density and efficiency, as well as their wide range of speed. The main drawback to PMSM drives is their use of rare-earth permanent magnets. Although rare-earth elements are not very scarce, some noteworthy circumstances to consider are:

- 50% of reserves are located in China.
- China additionally controls most (85%) of the world's rare-earth permanent magnet production.
- Demand is growing for permanent magnets in green industries, such as wind generation and electric vehicles.
- Historical volatility in the price of permanent magnets, as in 2011.

Given these circumstances, it is advisable to reduce the mass of permanent magnets in electric machines and perhaps even to dispense of them completely. Thus, there is presently great interest in developing permanent magnet-less (PM-less) electric drives, with the most relevant drives in this category being: induction motor (IM) drives, synchronous reluctance motor (SyncRM) drives and switched reluctance motor (SRM) drives. **Fig. 1** shows a basic cross-section of these motors; and their main advantages and drawbacks are listed, respectively, in Tables I and II [2-5].



Fig. 1: Cross-section of the three most relevant PM-less motors: IM (left), SyncRM (center) and SRM (right)

TABLE I. ADVANTAGES OF THE PM-LESS DRIVES UNDER CONSIDERATION

IM drives	SyncRM drives	SRM drives
Rotor losses can be significantly reduced by using a copper rather than aluminum squirrel cage.	Simplification of rotor construction because there are no magnets or embedded conductors that have to be inserted.	The simplicity of the stator and rotor construction helps reduce the cost of SRM machine manufacturing.
The drive-cycle efficiency of a well-designed induction machine can pose a challenge to that of an IPM machine in some applications.	Opportunity to achieve low rotor losses in the absence of magnets and conductors in the rotor.	SRM rotors typically have low moments of inertia compared to other machine types, thus improving acceleration and deceleration.
The magnetic field strength of a machine can be lowered via stator current to reduce losses under light load conditions, which is valuable for high-speed cruising.	The machine's saliency makes it an attractive candidate for rotor position self-sensing.	It achieves high CPSR values due to low magnetic coupling between phase windings. SRM fault tolerances are best among the evaluated machines.
The absence of magnets reduces an induction machine's vulnerability to damage from short circuit faults.	The absence of magnets reduces the SyncRM machine's vulnerability to damage from short circuit faults.	SRM machine efficiency during-high-speed, light-load operations do not suffer from any need for a stator current to cancel flux linkage.
The electronic power converter is the usual three-phase inverter used in AC machines.	The electronic power converter is the usual three-phase bridge inverter used in AC machines.	The number of SRM phases can vary from two to higher numbers by changing the number combinations of stator and rotor poles.

CPSR Constant power speed range  
PWM Pulse wide modulation

TABLE II. DRAWBACKS OF THE CONSIDERED PM-LESS DRIVES

IM drives	SyncRM drives	SRM drives
There are rotor losses whenever torque is generated.	Limits on achievable saliency ratio values reduce machine torque density in comparison to permanent machines.	The pulsed nature of stator winding excitation tends to result in high torque ripple when compared with other machines.
It requires a small air-gap to minimize the reactive current and maximize efficiency.	Increasing the inductance saliency ratio tends to reduce mechanical strength due to more flux barriers and increase pressure to reduce air-gap length.	High frequency radial forces on stator poles can result in undesirable acoustic noise due to excitation of stator mechanical resonant modes.
It is not adequate for high pole numbers, thus making them less attractive for lower speeds and direct drive applications.	It requires very high saliency ratios to achieve the CPSR values required in many traction applications.	The torque density and rated efficiency of SRM machines are lower than those of permanent magnet synchronous machines.
CPSR is more limited than internal permanent synchronous machines.	Achievable saliency ratio values result in a low power factor, thus increasing the inverter power rating.	The large amplitude of magnetic flux variations in rotor poles can lead to high rotor losses at high speeds.
Increasing CPSR requires reducing leakage reactance, thus generating additional PWM losses.	Not a good candidate for high pole number designs and, therefore, for high torque direct-drive applications.	It requires a small air-gap to maximize torque density.
It is not well suited to rotor position self-sensing at low speeds due to the absence of rotor saliency.		SRM performance depends on the accurate sensing of rotor position and tight control of current pulse timing.
		Each SRM phase winding requires two external terminals, thus doubling the number of excitation cables and connector pins in comparison to AC machines.
		The SRM electronic power converter does not use the standard three-phase inverter that is usually employed by all AC machines.
		Control characteristics are very non-linear due to the high magnetic saturation of SRM.

CPSR Constant power speed range  
 PWM Pulse wide modulation

## 1.2. SRM Basics

Although SRM drives present drawbacks such as large numbers of connections, the inability to use phase-leg power modules developed for inverters in SRM power converters, high torque ripple and acoustic noise; they do have advantages such as torque-speed characteristics that match very well with the needs of electric vehicle traction as well as a simple and robust construction. From the point of view of electromechanical conversion, SRM is a doubly salient pole device with single excitation that usually works under strongly saturated conditions [6,8]. Based on the air-gap flux direction, a rotary SRM can be classified as radial, axial or transverse flux [9]. In all cases, torque is produced by the rotor's tendency to move to a position that maximizes the inductance of the excited phase winding, i.e., it aligns with the stator and rotor poles. Therefore, a power converter with solid-state switches is needed to generate the right sequence of phase commutations and this requires knowing the rotor position. Figure 2 shows a block diagram of an SRM drive.

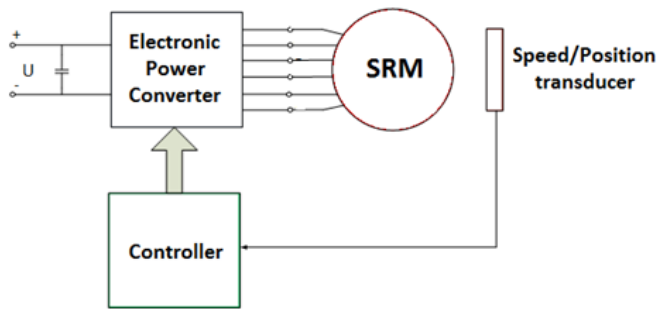


Fig. 2: Block diagram of an SRM drive

The electronic power converter in an SRM fulfills two functions. The first is to switch phases in the order established by the controller, based on the rotational position. The second is to ensure the rapid demagnetization of the SRM phases. The phase current in an SRM is unipolar so that, in principle, the switching can be performed sufficiently by only one switch per phase (unipolar electronic power converter). Once the switch is open, the demagnetization of the phase is carried out through a freewheeling diode with a series resistor that applies a reverse voltage to the phase terminals in order to force cancellation of the current. Nevertheless, the so-called asymmetric bridge power converter or classic converter is the most usual, Figure 3. It consists of two switches per phase – generally IGBTs – and the demagnetization circuit is completed by means of two diodes that, when the switches are opened, apply a negative voltage to the phase with the same value as the supply voltage. Although this converter uses a high number of power components and drive circuits, it maintains independence between phases, has a high fault tolerance, and offers many control options.

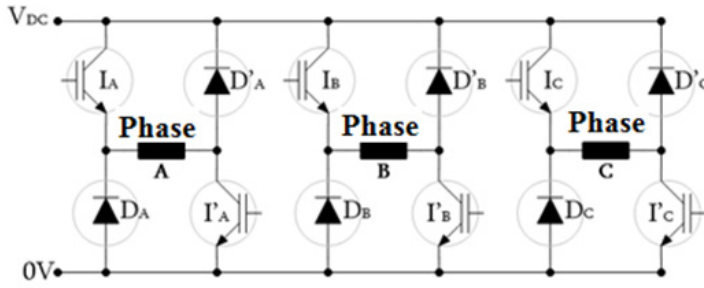


Fig. 3: Asymmetric bridge power electronic converter with two IGBTs and two diodes per phase

In variable speed applications, the SRM operates in one of the following three control modes: current mode (**Fig.4**); voltage mode (**Fig.5**); and single-pulse mode (**Fig.6**). Generally speaking, the SRM is controlled in the low speed range either by current control (hysteresis control) or by voltage control. The former sets a current reference ( $I_{ref}$ ) and maintains the current within a given hysteresis band, while the latter uses PWM with a variable duty cycle ( $D$ ). In both cases, the turn-on and turn-off angles, respectively,  $\theta_o$  and  $\theta_c$ , are maintained constant unless it is necessary to optimize torque ripple, efficiency or acoustic noise. At high speeds, single-pulse control is used with the voltage at the rated value in order to adapt the conduction period ( $\theta_o - \theta_c$ ) to the torque and speed requirements.

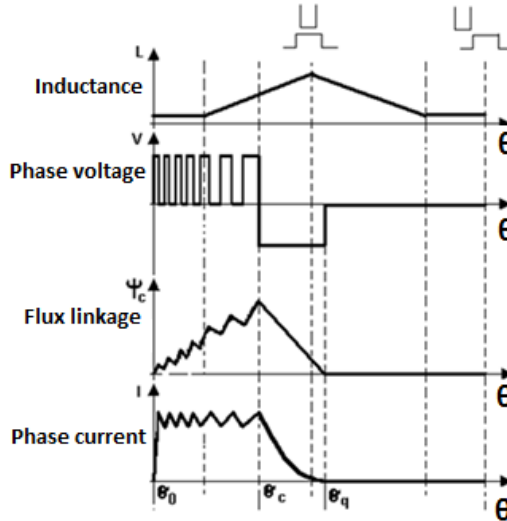


Fig.4: Hysteresis control with unipolar modulation or soft switching.

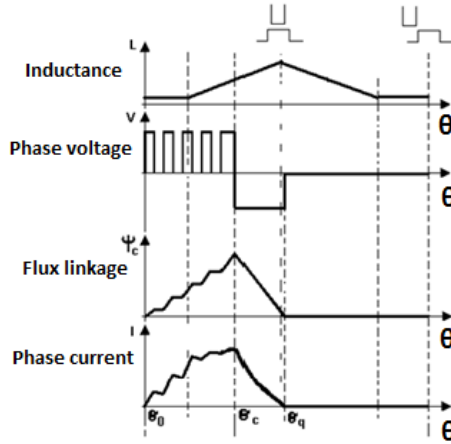


Fig.5: PWM control with unipolar modulation or soft switching.

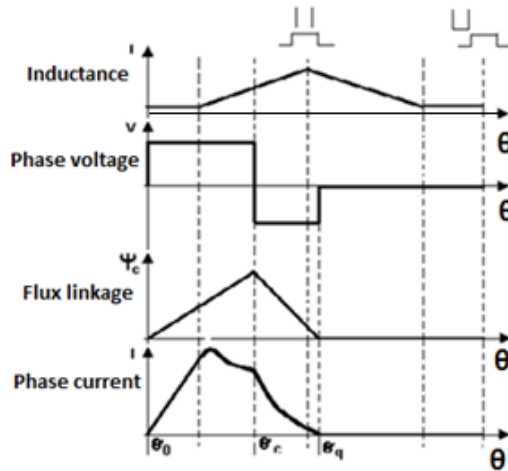


Fig.6. Single-pulse control

**Fig.7** shows the torque speed characteristic of an SRM for electric traction with three operational zones. In zone I, torque is constant at low speed and is controlled by hysteresis or voltage PWM. In zone II, medium speeds, the single-pulse control is utilized, the voltage is maintained at its rated value and the conduction period is increased (no more than half a rotor pole-pitch), which keeps a constant power. In zone III, high speeds, voltage remains at its rated value and turn-on and turn-off angles are also maintained at determined value following the natural characteristic. In addition, the torque decreases more or less with the square of the speed. The control strategies for the different zones of operation are summarized in Table II.

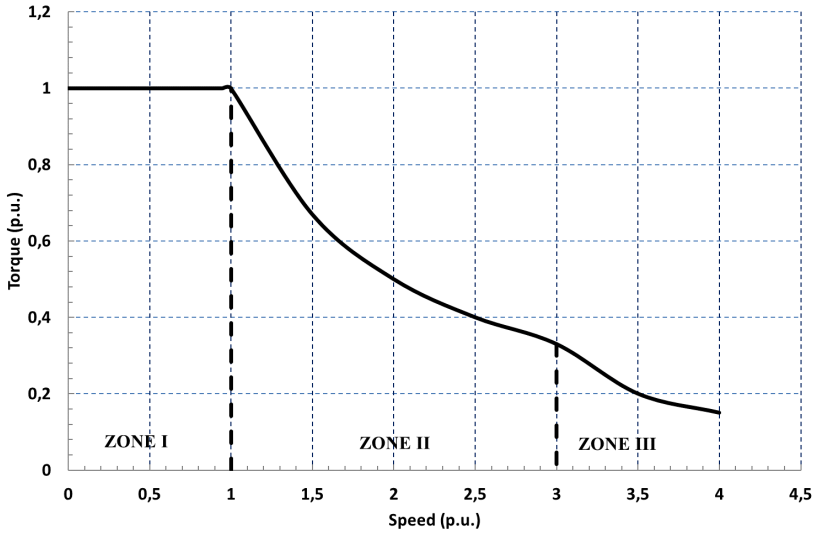


Fig. 7: Torque-speed characteristic of SRM

TABLE II. CONTROL STRATEGIES

Zone	Control	Operation	Variables	Constants
Zone I	Hysteresis	Constant torque	$I_{ref}$	$\theta_0$ and $\theta_c$
	PWM		D	
Zone II	Single-pulse	Constant power	$\theta_0$ and $\theta_c$	V
Zone III	Single-pulse	Natural		$\theta_0$ and $\theta_c$ V

### 1.3. SRM for electric traction

#### A. Early achievements

SRM has always been associated with electric traction, ever since the first documented switched reluctance motor appeared in the period 1837-1840 and one of its earliest applications (such as Robert Davidson's design) powered a locomotive on a section of railway between Glasgow and Edinburgh [6, 10]. However, the rapid development of D.C. motors in the second half of the 19th century eclipsed switched reluctance motors. The appearance of solid-state controlled switches initiated a renewed interest in switched reluctance motors, but the modern era of

SRM did not begin until the late 70s of the last century, thanks to a research project on battery powered electric vehicles carried out by the Universities of Leeds and Nottingham and sponsored by Chloride Technical Ltd. [11, 12]. Later, due to the renewed interest in electric vehicles at the end of the last century and the beginning of the current one, several major automobile manufacturers (Toyota [13], Daimler-Chrysler [14-15], Volkswagen [16], General Motors [17]) and a research agency (CSIRO) developed radial-flux switched reluctance motors as drive trains for their prototype electric cars [18]. Although some of these initiatives proved to be successful in test vehicles, they were not used in commercial cars. Nevertheless, at that time, the commercial electric motorcycle EMB-LECTRTRA [19] with a two-phase variable reluctance motor was launched and four 400 kW SRMs were used as traction motors in a LeTourneau L-1350 electric wheel loader [20]. Two other advances were also noteworthy: the motor/generator for a mild hybrid-electric powertrain that was developed by the SR drives® for the EC-funded project ELMAS [21]; and the hybrid electric bus constructed by Green Propulsion and SR drives® [22]. In recent years, great concern has emerged regarding the research and development of SRM in radial flux, axial flux and transverse flux for electric traction applications. The major trends in this research and development are reported below.

## B. Radial flux SRM

In radial flux SRM, the air-gap flux is mainly in the radial direction relative to the axis of rotation (see **Fig. 8**). This type of SRM usually has a cylindrical shape with a stator and rotor that can be either internal (the most common) or external. Great efforts are being made to improve SRM power and torque density in order to match the values of PMSM [23-28]. One attempt is to maintain the conventional structure of the SRM and use special soft magnetic materials with high performance [29]. Others are based on building structures that increase inductance in the alignment position and reduce it in the non-alignment position. Among these stands out the SRM with its segmented rotor, which has obtained good results [30-33]. It is also interesting to note the structures with higher numbers of rotor poles than stator poles [34, 35] and those with segmented stators, of which several variants have been presented [35-40]. Recently, alternative proposals have been made, such as the SRM double stator [41] and the SRM double rotor [42], both of which have delivered very promising results. Another option is the multistack (or multilayer) SRM [43], in which each phase of the machine is wound in independent parallel salient pole stators while the rotors corresponding to each stator shift between them at a determined angle. In order to facilitate the construction of the machine and increase its fault tolerance, some of these proposals are modular, i.e., they are built with independent yet common parts that are assembled to form the complete machine [44]. The presentation of Land Rover, at the 2013 Geneva Motor Show, of a range of new Defender electric vehicles powered by SRM units that were developed and built by Nidec SR Drives



Ltd., generated great expectations for applying SRM drives to electric traction [45].

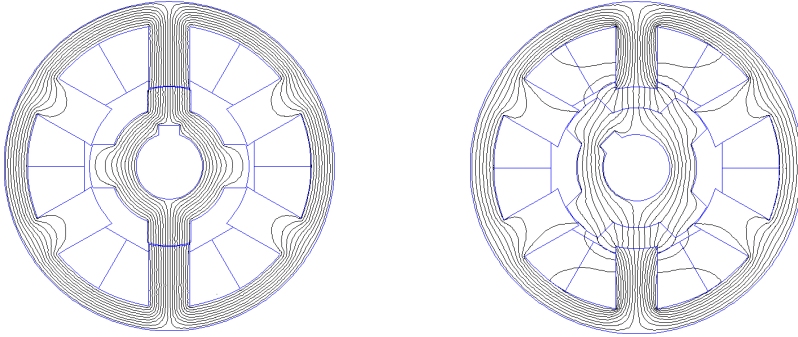


Fig. 8: Flux paths in a radial 6/4 SRM: (left) aligned position; (right) unaligned position

### C. Axial flux SRM

In axial flux SRM, the air-gap flux runs mostly parallel to the axis of rotation (see **Fig. 9**). The stator and rotor are parallel plates arranged perpendicular to the axis of rotation. Some studies carried out on axial flux SRM demonstrate that this type of machine can obtain higher torque density than do radial flux switched reluctance machines. These improved features of the axial flux SRM are due to the increased air-gap area, which depends on the diameter of the machine; while the air-gap area in the radial-type machine depends on the machine's length. Although, Unnewher and Koch reported the first variable reluctance axial flux motor as early as 1973 [46], it was not until recently that many authors have made important contributions to developing axial-flux SRM, as reported by Torkman [47]. Nevertheless, it is relevant to point out the following contributions that are of interest for electric traction. Arihara et al. have presented the basic design methodology for the axial counterpart of the classic radial flux SRM [48]. Murakami et al., have studied the optimization of an axial-flux 18/12 SRM [49]. Labak et al. have proposed a novel multiphase pancake-shaped SRM with a stator composed of a series of C-cores, each with an individually wound coil perpendicularly disposed to a rotor that is made of aluminum in which a suitable number of cubes, the rotor poles, of high permeability material have been added. The torque production in this machine results from the tendency of these cubes to align with the two poles of an energized C-core [50]. Madahvan et al. have contributed to developing the axial counterpart of a segmented rotor SRM in a machine with two rotors and a stator with toroidal-type winding [51]. Bo et al [52] designed an axial field SRM with a single teeth stator and segmental rotor. Recently, Potgieter et al. [53] have released a high-speed rotor two-phase axial-flux segmental SRM.

Andrada et al. have presented a new axial flux-switched reluctance machine with a particular distribution of stator and rotor poles that results in short flux paths without flux reversal. Furthermore, they propose two different types of rotors: one conventional [54] and the other segmented [55]. Some of the contributions cited above describe the manufacturing problems of these machines and propose using soft magnetic composite materials for building their magnetic circuits [53-56].

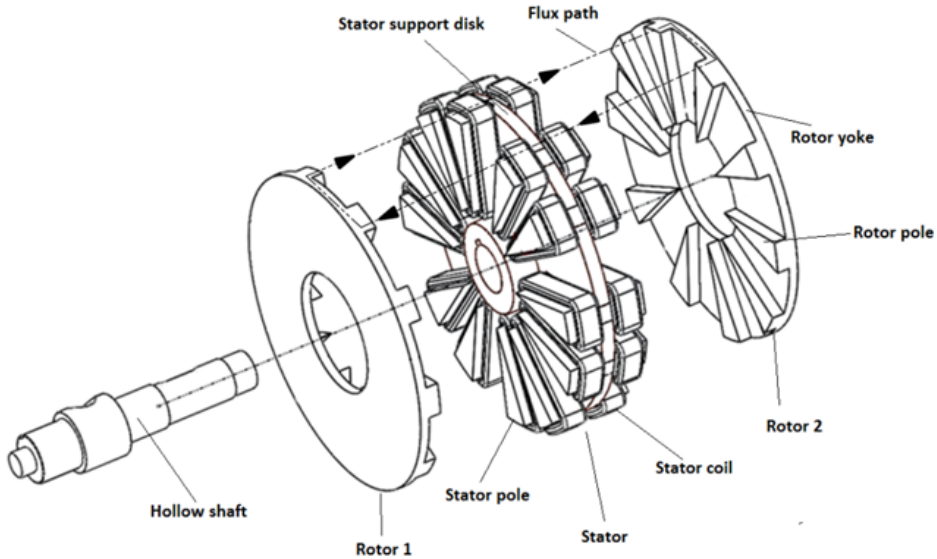


Fig.9: Flux path, aligned position, of an axial-flux SRM

#### D. Transverse flux SRM

In this class of machines, the flux is transverse to the direction of motion and is generated by the flow of a current through a toroidal coil that results in a homopolar magneto-motive force [57-60] (see **Fig. 10**). The phases are independent and disposed axially, with each one being formed basically by a U-shape stator with a toroidal (or hoop) coil along it and a rotor with the same number of salient poles as the stator. The torque production as in a conventional SRM is based on the rotor's tendency to find the minimum reluctance path when the winding is energized. Despite their cumbersome construction, the main advantages of these machines are that the number of poles can be increased without reducing the magneto-motive force per phase. What is more, due to the particular type and disposition of the windings, the copper volume is minimized and thus copper losses

are reduced [61]. Therefore, transverse flux SRM features high torque density and high efficiency at low rotational speeds, which makes it a good candidate for direct drive automotive applications [63-65].

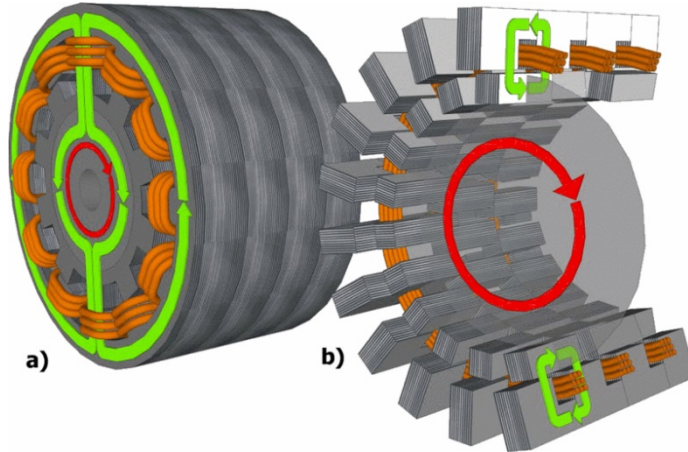


Fig. 10: Flux paths: a) in a radial SRM; b) in a transverse flux SRM [60]

#### 1.4. Conclusions

Despite the advantages indicated in Table I and the research efforts made in overcoming their drawbacks (which are outlined in the previous sections), SRM drives continue to be just one more option for the propulsion of BEV/PHEVs, as evidenced by the fact that, to date, they have not been used in any of the commercially available BEV/PHEVs [7,66]. The underlying justifications for this evidence are:

- Using soft magnetic materials that are different from the current silicon-iron laminations can improve the performance of SRM and make their construction possible, but they greatly increase the cost.
- New SRM structures increase power and torque density in radial, axial and transverse flux machines, but they clearly penalize the most relevant advantage of SRMs, namely their simplicity and robustness of construction – circumstance that have a clear negative impact on cost.
- Despite the great progress made in researching the causes of torque ripple and audible noise while seeking solutions that reduce and mitigate these to acceptable levels in both the mechanical design and electronic control of SRMs, these advances are, until now, insufficient in meeting the standards of the automotive industry [67].

- There are currently no commercial controllers on the market that are intended for switched reluctance motors [68].
- SRM drives are little known among engineers working in automotive industry. Furthermore, academia dedicates hardly any attention to them in courses on electric drives.

## 1.5. References

- [1] Global EV outlook 2019. International Energy Agency. May 2019.
- [2] S. Estenlund, M. Alaküla, A. Reinap. "PM-less machine topologies for EV traction: A literature review". ESARS ITEC 2016, Toulouse France 1-4, November 2016.
- [3] T. Jahns. "Getting rare-earth magnets out of EV traction machines: a review of the many approaches being pursued to minimize or eliminate rare earth magnets from future EV drive trains". IEEE Electrification Magazine, Issue 1, March 2017, pp. 6-18.
- [4] T. Raminosoa, D. A. Torrey, A. El-Refai, D. Pan, Stefan Grubic, Kevin Grace. "Robust non-permanent magnet motors for vehicle propulsion". 2015 IEEE International Electric Machines & Drives Conference (IEMDC). pp- 496 - 502,
- [5] A.El-Refai, T. Raminosoa, P.Reddy, S.Galioto, D. Pan, K. Grace, J. Alexander, K.K. Huh."Comparison of traction motors that reduce or eliminate rare-earth materials".2016 IEEE Energy Conversion Congress and Exposition (ECCE), pp. 1-8.
- [6] T. J. E. Miller. Electronic Control of Switched Reluctance Machines. Newnes Power Engineering Series. 2001.
- [7] B. Bilgin, J.W. Jiang, A. Emadi. "Switched reluctance motor drives". CRC Press, 2019.
- [8] R. Krishnan. Switched Reluctance Motor Drives: Modeling, Simulation, Analysis, Design, and Applications, CRC Press, 2001.
- [9] Y. Gao and M.D. McCulloch. "A review of high power density switched reluctance machines suitable for automotive applications". ICEM 2012 Marseille (France), pp. 2610-2614.
- [10] J.W. Ahn and G.F.Lukman. "Switched reluctance motor: research trends an overview".CES Transactions on Electrical Machines and Systems, Vol 2, No 4, December 2018, pp.339-347.
- [11] P. J. Lawrenson, J. M. Stephenson, P. T. Blenkinsop, J. Corda, N. N. Fulton. "Variable-speed switched reluctance motors". IEE Proceedings B - Electric Power Applications, 1980, Vol 127, Issue: 4, pp. 253-265.
- [12] W.F. Ray and R.M Davis. 'Inverter drive for doubly salient reluctance motor', IEE. J. Electr. Power Appl, 1979, 2, (6), pp.185-193.
- [13] T. Uematsu and R.S. Wallace. "Design of 100 kW switched reluctance motor for electric vehicle propulsion". Proc. IEEE APEC, 1995, pp. 411-415.

- [14] H. Baush, A. Greif, B. Lange, R. Bautz. "A 50 kW/15000 rpm switched reluctance drive for an electric vehicle: Current control and performance characteristics". ICEM 2000, 28-30 August, Espoo, Finland, pp. 603-607.
- [15] H. Bausch, A. Greif, A.B.A. Nickel. "A switched reluctance and an induction machine in a drive train for an electrical vehicle under the conditions of car application". ICEM 2000, 28-30 August, Espoo, Finland, pp. 1313- 1316.
- [16] R.B.Inderka, J-P. Altendorf, L.Sjöberg, R.W. De Doncker. Design of a 75 kW Switched Reluctance Drive for Electric Vehicles". EVS 18 Berlin 2001.
- [17] K.M. Rahman & S.E.Schulz. "Design of high efficiency and high density switched reluctance motor for vehicle propulsion". IAS'2001, Chicago, pp. 2104-2110.
- [18] W. Wu, H. C. Lovatt, J. B. Dunlop."Optimisation of switched reluctance motors for hybrid electric vehicles" 2002 International Conference on Power Electronics, Machines and Drives (Conf. Publ. No. 487), pp.177-182.
- [19] LECTRA. <http://www.electricmotorbike.org/index.php?page=lectra>
- [20] LeTourneau. <http://www.srdrives.com/wheel-loader.shtml>
- [21] Mild hybrid-electric powertrain. <http://www.srdrives.com/hybrid-powertrain.shtml>
- [22] Hybrid electric bus. <http://www.srdrives.com/green-propulsion.shtml>
- [23] K. Boynov, J.H. Paulides, E.A. Lomonova. "Comparative analysis of the SRM as an alternative to the PM motor for automotive applications". COMPEL: The International Journal for Computation and Mathematics in Electrical and Electronic Engineering Vol. 33 No. 5, 2014 pp. 1-14.
- [24] E.Bostanci, M. Moallem, A.Parsapour and B.Fahimi. "Opportunities and Challenges of Switched Reluctance Motor Drives for Electric Propulsion: A Comparative Study". IEEE Transactions on Transportation Electrification, Vol. 3, No. 1, March 2017, pp. 58-75,
- [25] Q.Yu, B.Bilgin, A.Emadi."Design considerations of switched reluctance machines with high power density".2016 IEEE Transportation Electrification Conference and Expo (ITEC), pp. 1-5.
- [26] B. Burkhart, A. Klein-Hessling, I. Ralev, C.P. Weiss, R. W. De Doncker. "Technology, Research and Applications of Switched Reluctance Drives". CPSS Transactions on Power Electronics and Applications, Vol 2, No1, March 2017, pp. 12-26.
- [27] O. Argiolas, E. Nazera, O. Hegazyl, J. De Backer, A. Mohammadi and J. Van Mierlo. "Design Optimization of a 12/8 Switched Reluctance Motor for Electric and Hybrid Vehicles" Twelfth International Conference on Ecological Vehicles and Renewable Energies (EVER) 2002, pp. 177-182
- [28] S. Faid, P. Debal, S. Bervoets. "Development of a switched reluctance motor for automotive traction application" The 25th World Battery, Hybrid o Fuel cell Electric Vehicle Symposium & Exhibition, EVS-25 Shenzhen, China Nov. 5-9, 2010.
- [29] A. Chiba, K. Kiyota, N. Hoshi, M. Takemoto, S. Ogasawara. "Development of a rare-earth-free SR motor with high torque density for hybrid vehicles". IEEE Transactions on Energy Conversion. Year: 2015, Volume: 30, Issue: 1; pp. 175-182.

- [30] B.C. Mecrow, J.W. Finch, E.A. El-Kharashi and A.G. Jack. "Switched reluctance motors with segmental rotors". IEE Proc. Electr. Power Appl. Vol 149. No 4, July 2002, pp. 245-253.
- [31] T. Celik. "Segmental rotor switched reluctance drives". Phd Thesis. University of Newcastle upon Tyne. School of Electrical, Electronic and Computer Engineering. August 2011.
- [32] J.D. Widmer and B.C. Mecrow. "Optimized segmental rotor switched reluctance machines with greater number of rotor segments than stator slots". IEEE Transactions on pp. Industry Applications. Vol. 49, No 4, July/August 2013, pp. 1491-1498.
- [33] J.D. Widmer, R. Martin, B.C. Mecrow. "Optimization of a 80 kW segmental rotor switched reluctance machine for automotive traction." IEEE Transactions on Industry Applications. Vol.51, No 4, July/August 2015, pp. 2990-2999.
- [34] P.C. Desai, M. Krishnamurthy, N. Schofield and A. Emadi. "Novel switched reluctance machine configuration with higher number of rotor poles than stator poles: concept and implementation". IEEE Transactions on Industrial Electronics, Vol. 57, No 2, February 2010, pp. 649-659.
- [35] N. Zabihi and R. Gouws. "A Review on Switched Reluctance Machines for Electric Vehicles". 25th IEEE International Symposium on Industrial Electronics (ISIE), Santa Clara, California (USA), 2016, pp 799-804.
- [36] J.R. Hendershot. "Switched reluctance brushless DC motors with low loss magnetic circuits". Proceedings Intelligent Motion, October 1989.
- [37] J.R. Hendershot. "Polyphase electronically commutated reluctance motor". US Patent 4883999, Filed: August 15, 1988.
- [38] C. Hancock and J.R. Hendershot. "Electronically commutated reluctance motor". US Patent 5015903, Filed: March 28, 1989.
- [39] T. Burress, C. Ayers. "Development and experimental characterization of a multiple isolated flux path reluctance machine". 2012 IEEE Energy Conversion Congress and Exposition (ECCE), pp. 899-905.
- [40] S. R. Mousavi-Aghdam, M. Reza Feyzi, N. Bianchi, M. Morandin, "Design and analysis of a novel high-torque stator-segmented SRM". IEEE Transactions on Industrial Electronics, Vol. 63, No. 3, March 2016, pp. 1458-1466.
- [41] M. Abbasian, M. Moallem, B. Fahimi. "Double-Stator Switched Reluctance Machines (DSSRM): Fundamentals and Magnetic Force Analysis". IEEE Transactions on Energy Conversion, Vol. 25, No. 3, September 2010, pp 589-597
- [42] Y. Yang, N. Schofield, A. Emadi. "Double-rotor switched reluctance machine design, simulations and validations". IET Electrical System in Transportation Vol. 6, Iss. 2, 2016, pp. 117-125.
- [43] E.S. Afjei and H. A. Toliyat. "A Novel Multilayer Switched Reluctance Motor". IEEE Transactions on Energy Conversion, Vol. 17, No. 2, June 2002, pp 217-221
- [44] M. Ruba, I. A. Viorel, L. Szabó. "Modular stator switched reluctance motor for fault tolerant drive Systems". IET Electr. Power Appl., 2013, Vol. 7, Iss. 3, pp. 159-169.

- [45] Land Rover Defender electric. <http://www.srdrives.com/land-rover.shtml>.
- [46] L. E. Unnewehr and W.H. Koch. "An axial air-gap reluctance motor for variable speed applications", Jan./Feb. 1974, IEEE Transactions on Power Apparatus and Systems.
- [47] H. Torkaman, A. Ghaheri, A. Keyhani. Axial flux switched reluctance Machines: a comprehensive review of design an topologies. IET Electric Power Applications, 2019, Vol. 13, Iss. 3, pp. 310-321.
- [48] H. Arihara and K. Akatsu."Characteristics of axial type switched reluctance motor". 2011 Energy Conversion Congress and Exposition, pp 3582-3589.
- [49] S. Murakami, H. Goto, O. Ichinokura. "A study about optimum stator pole design of axial-flux switched reluctance motor". ICEM 2014 Berlin, pp.975-980.
- [50] A. Labak, N.C. Kar. "Designing and prototyping a novel five-phase pancake-shaped axial flux SRM for electric vehicle application through dynamic FEA incorporating flux-tube modeling". IEEE Transactions on Industry Applications, Vol. 49, No 3, May/June 2013, pp. 1276-1288.
- [51] R. Madhavan and B.G. Fernandes. "A novel axial flux segmented SRM for electric vehicle application". XIX ICEM 2010, Roma, pp. 1-6.
- [52] W. Bo and J. Ahn. "Design and characteristic analysis of a novel axial field SRM with single teeth stator and segmental rotor". ICEMS, Oct. 26-29, 2013, Busan, Korea, pp. 571-576.
- [53] H.J. Potgieter, F.M. Márquez-Fernández, A.G. Fraser, M.D. McCulloch. "Design optimization methodology of a high-speed switched reluctance motor for automotive traction applications". 8th IET International Conference on Power Electronics, Machines and Drives. Glasgow Scotland, UK, 2016, pp. 1-6.
- [54] P. Andrada, E. Martínez, B. Blanqué, M. Torrent, J.I. Perat, J.A. Sánchez. "New axial-flux switched reluctance motor for E-scooter". ESARS ITEC Toulouse (France), 2-4 November 2016.
- [55] P. Andrada, E. Martínez, M.Torrent, B.Blanqué, J.I. Perat. "Novel in-wheel axial-flux segmented switched reluctance motor" EPE 2017 Warsaw (Poland), pp 1-8.
- [56] T. Lambert, M. Biglarbegian, S. Mahmud. "A novel approach to the design of axial-flux switched reluctance motors". Machines 2015, 3, pp. 27-54.
- [57] H.M. Amreiz, B.C. Mecrow, C. Weiner. "Switched reluctance machines with simple hoop windings". 2002 International Conference on Power Electronics, Machines and Drives (Conf. Publ. No. 487), 2002, pp. 522-527.
- [58] R. Kruse, G. Pfaff, C. Pfeiffer. "Transverse Flux Reluctance Motor for Direct Servodrive Applications" Conference Record of 1998 IEEE Industry Applications Conference. Thirty-Third IAS Annual Meeting, Vol.1, pp 655-662.
- [59] Yang, C. Gu. "Analytical design and modeling of transverse flux switched reluctance machine" 2008 International Conference on Electrical Machines and Systems, pp. 3414-3416
- [60] Jacek Borecki ; Holger Groke ; Bernd Orlik ; Matthias Joost. "Current waveform optimization for ripple-free output torque of transverse flux reluctance machines".



- 2015 International Symposium on Advanced Electromechanical Motion Systems (ELECTROMOTION), pp.269-273.
- [61] H.M. Amreiz. "A comparison between transverse flux and conventional switched reluctance Machines". XIX International Conference on Electrical Machines, ICEM 2010, Rome Italy.
  - [62] J. Doering, G. Steinborn, W. Hofmann, "Torque, power, losses, and heat calculation of a transverse flux reluctance machine with soft magnetic composite materials and disk-shaped rotor", IEEE Transactions on Industry Applications, Vol. 51, No. 2, March/April 2015, pp. 1494-1504.
  - [63] Bolognesi, "Design and manufacturing of an unconventional variable reluctance machine," in Proceedings of the 4th IET Conference on Power Electronics, Machines and Drives (PEMD '2008) York (UK), 2008, pp. 45-49.
  - [64] B.R. Carlisle. Transverse flux switched reluctance motor and control methods. US Patent 2006009 1755A1. Filed: Oct. 28, 2004.
  - [65] D. Krammer. Transverse flux, switched reluctance, traction motor with bobbin wound coil, with integral liquid cooling loop. US Patent 20080179982A1. Filed: Jan. 30, 2007.
  - [66] P. Andrada, M. J. Dougan, F.M. Márquez-Fernández, A. Egea, L. Zsabo. "Are SRM drives a real alternative for EV powertrain? Workshop on SRM an alternative for E-traction. Vilanova i la Geltrú, Barcelona, Spain February 2, 2018.
  - [67] A.M. Omekanda. "Switched reluctance machines for EV and HEV propulsion: State-of-the-art". 2013 IEEE Workshop on Electrical Machines Design, Control and Diagnosis (WEMDCD), pp.70-74.
  - [68] P. Andrada, B. Blanqué, M. Capó, G. Gross, D. Montesinos. Switched Reluctance Motor Controller for Light Electric Vehicles. In Proceedings of the 20th European Conference on Power Electronics and Applications, EPE'18 ECCE Europe, 2018, P1-P11.



# Soft Magnetic Materials for Switched Reluctance Machines

Pere Andrada

## 2.1. Introduction

In 2011, the sharp increase in raw material costs for rare-earth permanent magnets resulted in automakers seriously considering reductions in the mass of magnets and even eliminating them entirely from powertrains for electric and hybrid vehicles (EV/HEVs). This led to increased research in permanent magnet-less motors, such as: induction motors (IM), synchronous reluctance motors (SyncRM) and switched reluctance motors (SRM) [1]. Although IMs and SyncRMs, mainly the first ones, are strong competitors for the substitution of permanent magnet synchronous motors in electric traction, SRMs still offer viable options in meeting the challenge, above all due to their simple construction.

Much work is currently being dedicated to improving conventional SRMs and in seeking new SRM topologies. In this regard, materials – especially soft magnetic materials – play a key role in developing SRMs with higher values of power/torque density and efficiency for E-traction. Some authors have presented up-to-date research in developing soft magnetic materials for electric machines [2-6] and even for use in SRMs [7]. This chapter provides a survey of the trends in soft magnetic materials for SRMs, with special attention to their applications for traction motors in electrical vehicles.

## 2.2. Requirements of soft magnetic materials for SRM application in E-traction

This section first describes the requirements of soft magnetic materials for SRMs, then considers the demands of these materials in traction motors for electric vehicles.

### A. Requirements of soft magnetic materials for SRMs

As is well known, the instantaneous electromagnetic torque of an SRM is given by the partial derivative of co-energy,  $W'$ , versus position, keeping current constant, that is

$$T = \left( \frac{\partial W'}{\partial \theta} \right)_{i=cte} \quad (2.1)$$

The co-energy is given by

$$W' = \int_0^i \psi di \quad (2.2)$$

With  $\psi = \psi(i, \theta)$  the magnetization curve.

In **Fig.1**, the magnetization curve for the end of conduction, point B, is represented by two straight lines: OA and AB. The magnetization curve for the unaligned position is represented by the line OC.

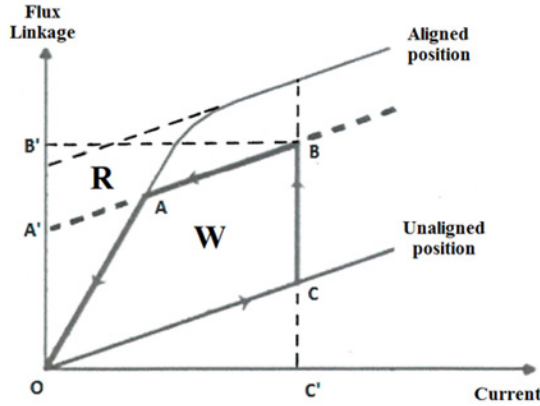


Fig. 1: Magnetization curves and energy conversion loop

The SRM is a single electromechanical converter in which part of the absorbed electrical energy is converted into mechanical energy. This mechanical energy is the area,  $W$  (OABCO), enclosed by the energy loop between the magnetization curve for the unaligned position, the evolution of the current during the period of conduction of one phase and the magnetization curve for the end of conduction (see **Fig.1**). Therefore, the average torque,  $T_{AV}$ , will be the product of this energy by the number of times the cycle is repeated throughout a revolution [8], that is:

$$T_{AV} = \frac{mN_r}{2\pi} W \quad (2.3)$$

With

$m$  being the number of phases and

$N_r$  being the number of rotor poles

The energy ratio,  $E$ , is the relationship between energy converted in mechanical work and the energy supplied [9], taking into account the energy returned by the motor to the supply,  $R(OB'BAO)$ , is given by

$$E = \frac{W}{W + R} \quad (2.4)$$

A high energy ratio requires that low energy be returned to the supply. Ideally, most of the energy supplied has to be converted into mechanical work, which implies that line  $OA'$  overlaps with the ordinate axis, while line  $A'B$  maintains the same slope as line  $AB$ . The coordinate axes of **Fig. 1**, can represent on another scale, the ordinate axis the magnetic induction,  $B$ , and the abscissa axis the magnetic field strength,  $H$ . Therefore, in addition to low core losses, the magnetic material used to channel the flux in an SRM should have high permeability values and high magnetic flux density of saturation.

## B. Requirements of soft magnetic materials used in E-traction.

The usual torque-speed characteristic of a traction motor for EV/HEVs is shown in **Fig. 2**. In the case of direct drive traction, demands of speed are no so high thus the requirements of torque are even higher.

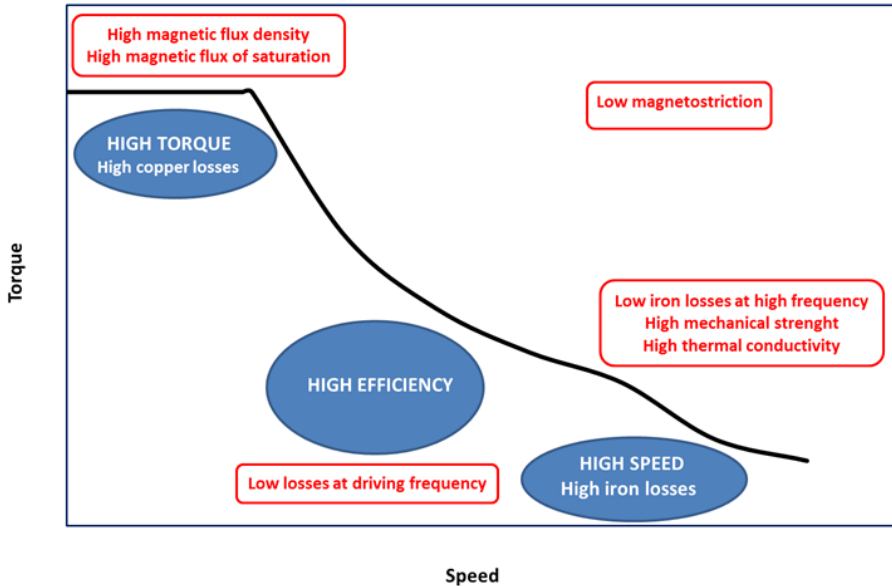


Fig. 2: Torque-speed profile of an EV/HEV and properties required for soft magnetic materials [10]

From **Fig. 2**, it is clear that high torque is required at low speeds (starting, accelerating, hill climbing), with copper losses being dominant. Therefore, soft magnetic material requires high magnetic flux density and high magnetic flux density of saturation. At high speeds, the iron losses are dominant and, hence, the soft magnetic materials must have: low iron loss at high frequency; high mechanical strength; high thermal conductivity; and low magnetostriction in order to reduce noise. Obviously, the soft magnetic material must be efficient in the speed range at which the vehicle is most frequently driven [10].

**Fig. 2** outlines the properties required for the soft magnetic materials used in EV/HEVs. In summary, the requirements of soft magnetic materials to be applied in SRM for E-traction are:

- High permeability
- High magnetic flux density of saturation
- Low losses at driven and at high speeds
- High mechanical resistance
- High thermal conductivity
- Low magnetostriction

In addition, the material must be able to easily take the shape of the stator and rotor of the SRM being built.

### 2.3. Laminated soft magnetic materials

In rotary electric machines, the magnetic core is usually made by stacking sheets of soft magnetic materials that have been previously cut in the shape required by the machine's magnetic circuit. The most usual cutting process is stamping, although laser cutting is suitable for prototypes. The laminated soft magnetic materials most commonly used are alloys made of silicon-iron (SiFe), nickel-iron (NiFe) and cobalt-iron (CoFe), in this category can be included the new dual-phase magnetic materials.

#### A. SiFe

The first choice and the most often used material in electric machines for channeling the magnetic flux is iron alloyed with some content of silicon, usually between 0.5 and 3%. There is SiFe in grain-oriented state (GO steel) or anisotropic, with better magnetic properties in the rolling direction, and non-oriented state (non-GO steel) or isotropic with the same magnetic properties in all directions. Isotropic SiFe is used mostly in the manufacturing of electric machines. Non-GO steels are available as both semi-processed and fully processed products. Semi-processed non-GO steels require annealing after stamping to remove stress and excess carbon. Furthermore, they are delivered without any superficial coating in order to electrically insulate laminations from each other once stacked. Fully

processed steels are delivered annealed and with the desired coating so that they are ready for use without any additional processing. Low loss standard grades of non-GO steels are always presented as fully processed laminations, with thicknesses of 0.35, 0.5, 0.65 or 1 mm.

In the design of SRMs for electric traction with high power/torque density and low loss standard grades (EN 10106), such as M 270-50 A (see **Fig. 3**), either M250-50A or M235-35A [11] are usually used. Some electric steel manufacturers provide specific non-Go steels with better properties. ArcelorMittal offers its iCARE® range of electrical steels, which includes iCARE® Save with very low losses, iCARE® Torque electric steels with high permeability and iCARE®Speed, electric steels for high speed rotors [12]. JFE Steel introduced distinctive non-GO steels such as its JNETM series for energy efficient motors, JNPTM series for high torque motors, the JNEHTM series for high frequency motors, and the JNTTM series for high speed rotors [13, 14].

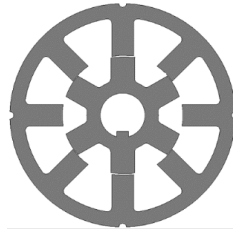


Fig.3: SiFe (M 270-50 A) stator and rotor lamination of an 8/6 SRM

In order to reduce eddy current losses in high frequency machines, interest is currently increasing in thinner laminations of thin gauge non-GO steel (EN10303) with thicknesses of between 0.1 to 0.3 mm.

In addition, alloys with higher silicon content of up to 6.5% are being used. Although the increase in silicon content has some drawbacks such as the reduction of saturation and permeability as well as complications in the manufacturing process due to increased brittleness and hardness, eddy current losses are reduced as a result of their high resistivity. Hiyashi et al. have demonstrated that an SRM built using SiFe laminations with 6.5% silicon content and Super Core™ 10JFX900 [15] can achieve efficiency values that are comparable to interior permanent magnet synchronous machines (IPMSM) [16, 17]. Furthermore, J.W. Jiang built a three-phase 24/16 SRM using this same material for a hybrid electric powertrain that delivered very good performance [18].

Although grain-oriented SiFe is used in transformers, an SRM was recently built using GO steel in the stator and rotor poles and non-GO steel in the rest of its magnetic circuit, and it reportedly provided higher torque and lower losses than the same motor built exclusively with non-oriented SiFe [19].

## B. NiFe

NiFe alloys, commonly named permalloy, typically have a Ni content of between 40% to 50%. These alloys present very low coercivity that results in very high permeability, but their main drawbacks are their low saturation and small magnetic flux density.

## C. CoFe

CoFe alloys, commercially known as permendur, exhibit the highest saturation levels (2.43 T). Typically, they have a Co composition of 49%, Fe of 49% and V of 2%. They also have high mechanical strength, for which they are recommended in the construction of high-speed rotor cores. Due to their high cost, their use is limited to high performance machines. Some SRMs have been built with CoFe alloys, such as the high speed 250 kW starter/generator system used for starting and secondary electrical power extraction from an aircraft propulsion gas turbine [20]. Also notable is the comparative study of two 12/8 SRMs with the same dimensions but comprising different core materials: one with conventional non-GO steel and the other with permendur. The experimental results showed that the SRM made of permendur achieved higher torque and efficiency than the conventional SRM [21].

## D. Dual-phase magnetic materials

Recently dual-phase magnetic materials have been developed [3, 22], with these materials having intermixed first and second regions, the first a magnetic region and the second a non-magnetic region. Both regions contain only limited amounts of carbon: less than about 0.05 % of the total weight. The second region includes greater than 0.4 % of the total nitrogen weight. The material is prepared according to the method described in [22]. From a magnetic point of view, using this kind of material can facilitate the construction of segmented SRMs and maintain the rotor pole saliency in conventional SRMs, while the air-gap remains constant and thus reduces windage losses and torque ripple (see **Fig. 4**).

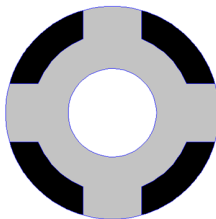


Fig.4: Dual phase lamination of a 6/4 SRM rotor: magnetic region (in grey) and non-magnetic region (in black).

## 2.4. Amorphous magnetic materials

Amorphous metals are non-crystalline materials that have a glass-like structure. The boron, silicon, and phosphorus alloys, as well as other glass formers with magnetic metals (iron, cobalt, and nickel) have high magnetic susceptibility, low coercivity and high electrical resistance. The conductivity of metallic glass is of the same low order of magnitude as molten metal at just above the melting point. The high resistance leads to low losses from eddy currents when subjected to alternating magnetic fields. The amorphous magnetic materials are provided as thin metal sheets (25  $\mu\text{m}$ ) in the shape of a rolled ribbon. These materials are used in wound core transformers in order to reduce iron losses. Due to their thinness and brittleness, their use in electrical machines is more cumbersome and they are thus limited to cores with simple geometries. The core is usually made by punching-out or by laser cutting a layered block made of ribbons of amorphous magnetic material that are held together by an adhesive. Some switched reluctance machines have been built using amorphous magnetic materials that achieve higher values of efficiency than those using conventional SiFe alloys [23, 24].

## 2.5. Soft magnetic composites

The use of powder metallurgical materials provides all the advantages of powder metallurgical production, such as low cost, tight tolerances, complicated forms and minimum material waste [25]. Soft magnetic composites (SMC) are powder metallurgical materials that can provide magnetic properties comparable to SiFe laminations at medium and high frequencies [26]. SMC materials are made of iron powder particles coated with an electrically insulating layer and can be formed into complex shapes by means of powder metallurgy, thereby allowing for three-dimensional magnetic circuit designs that open up the possibility of building axial or transverse flux motors – which would be impossible or prohibitively expensive if using laminated soft magnetic materials. Nevertheless, complex designs are restricted by the compacting process in order to get a uniform pressure and as a consequence density in the piece. The mechanical properties of SMC are lower than laminated magnetic materials. SMC materials have very high resistivity, which means low eddy current losses. The main drawbacks of SMC are its low permeability, as well as the fact that its flux density for the same magnetic field strength is lower than that of laminated magnetic materials. Manufacturing SMC consists of mixing iron powder with a binder, compacting the material at high pressures (500-800 MPa) in a mold and then curing it at relatively low temperatures of 200-650°C. Most SMC manufacturers provide specific material for prototyping; these are machined blanks that suffer little change from subsequent machining processes [27]. Vijayakumar et al. [28, 29] compared the torque and made a dynamic analysis based on the geometry of a 6/4 SRM built first using non-Go steel (M-19) and then two types of SMC (Somaloy 500 and 1000). Many authors have used SMC to construct new types of axial-flux SRMs [30-32] that

would not have been possible using laminated soft magnet materials. **Fig.5** shows the stator and rotor pole pieces of an axial flux motor made using SMC.

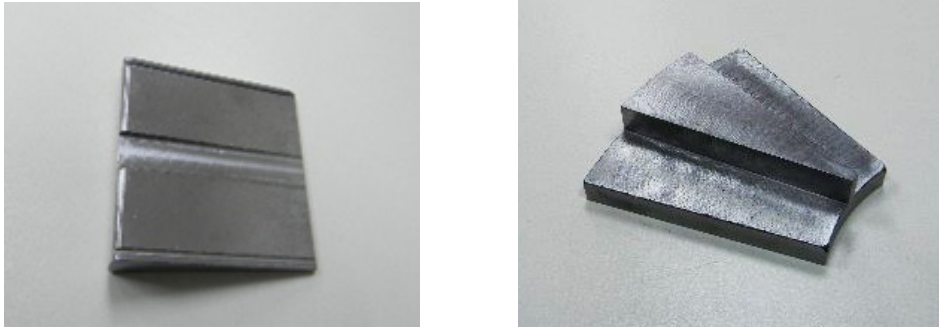


Fig. 5: SMC pieces of an axial flux SRM [31]

## 2.6. Conclusions

None of the materials described in the previous sections meet all the soft magnetic material requirements for applying SRM in E-traction. Nevertheless, each one stands out in some way. For example, NiFe alloys have the highest permeability; CoFe alloys achieve the highest magnetic flux saturation while also standing out for their mechanical properties; amorphous metals have the lowest iron losses; SMC allows making magnetic circuits in complicated shapes; and the different SiFe alloys provide a cheap solution in most cases. Table I lists some of the physical and magnetic properties of the soft magnetic materials that are most commonly used in these kinds of applications, while table II compiles their corresponding iron losses. Undoubtedly, a CoFe alloy would be the best alternative for a radial-flux SRM that can handle the same speed characteristics as those illustrated in Fig. 2. However, its high cost may discourage its use in favor of 6.5% non-GO steel. In the case of a direct drive motor, it would be better to opt for specific non-GO steel for high torque. Given the complex construction of a medium or high frequency axial-flux motor, the best option would be to use SMC. There presently remains much to investigate, not only in terms of materials that improve on the properties of those currently in use, but also in regard to materials that can be additively manufactured [33].



TABLE I. COMPARISON OF MAGNETIC CHARACTERISTICS

Alloy	Type	Thickness (mm)	Density (g/cm <sup>3</sup> )	Resistivity ( $\mu\Omega\text{cm}$ )	B at 0.8 kA/m	B at 2,5 kA/m
	M250-35	0,35	7.6	55	-	1.53
	M250-50	0,5	7.6	59	-	1.55
<b>SiFe</b>	Thin Non-Go	0,1	7.65	52	1.15	1.63
	Non-GO Si 6,5% <b>10JNEX900</b> [15]	0,1	7.42	82	1.29	1.40
<b>CoFe</b>	49% Co, 49% Fe, 2% V <b>VACOFLUX 48</b> [34]	0.35	8.12	42	2.1	2.23
<b>Amor- phous</b>	Fe-based amorphous	0.025	7.18	130	1.38	-
<b>SMC</b>	<b>Somaloy 700 3P</b> [35]	solid	7.57	20000	0.74	1.25

TABLE II. COMPARISON OF SPECIFIC IRON LOSSES

Alloy	Type	Losses W/kg 1T/50Hz	Losses W/kg 1T/400Hz	Losses W/kg 1T/1kHz
	M250-35	0.98	17.1	72.6
	M250-50	1.02	23.4	113
<b>SiFe</b>	Thin Non-Go	0.8	8.5	27.1
	Non-GO Si 6,5% <b>10JNEX900</b> [15]	0.5	5.7	18.7
<b>CoFe</b>	49% Co, 49% Fe, 2% V <b>VACOFLUX 48</b> [34]	1.6 (1.5 T/ 50 Hz)	31 (1.5 T/ 400 Hz)	147 (1.5 T/ 1kHz)
<b>Amorphous</b>	Fe-based amorphous	0.1	1.5	5.5
<b>SMC</b>	<b>Somaloy 700 3P</b> [35]	5.0/6.1	45	132

## 2.7. References

- [1] T. Jahns. "Getting rare-earth magnets out of EV traction machines: a review of the many approaches being pursued to minimize or eliminate rare earth magnets from future EV drive trains". IEEE Electrification Magazine, Issue 1, March 2017, pp. 6-18.
- [2] M.D. Calin, M.C. Georgescu, E. Helerea. *Magnetic Materials for Electric Machines Used in Transportation*. Lambert Academic Publishing, 2015.
- [3] A.M. El-Refaie. "Role of advanced materials in electrical machines". 20th International Conference on Electrical Machines and Systems (ICEMS), 2017.
- [4] N. Fernando, F. Hanin. "Magnetic materials for electrical machine design and future research directions: a review". 2017 IEEE International Electric Machines and Drives Conference (IEMDC)
- [5] A. Krings, A. Boglietti, A. Cavagnino, S. Sprague. "Soft magnetic material status and trends in electrical machines". IEEE Transactions on Industry Electronics, Vol 64, No 3, March 2017, pp. 2405-2414.
- [6] A. Krings, M. Cossale, A. Tenconi, J. Soulard, A. Cavagnino, A. Boglietti. "Magnetic Materials Used in Electrical Machines: A Comparison and Selection Guide for Early Machine Design". IEEE Industry Applications Magazine, 2017, Vol. 23, No 6, pp. 21-28.
- [7] F. Rebahi, A. Bentounsi, A. Lehair, T. Benamimour. "Soft magnetic materials for switched reluctance machine: finite element analysis and perspective". 2014 International Conference on Electrical Sciences and Technologies in Maghreb (CISTEM).
- [8] T.J.E. Miller. "Converter volt-ampere requirements of the switched reluctance motor drive". IEEE Transactions on Industry Applications, Vol 21, No 5, September/October 1985, pp 1136-1144.
- [9] T.J.E. Miller. *Switched reluctance motors and their control*. Magna Physics Publishing Oxford Science Publications, 1993.
- [10] T. Wakisaka, S. Arari, Y. Kurosaki. "Electrical steel sheet for traction motor of hybrid/electrical vehicles. Nippon Steel Technical report, No 103, May 2013, pp. 16-120.
- [11] M. Besharati ; K. R. Pullen ; J. D. Widmer ; G. Atkinson ; V. Pickert. "Investigation of the mechanical constraints on the design of a super-high-speed switched reluctance motor for automotive traction". 7th IET International Conference on Power Electronics, Machines and Drives (PEMD 2014) 2014, pp. 1-6.
- [12] S. Jacobs, D. Hectors, F. Henrotte, M. Hafner, M. Herranz Gracia, K. Hameyer, P. Goes, D. Ruiz Romera, E. Attrazic, S. Paonelinelli. A. "Magnetic material optimization for hybrid vehicle PMSM drives". EVS24 International Battery, Hybrid and Fuel Cell Electric Vehicle Symposium Stavanger, Norway, May 13 - 16, 2009, pp.1-9.
- [13] O.Yoshihiko, O.Tomoyuki, T. Masaaki. "Recent Development of Non-Oriented Electrical Steel in JFE Steel". JFE TECHNICAL REPORT. No. 21 (Mar. 2016), pp. 7-13.
- [14] H. Toda, and K. Senda, "Influence of various non-oriented electrical steels on motor efficiency and iron loss in switched reluctance motor", IEEE Trans. on Magnetics, Vol. 49, No. 7, 2013.

- [15] JFE Steel Corporation, "Super Core," 2015. [Online]. Available: <http://www.jfes-steel.co.jp/en/products/electrical/catalog/f1e-002.pdf>. [Accessed: 23- Nov- 2019].
- [16] H. Hayashi, A. Chiba, T. Fukao, "Efficiency comparison of switched reluctance motors with low loss materials". 2007 IEEE Power Engineering Society General Meeting, 2007, pp.1-6
- [17] A. Chiba, K. Kiyota, N. Hoshi, M. Takemoto, S. Ogasawara. "Development of a rare-earth-free sr motor with high torque density for hybrid vehicles". IEEE Transactions on Energy Conversion. Year: 2015, Vol. 30, Issue: 1; pp 175 – 182.
- [18] J. W. Jiang. Three-phase 24/16 switched reluctance machine for hybrid electric powertrains: design and optimization. PhD thesis McMaster University, December 2015.
- [19] Y. Sugawara, and K. Akatsu, "Characteristics of Switched Reluctance Motor using Grain-Oriented Electric Steel Sheet", 2013 IEEE ECCE Asia, 3-6 June 2013 Melbourne, pp. 1105-1110.
- [20] E. Richter, C. Ferreira. "Performance evaluation of a 250 kW switched reluctance starter/ generator". IAS '95. Conference Record of the 1995 IEEE Industry Applications Conference Thirtieth IAS Annual Meeting, 1995, pp. 434 -440.
- [21] E. Y. Hasegawa, K. Nakamura, O. Ichinokura. "Experimental verification of performance of a switched reluctance motor made of permendur". The XIX International Conference on Electrical Machines - ICEM 2010 , Rome 2010.
- [22] L. Cerrully, R. DiDomizio, F. Johnson. Dual phase magnetic material component and method of forming. US Patent 2015/0115749 A1, Filed: October 31, 2013.
- [23] A. Chiba, H. Hayashi, K. Nakamura, S. Ito, K. Tungpimolrut, T. Fukao, M. Azizur Rahman, M. Yoshida. "Test results of an SRM made from a layered block of heat-treated amorphous alloys", IEEE Transactions on Industry Applications Vol. 44, No. 3, May/June 2008, pp. 699-706.
- [24] S. Ito, A. Chiba, T. Fukao, M. Yoshida, "A Test Results of a SRM made of layered Block of Heat-Treated Amorphous". IAS2005, Vol. 4, pp.2698-2703.
- [25] M.J. Dougan."Powder metallurgical materials and processes for soft magnetic applications". Workshop on SRM an alternative for E-traction. Vilanova i la Geltrú Barcelona Spain. February 2, 2018, pp. 11-18.
- [26] A. Schoppa, P. Delarbre, A. Schaetz. "Optimal Use of Soft Magnetic Powder Composites (SMC) in Electrical Machines". [Online] Available: [https://www.pmg-sinter.com/scripts/PowderMet\\_2013\\_Chicago.pdf](https://www.pmg-sinter.com/scripts/PowderMet_2013_Chicago.pdf). [Accessed: 23- Nov- 2019].
- [27] Höganäs, Somaloy prototyping material, SPM. [Online] Available: [https://www.hoganas.com/globalassets/download-media/sharepoint/brochures-and-datasheets-all-documents/somaloy-prototyping-material\\_march\\_2016\\_1334hog.pdf](https://www.hoganas.com/globalassets/download-media/sharepoint/brochures-and-datasheets-all-documents/somaloy-prototyping-material_march_2016_1334hog.pdf). [Accessed: 23- Nov- 2019].
- [28] K. Vijayakumar, R. Karthikeyan and R. Arumugan. "Influence of soft magnetic composite material on the electromagnetic torque characteristics of switched reluctance motor". 2008 Joint International Conference on Power System Technology and IEEE Power India Conference, 12-15 Oct. 2008, New Delhi, India.

- [29] K. Vijayakumar, R. Karthikeyan, S. Kannan, G. Prem Sunder and R. Arumugam. "Dynamic Analysis of Switched Reluctance Machine using Soft Magnetic Composite Material", 2010 Joint International Conference on Power Electronics, Drives and Energy Systems & 2010 Power India.
- [30] T. Kellerer, O. Radler, T. Sattel, S. Purfürst, S. Uske. "Axial type switched reluctance motor of soft magnetic composite" Innovative Small Drives and Micro-Motor Systems 19-20 september 2013, Nuremberg, Germany, pp. 29-34.
- [31] P. Andrada, B. Blanqué, E. Martínez, J.A. Sánchez, M. Torrent. "In wheel-axial-flux SRM drive for light electric vehicles". Workshop on SRM an alternative for E-traction. Vilanova i la Geltrú Barcelona Spain. February 2, 2018, pp. 39-46.
- [32] J. H.J-Potgeister, F. Márquez-Fernández, A.G.Fraser, M.D. McCulloch. "Effects observed in the characterization of soft magnetic composite for high frequency, high flux density applications". IEEE Transactions on Industry Electronics, Vol 64, No 3, March 2017, pp 2485-2493.
- [33] F. Wu, A. M. El-Refaie. "Towards fully additively-manufactured permanent magnet synchronous machines: opportunities and challenges. 2019 IEEE International Electric Machines & Drives Conference (IEMDC), pp. 2225-2232.
- [34] Soft magnetic cobalt-iron alloys Vacoflux and Vacodur. VAC Vacuumschmelze. [Online] Available: <https://vacuumschmelze.com/Assets/Cobalt-Iron%20Alloys.pdf>. [Accessed:23- Nov-2019].
- [35] Höganäs. Somaloy® 3P Material data. [Online] Available [https://www.hoganas.com/globalassets/download-media/sharepoint/brochures-and-datasheets---all-documents/somaloy-3p\\_material-data\\_june\\_2018\\_2273hog.pdf](https://www.hoganas.com/globalassets/download-media/sharepoint/brochures-and-datasheets---all-documents/somaloy-3p_material-data_june_2018_2273hog.pdf). [Accessed:23- Nov-2019].

## PM to RSM Rotor Replacement Study on Traction Machines

Avo Reinap

### 3.1. Introduction

Transport electrification gains uninterruptedly interest as this is apparently one of the promising ways towards sustainable, energy efficient and environmentally friendly future. No pain, no gain – all electric drive system components are under continuous research and examination in order to increase the power density, efficiency, reliability while seeking for suitable materials and production technologies for the sake of more affordable solutions and sustainable products. Since the transportation means motion, mechanical energy needs to be present and unquestionably the electrical machine or machines take place in this system. Is it matter of taste, how the vehicle looks like or what components are used to achieve the desired unfailing functionality? Well, usually the prosperity advances living environment, which can be exemplified by the abrupt change of raw material price in permanent magnet (PM) in 2011 that concern is clearly seen in publications and research headlines as a cost issue. Inopportunately the environmental issues related to material engineering and technology development are seldom if ever reflected in context of electrical machine design. Positively, the cost concern of PM materials has triggered research towards PM-less machine topologies, e.g. reluctance machines (RM), and judge different options for system development instead of selecting hastily a PM-machine topology in order to increase simultaneously torque density, power density, efficiency and so forth and on. Electrical machine design and engineering is multidisciplinary wherever competency should not be replaced by effectiveness. Diversity of electric drive system requirements can take functional advantages of the specific features that an explicit type of electrical machine can provide. As a matter of fact, the implication on high speed and temperature capability, higher reliability over wider constant power speed range favor reluctance type of machines to any other types. This objectionable exaggeration is based to facts that switched reluctance type of machines (SRM) are used in aircraft as generators

[1][2][3] and auxiliary drives [4], turbo machines [5] where desirable high power density is not gained from increasing the torque per unit of machine rather than increasing the speed. Fascinatingly, RM types of machines have found a way into wind turbines [6][7] as this low speed application challenges machine designers when looking for direct gearless, reluctance generators as prospectively pm-less and fault tolerant solutions. These prototypes were designed and evaluated 100-115 rpm at output load partly or completely fulfilling the targeted 10 kW [6] and 20 kW [7]. However, vehicular electric propulsion machines and drives is application area where the low price can be more valuable than the weight and size [8]. As a matter of fact, the collected experience on machine modelling and development of reluctance type of machines [9] compared to various design challenges and practical realizations [10] encourages researchers working on reluctance machines and drives. The challenging design aspects of RM, which reduces their ranking [11], is torque ripple and noise which is directly connected to torque production and torque capability of these type of machines. The main target of this chapter is road bound transportation and traction machines, which could take advantage of less permanent type of machines. The disposition of this work is not restudying what previously is done rather than providing evaluation example of a PM and its' RM counterpart with the focus on torque production capability and quality when exploring the magnitude and force distribution in the air-gap. The study starts from general machine construction, moves into the air-gap of selected machines, focuses on the magnetic shear stress distribution along the gap circumference and compares the torque production.

The objective of this chapter is not praising reluctance machines nor do comparing alternative PM-less machines rather than putting RM into content of PM traction machines. This contextualization is based to replacement of PM to RM rotor and comparison of torque capability. However, since the PM machines need to operate over relatively wide speed range the feature is achieved either by rotor design or usage of distributed concentrated windings. Furthermore, as the stator layout takes advantage of inserted windings or core segments the machine layout reminds apparently switched reluctance machines. As a matter of fact, constructional modularity and simplicity are often awaited features that not only production technology but also faultless drive can take advantage on behalf of machine topology selection and design. Some efforts are made to demonstrate the torque producing force distribution in the air-gap that is more concentrated peaks in RM machines compared to PM machines. However, the machine specification and design are driven by the system requirements towards application and likely there are many options, solutions and valuable candidates that should not be related only to torque capability or ripple.

3.2. Machine topologies

When considering that origin of torque in any electrical machine is based to excitation and reluctance torque or in combination of these two then the machine topologies can simply divided into non-excited, temporal (electrically) excited and permanent excited machines, where the first category can take advantage only of reluctance torque. This nomenclature of none-excited and temporary excited is more unconventional as terminology of single-fed and double-fed machines. The purpose of recalling the machine topologies differently is to distinguish machine types that are naturally capable to higher torque and the others which are better suited operating over wide speed range. Obviously electrical machines for transportation need to provide both, and not only, reliability and fault tolerant operation are some of the features where RM becomes beneficial.

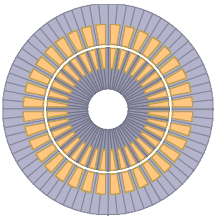
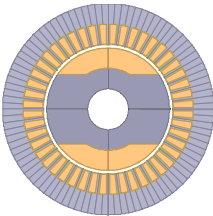
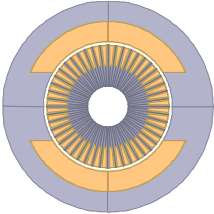
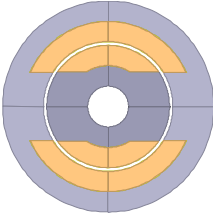
The topology classification is made in two levels according to

- A. electromagnetic and geometric arrangement – excitation and saliency
- B. electromagnetic mechanic interaction – more focus on machines with no rotor excitation

A. Excitation and saliency

The geometric electromagnetic arrangement of electrical machines can be sorted among none, single, or double-salient and single or double-fed machines. Table I demonstrates machine layouts that have coils in stator and rotor and formation of stator and rotor saliency that result double salient structure used in variable and switched reluctance machines.

TABLE I MACHINE CLASSIFICATION ACCORDING TO GEOMETRIC ELECTROMAGNETIC ARRANGEMENT

		ROTOR SALIENCY	
STATOR SALIENCY			
			

The geometric arrangement of radial flux machines (Table I) can have even dual rotor or stator but this does not provide any obvious benefits and common for all topologies the saturation limit to magnetic loading and temperature limit to electric loading are the main constraints to torque capability. Ideally, the torque would be generated all around rotor belt, but practically the force distribution between the machine parts is rather local and concentrated. The machine layouts (Table I) can reveal a subjective guesstimate of tangential forces behind torque generation and structural loads behind noise generation.

## B. Electromagnetic mechanic interaction

Starting from control involvement and maximizing torque product, the reluctance type machines RM are mostly known as variable reluctance, switched reluctance and synchronous reluctance. It is just unfair to locate or limit (us) in the UK or few references but the RM knowledge established by T.J.E. Miller [12], A.G. Jack, and B. Mecrow [13], the continuous contribution by Z.Q. Zhu [14] provides rather adequate overview, outline and challenges of the development on RM type of machine related topologies. As a matter of fact, there are considerably more engineers and researches who have contributed to RM machine and drive system development. When considering machine construction then the common nominator of all these contributions is based to a geometrically undemanding salient rotor core that takes advantage of simplicity, fault tolerance, high speed and high (rotor) temperature operation. **Fig. 1** gives an example of research interest and demonstrates rotor alternation from conventional (in the left), to unconventional (in the middle) and further on to eccentric (in the right). The RM layouts that were irrational or unthinkable in 1980s have received intention this century [15][16]. The eccentric RM has been an effort to merge cycloid gear directly to electromagnetically excited ring gear [17] and if nothing else so has this “invention” triggered modal analysis of forces in order to understand the behavior of the actuator.

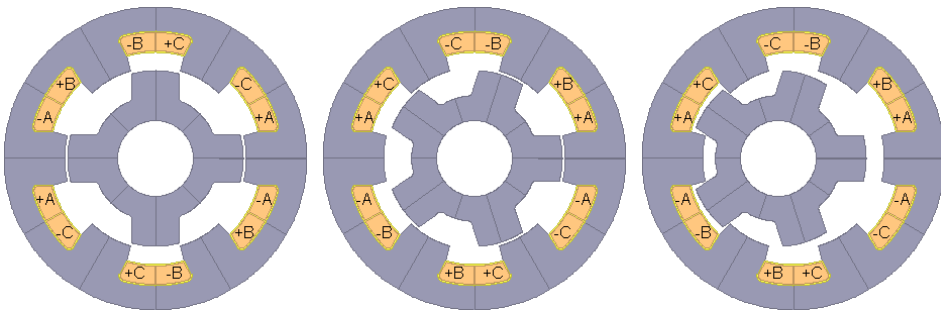


Fig. 1: 6-tooth stator 4-tooth rotor 6S4R (left), centric 6S5R (middle) and eccentric 6S5R (right)



Electromagnetic mechanic interaction in magnetic field is important aspect when comparing or developing RM type machines. Radial magnetic force is recognized as main contributor to the noise [18] and satisfactory operation over the wide power speed range including the unbalanced magnetic force requires powerful models to understand the complex rotor dynamic interactions [19]. The electromagnetic forces applied to machine cores and analysis of structural response modes facilitate understanding the origin of noise generation and propagation in RM [20]. The RM can be operated into deep saturation for the sake of maximizing torque and consequently the over-forced salient structures are more tend to audible noise than cylindrical medium forced machines. RM machines appear in various stator tooth to rotor tooth configurations from reluctance Vernier machine to a conventional few tooth configuration (**Fig. 1** right). Similarly, the coil arrangements appear from single layer to double layer winding (coils sharing the same slot) and from single-fed to double-fed machine when considering that armature coil and field coils are both integrated into the stator core to facilitate flux switching and variable flux topologies. The core development contributes also to RM, as it can take advantage of c-cores, have portioned cores and integrate machines towards magnetic gears. However, PM integrated RM types, where PM is part of stator structure has the majority but RM with dual stator windings and related research is well presented.

### 3.3. Core material selection

Since the RM can operate to high saturation and the gap length is a few % of magnetizing path the high flux density magnetic cores become stimulating design option. Soft magnetic material development towards higher speed (frequency) gives obviously satisfactory results of reduced power losses [21] while higher magnetic flux and torque capability may not result to expected upgrading on specific torque [22]. In this evaluation 6 different grades are compared (Table II).

TABLE II SOFT MAGNETIC CORE MATERIALS

Grade	Material	Density [g/cm <sup>3</sup> ]	Thickness [mm]	Saturation [T]	Losses @1kHz 1.5T [W/kg]
Vacoflux 48	Fe Co	8.12	0.1	2.3	38.0
Vacodyr 49	Fe Co	8.12	0.15	2.3	100
Vacodur X1	Fe Co	7.9	0.2	2.1	146
Arnon-5	Fe Si	7.65	0.127	1.9	78.7
HI-LITE NO10	Fe Si	7.65	0.1	1.8	83.7
M250-35A	Fe Si	7.6	0.35	1.8	191

Initially the selected machines are evaluated using FeSi core M250-35A, whereas RM machines are also evaluated by using FeCo core Vacoflux 48 and (cost) optimized FeCo core Vacodur X1. Material data are provided by material developers and producers [23][24][25][26].

### 3.4. Torque generation

The primary purpose of an electrical machine is to produce the torque – driving or braking, which means that the question for electrical machine engineer is where (in design), when (in control) and what conditions (in physics) the construction provides the desired forces for torque. The exploration of flux density distribution and the resulting magnetic forces improves the understanding on the origin of forces and the capabilities and design issues of different machine topologies rather than developing comparisons between apples and pineapples. Usually, the comparison condition is made simple as the criterion is which machine provides most torque (consequently also power) and lowest price at given space. This work provides the same type of unfair comparison as it evaluates two different stator layouts with two different types of rotors. The initial machines are “optimized” PM machines for use in traction application and they take advantages of 3-phase vector control. Meanwhile, the proposed RM counterpart uses a simple switching sequence with one-phase energized only and the proposed rotor geometry, which replaces the PM rotor, is not optimized to take advantage of SRM drive or use sinewave currents from conventional voltage source inverter as PM machine [27]. The torque generation analysis is done as following

1. Flux density distribution and resulting forces at a single rotor position is compared to demonstrate the conditions and outcomes for comparison
2. Static torque characteristics are obtained at different rotor position and current levels in order to compare low-speed torque capability of selected topologies

### 3.5. Case studies

The selection of electrical machines for comparison are shown in **Fig. 2** and further specified in TABLE III. One of the initial machines (12-tooth 8-pole **Fig. 2**), which is initially with interior permanent magnet (IPM) rotor, are discussed in [28] whereas the investigation on cooling integration and thereby improving the torque capability of the machines are presented in [29] (12T8P) and [30] (18T16P). The number of turns per phase and maximum reference current is chosen so that the selection of machines becomes somehow comparable and place the current level in content of previous thermal analyses. 0.7 mm air-gap is used in counterpart RMs.

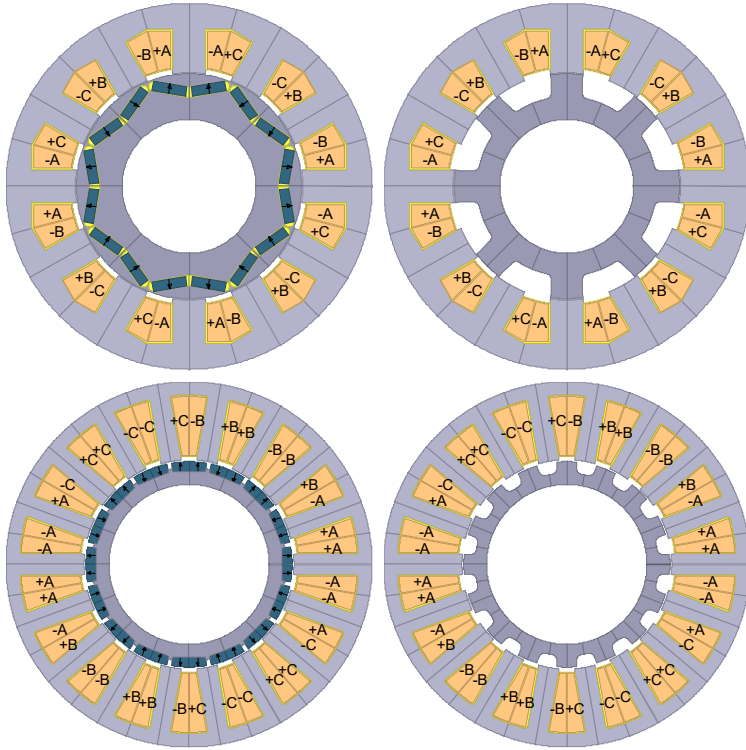


Fig. 2: 12-tooth 8-pole, 12T8P (top) and 18-tooth 16-pole 18T16P (bottom) machines

TABLE III SPECIFICATION OF 12-TEETH 8-POLE (LEFT)  
AND 18-TEETH 16-POLE (RIGHT) MACHINES

Quantity, symbol [Unit]	12-teeth 8-pole (12T8P)	18-teeth 16-pole (18T16P)
Outer diameter, $D_o$ [mm]	246	240
Active length, $H$ [mm]	27	200
Number of turns, $N$ [turns]	4x11	6x7
Reference current, $I$ [A]	300	300
Active weight, $m$ [kg]	12	45

The active length means that the axial length of overhangs is excluded and in case of weight the housing, shaft and bearings are excluded. The weight approximation is made for PM type of machine.

### 3.6. 12-Tooth 8-pole machine

This machine is used mainly as generator for light vehicles with some evaluation presented in [28] and research on development of direct cooled windings is presented in [29].

#### A. Magnetic loading

The purpose of magnetic analysis is to visualize flux density distribution of the loaded machine with different rotors (**Fig. 3**) and investigate tangential force distribution around rotor in the air-gap (**Fig. 4**). As the PM machine have two coils excited and RM only one then the current is doubled in RM machine in order to show that the machines have the same MMF. The magnetic loading is shown with FeSi core (M250-35A), optimized FeCo core (Vacodur X1) and high flux density FeCo core (Vacoflux 48) in Fig. 3. Fig. 4 compares the machines with FeSi core.

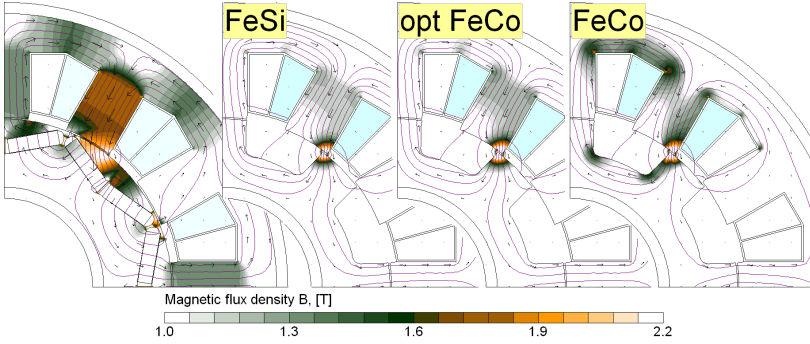


Fig. 3: Flux density distribution of IPMSM at 150 A at two phases (left) and SRM at 300 A at single phase

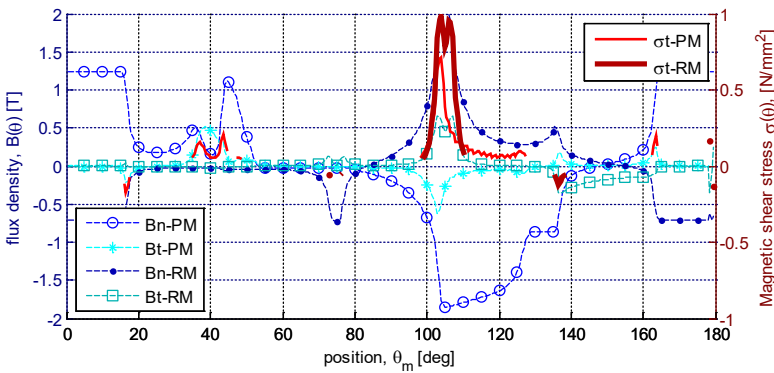


Fig. 4: Flux density distribution along the air-gap from 0 to 90 mechanical degrees and resulting tangential magnetic stress component ( $\sigma_t$ ) of 12T8P machine

The resulting torque for these machines at given rotor position is 33.9 vs 59.8 Nm, respectively for SRM and IPMSM machine. As the instantaneous value of torque contains ripple the torque values for specific position are not clearly comparable. However, this comparison demonstrates the tangential flux and tangential force distribution as a character of torque production.

## B. Torque capability

The focus is on low-speed torque of the previously presented RM. **Fig. 5** demonstrates static torque as a function of rotor position from un-alignment to alignment, from unstable equilibrium position to stable equilibrium position and the currents at different level are kept constant. If the excitation sequence that consists of  $60^\circ$  constant current pulses from  $\theta_e = \{40^\circ - 100^\circ\}$  (**Fig. 5**) then the (static) torque capability can be compared for the machines (**Fig. 6**)

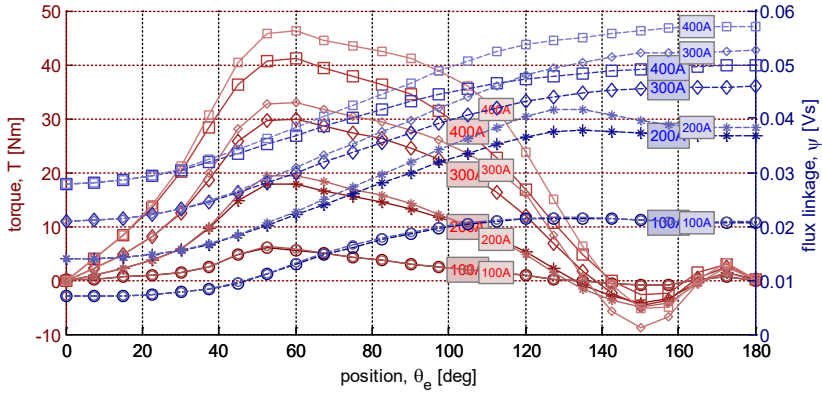


Fig. 5: Static torque characteristics of 12T8P machine at constant current

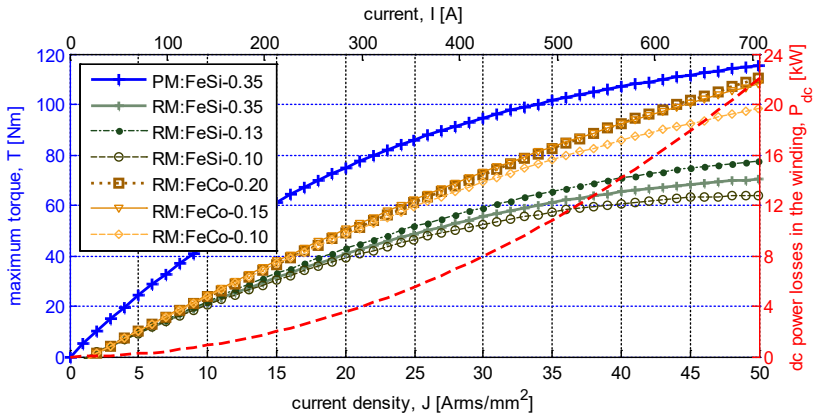


Fig. 6: Torque as function of current related to current density and power losses

**Fig. 5** compares FeSi (M250-35A) core to FeCo (Vacoflux 48) core where lighter curves with smaller labels belong to high flux density material. **Fig. 6** extends this comparison to other core materials. Different cores can be distinguished by the materials used (FeSi or FeCo) and lamination thickness between 0.10 and 0.35 mm. The remaining challenge is to establish a fair comparison condition and to interpret the equal amount of current in PM and RM. PM machine consumes 3-phase currents followed by maximum torque per ampere (MTPA) line. RM has 1/3 duty or rectangular wave excitation, which means that the dc current levels in **Fig. 5** are adjusted by  $\sqrt{3}$  for the same heating power. As **Fig. 6** shows in this comparison, the RM is capable of 40-50 Nm depending on core type at 300A while PM machine would be capable of 80 Nm.

### 3.7. 18-Tooth 16-pole machine

This machine with surface mounted magnets (SPM) is used for traction in an off-road vehicle. The evaluation of power losses and integrated direct cooled windings of this machine is presented in [30].

#### A. Magnetic loading

Similar to previous machine example, the flux density distribution of the loaded machine with different rotors (**Fig. 7**) and investigation of tangential force distribution around rotor in the air-gap (**Fig. 8**) are shown. The core material is changed and presented as previously in order to study the benefits of replacing core of RM machines for higher torque capability.

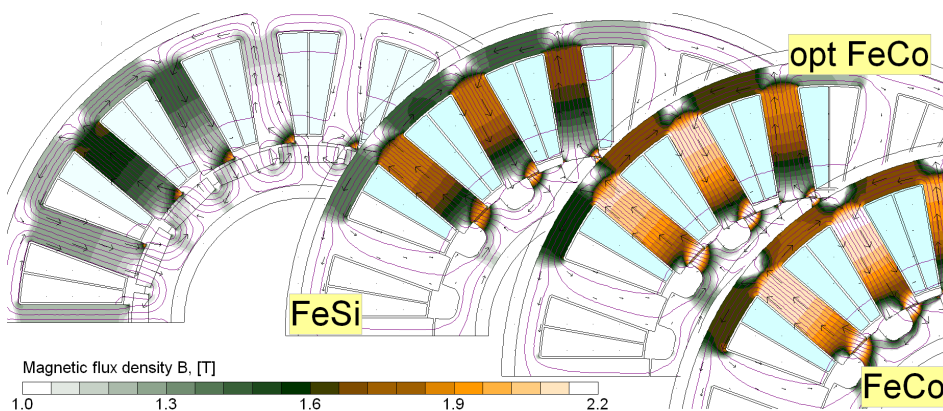


Fig. 7: Flux density distribution of 18T16P SPMsM at 150 A at two phases (left) and SRM at 300 A at single phase

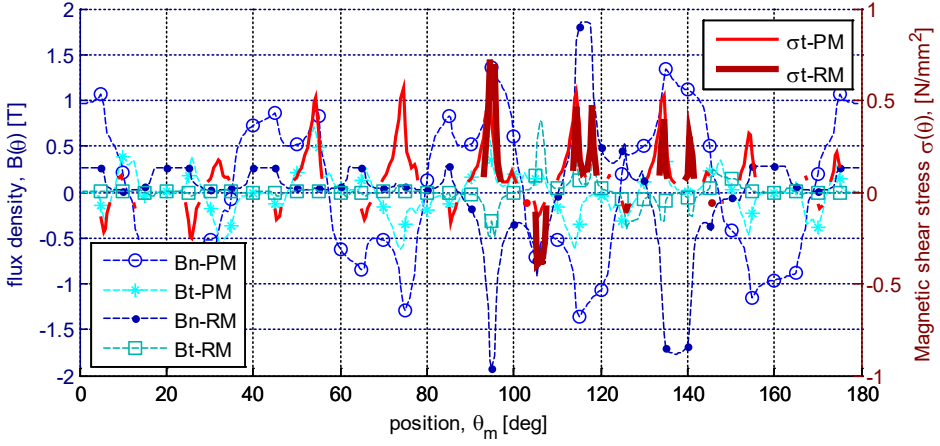


Fig. 8: Flux density distribution along the air-gap from 0 to 180 mechanical degrees and resulting tangential magnetic stress component ( $\sigma_t$ ) of 18T16P machine

The resulting torque for these machines at given position is 91 Nm and 281 Nm, respectively for SRM and SPMSM machine. The first impression is that the difference becomes larger than for the previous case. This is acceptable since if the previous machine took advantage of PM and RM excitation to maintain high speed torque then this purely surface mounted PM machine takes advantage of stator reactance for high speed operation. However, this reactance is not favor for RM counterpart and the discrepancy between the machines with different cores becomes larger. Similar to **Fig. 4**, **Fig. 8** demonstrates the significance of shear stress, which is the tangential pressure that produces torque, and which becomes thornier and less distributed in case of RM.

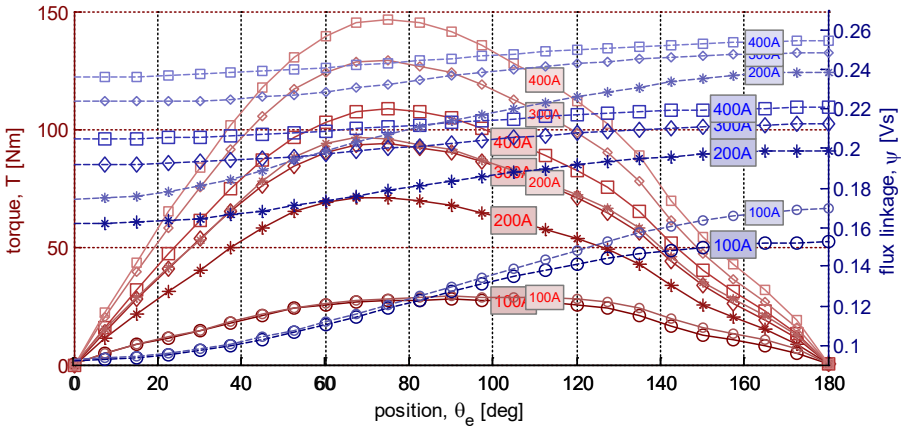


Fig. 9: Static torque characteristics of 18T16P machine at constant current



## B. Torque capability

Even if **Fig. 9** shows noticeable increase in torque when replacing FeSi material to FeCo material the improvement is insignificant to the initial machine with PM rotor (**Fig. 10**). The static torque for 18T16S RM as a function of rotor position from un-alignment to alignment is proceeded identically to previous calculation shown in **Fig. 5**.

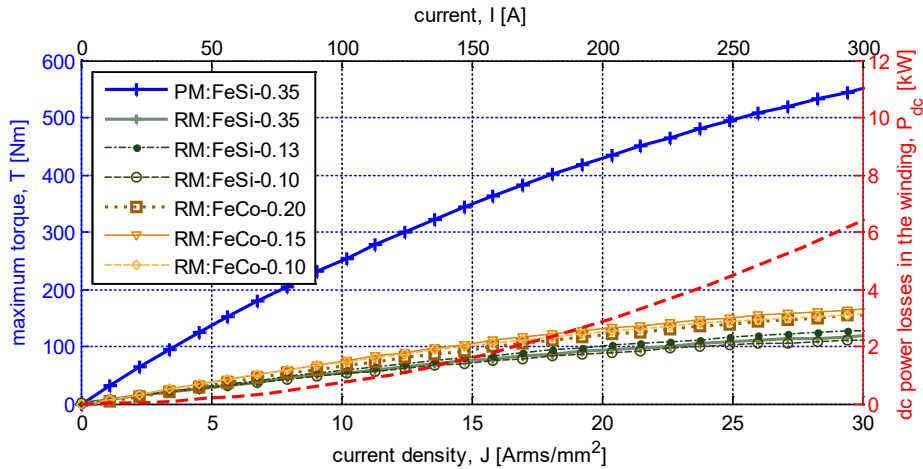


Fig. 10: Torque as function of current related to current density and power losses

**Fig. 10** reveals that simple replacement of PM rotor against RM rotor results vast loss of torque, which due to machine layout that has rather large stator reactance compared to reluctance change that the relatively small rotor is able to produce. These outcomes convince that simple replacement of machine components such as machine parts or materials when replacing the core does not provide direct revenue in machine performance.

## 3.8. Conclusions

This chapter evaluates and compares two electrical machines when replacing PM rotor with RM rotor. The comparison is rather limited and underestimates the double salient reluctance machines as the machine type is not specifically designed for the designated design space and mission. However, as the rotor replacement demonstrates of these examples the torque capability can be reduced by half or by factor 5! The latter is a machine where surface mounted magnets keep up the magnetization of the stator with distributed concentrated winding that have already a large inherent reactance for wide speed range capability. This weakness of torque capability in SRM machines is changed when considering the advantageous features of SRM drives such as wide speed range and more hazardous conditions and fault tolerant drive.



### 3.9. References

- [1] V. Madonna, P. Giangrande, M. Galea, "Electrical Power Generation in Aircraft: Review, Challenges, and Opportunities", *IEEE Transactions on Transportation Electrification*, V 4 n 3, Sep. 2018, pp.646-659
- [2] E. Richter, C. Ferreira, "Performance evaluation of a 250 kW switched reluctance starter generator", *Conf. Rec. 1995 IEEE Industry Applications*, vol. 1, pp. 434-440, 1995.
- [3] A. V. Radun, C. A. Ferreira, E. Richter, "Two-channel switched reluctance starter/generator results", *IEEE Transactions on Industry Applications*, V 34 n 5, Sep. 1998, pp.1026-1034
- [4] A. Boglietti, A. Cavagnino, A. Tenconi, S. Vaschetto, P. di Torino, "The safety critical electric machines and drives in the more electric aircraft: A survey", 2009 35th Annual Conference of IEEE Industrial Electronics, Nov 2009, pp.2587-2594
- [5] Ma Xiaohe et al., "Review of high speed electrical machines in gas turbine electrical power generation," *TENCON 2015 - 2015 IEEE Region 10 Conference*, Macao, 2015, pp. 1-9.
- [6] M. A. Mueller, "Design and performance of a 20 kW, 100 rpm, switched reluctance generator for a direct drive wind energy converter", *IEEE International Conference on Electric Machines and Drives*, 2005., May 2005, pp.56-63
- [7] Y. J. Bao, K. W. E. Cheng, X. D. Xue, J. Chan, Z. Zhang and J. K. Lin, "Research on a novel switched reluctance generator for wind power generation," 2011 4th International Conference on Power Electronics Systems and Applications, Hong Kong, 2011, pp. 1-6.
- [8] A. G. Jack, B. C. Mecrow, C. Weiner, "Switched reluctance and permanent magnet motors suitable for vehicle drives – a comparison", *IEEE*, pp. 505-507, Jul. 1999.
- [9] E. Bostanci, M. Moallen, A. Parsapour, B. Fahimi, "Opportunities and challenges of switched reluctance motor drives for electric propulsion: A comparative study", *IEEE Trans. Transportation Electrification*, vol. 3, no. 1, pp. 58-75, March 2017.
- [10] S. Li, S. Zhang, T.G. Habetler, R.G. Harley, "Modeling, design optimization, and applications of switched reluctance machines – a review", *IEEE Trans. Ind. Appl.*, vol. 55, no. 3, pp. 2660-2681, May/June 2019.
- [11] E. Ganev, "Selecting the Best Electric Machines for Electrical Power-Generation Systems: High-performance solutions for aerospace More electric architectures.," in *IEEE Electrification Magazine*, vol. 2, no. 4, pp. 13-22, Dec. 2014.
- [12] T. J. E. Miller, "Optimal design of switched reluctance motors", *IEEE Trans. Ind. Electron.*, vol. 49, no. 1, pp. 15-27, Feb. 2002.
- [13] A. G. Jack, B. C. Mecrow, J. A. Haylock, "A comparative study of permanent magnet and switched reluctance motors for high-performance fault-tolerant applications", *IEEE Trans. Ind. Appl.*, vol. 32, no. 4, pp. 889-895, Jul. 1996.

- [14] X. Y. Ma, G. J. Li, G. W. Jewell and Z. Q. Zhu, "Recent development of reluctance machines with different winding configurations, excitation methods, and machine structures", CES Transactions on Electrical Machines and Systems, V 2 n 1, March 2018, pp.82-92
- [15] P. C. Desai, M. Krishnamurthy, N. Schofield, A. Emadi, "Novel switched reluctance machine configuration with higher number of rotor pole than stator poles: Concept to implementation", IEEE Trans. Ind. Electron., vol. 57, no. 2, pp. 649-659, Oct. 2009.
- [16] X. Liu and Z. Q. Zhu, "Stator/Rotor Pole Combinations and Winding Configurations of Variable Flux Reluctance Machines", IEEE Transactions on Industry Applications, V 50 n 6, Nov 2014, pp.3675-3684
- [17] A. Reinap, M. Alaküla and G. D. Olavarria, "Direct electromagnetic actuation on high ratio gears," 2016 XXII International Conference on Electrical Machines (ICEM), Lausanne, 2016, pp. 743-749.
- [18] D. H. Cameron, J. H. Lang, S. D. Umans, "The origin and reduction of acoustic noise in doubly salient variable-reluctance motors", IEEE Trans. Ind. Appl., vol. 26, no. 6, pp. 1250-1255, Dec. 1992.
- [19] N. R. Garrigan, W. L. Soong, C. M. Stephens, A. Storace, T. A. Lipo, "Radial force characteristics of a switched reluctance machine", Proc. 34th IAS Annu. Meeting Conf. Rec. IEEE Ind. Appl. Conf., pp. 2250-2258, Oct. 1999.
- [20] A. Dorneles Callegaro and J. Liang and J. W. Jiang and B. Bilgin and A. Emadi, "Radial Force Density Analysis of Switched Reluctance Machines: The Source of Acoustic Noise", IEEE Transactions on Transportation Electrification, V 5 n 1, March 2019, pp.93-106
- [21] O. Bottauscio, G. Serra, M. Zucca, M. Chiampi, "Role of Magnetic Materials in a Novel Electrical Motogenerator for the More Electric Aircraft", IEEE Transactions on Magnetics, V 50 n 4, April 2014, pp.1-4
- [22] N. Fernando, G. Vakil, P. Arumugam, E. Amankwah, C. Gerada, S. Bozhko, "Impact of Soft Magnetic Material on Design of High-Speed Permanent-Magnet Machines", IEEE Transactions on Industrial Electronics, V 64 n 3, March 2017, pp.2415-2423
- [23] "Soft magnetic cobalt-iron alloys", Vacuumschmelze ([available online](#))
- [24] "Lamination Stacks made of VACOFLUX X1", Vacuumschmelze ([available online](#))
- [25] "Energy Savings with Thin Gauge for Motors, Generators, Transformers and Inductors", Arnold Magnetic Technologies, ([available online](#))
- [26] "Arnon thin and ultra-thin silicon iron datasheet", Arnold Magnetic Technologies, ([available online](#))
- [27] X. Y. Ma, G. J. Li, G. W. Jewell, Z. Q. Zhu, H. L. Zhan, "Performance comparison of doubly salient reluctance machine topologies supplied by sinewave currents", IEEE Trans. Ind. Electron., vol. 63, no. 7, pp. 4086-4096, Mar. 2016.

- [28] M. Olszewski, "Evaluation of the 2010 Toyota Prius hybrid synergy drive system" Oak Ridge National Laboratory, U.S. Department of energy, 2011
- [29] A. Reinap, F. J. Marquez-Fernandez, M. Alaküla, R. Deodhar and K. Mishima, "Direct Conductor Cooling in Concentrated Windings," 2018 XIII International Conference on Electrical Machines (ICEM), Alexandroupoli, 2018, pp. 2654-2660.
- [30] A. Reinap, C. Högmark, F. J. Marquez-Fernandez, M. Alaküla and M. Andersson, "Power Losses and Heat Extraction in a Stator with Directly Air-Cooled Laminated Windings," 2018 XIII International Conference on Electrical Machines (ICEM), Alexandroupoli, 2018, pp. 2675-2681.



# Variable Reluctance Motors for Automotive Applications. The Modular Construction Approach

Loránd Szabó

## 4.1. Introduction

Nowadays, the automotive industry faces significant technological changes, mainly connected to the inherent transit to hybrid and full electric cars. Beside the integration of new drivelines based on electrical machines, the electrical drive systems gain more and more importance also for the car auxiliaries, basically due to the spread of x-by-wire (XBW) systems proposed for diverse vehicle controls, as throttle, braking, steering, shifting, clutch, etc. All for these purposes advanced, low cost, high efficiency, fault tolerant electrical machines are needed, which can operate also at high temperatures [1], [2].

For such automotive applications, variable reluctance machines (VRMs) are well-fitted due to their various advantages. Their construction is very simple, robust and reliable, as they do not have in their rotor windings or cages, only possibly in some special cases permanent magnets (PMs). The passive rotor is generating low quantity of heat; therefore, the cooling is straightforward. Generally, they have high efficiency and strong overload capacity. Supplementary, they can be easily integrated in digital systems, as being driven in an advanced way by means of electronic controllers, which usually implies the need of position sensors.

As most of VRMs are PM free, they do not face the numerous problems related to the nowadays use of rare earth PMs. The demerits connected these magnetic materials are connected to their high prices, lower maximum allowable temperature and weak resistance to corrosion. Furthermore, there are several discouraging economy-related matters in relation with them, as unpredictable price due to the market monopoly of China, rapid depletion of ore reserves, etc. [3].

The VRMs have two basic configurations, the simple salient type or the double salient type. In both variants, the VRMs may have distributed, concentrated or homopolar windings, and eventually PMs placed in the stator or in the rotor.

VRMs work upon the minimum magnetic reluctance principle. Their passive salient rotor moves in such an angular position where the minimum reluctance (magnetic resistance) is achieved, i.e. when the poles on the two armatures are aligned. In this situation, the axis of the magnetic field produced in the stator will match the axis of the magnetic flux passing through the rotor. As a result, the magnetic field in the active poles and the inductance of the supplied coils are at their maximum value [4]. Another of their benefits is that they can be built up in an advantageous modular way [5], [6].

Upon the definition of the modularity, different parts of a system comprise of smaller subdivisions (modules), which can be designed and manufactured separately, and only later connected together to work as a sole unit [7]. In the case of electrical machines, the modular approach means that their main parts (the stator and the rotor) can have a segmental construction. This design not only enables easy manufacturing and maintenance, and increased efficiency, but assures in several cases also a high fault tolerance of the electrical machines [8].

The "modular motor" concept originally came out as a response to increasing safety and reliability requirements for the electrical machines. First time it was used in 1977 when a modular motor was patented by C.R. Carlson Jr. and M.J. Hillyer [9].

The chapter is a survey of the main modular VRMs. The investigation is focusing especially on the machines proposed to be used in diverse automotive applications, including the traction drive and the auxiliaries.

The greatest part of the modular VRMs which were developed upon the modular approach are switched reluctance machines (SRMs). They can have segmented stator or rotor iron core, but also several variants having both armatures modularized are cited in the literature. The survey also covers other modular VRMs, as of transverse flux type or doubly salient ones.

The final part of the chapter is an overview of the advancements brought by the iron core segmentation to the developments in the field of electrical machines.

## 4.2. Modular switched reluctance machines

Due to the simplicity of the SRMs, they can be easily constructed modularly. By the segmentation of the iron core, the magnetic flux in the machines can be increased, resulting in higher torque. Moreover, due to the optimized (shortened) flux paths, the iron core losses can be diminished.

The main challenge in designing such machines is to find an efficient way of joining together the modules in a way as to maintain the robustness of the classical construction SRMs.

### A. Variants with modular stator

In the case of modular stator type SRMs, the stator is usually made of several, C- or E-shaped electrical steel laminated segments.

C. Lee made significant efforts to reduce by 20% both the copper and iron requirements of a two-phase SRM by applying E-shaped stator iron core modules (see **Fig. 1**) [10].

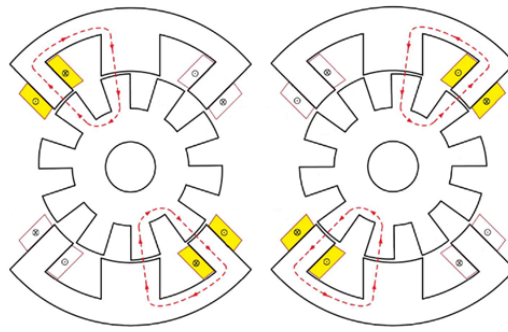


Fig. 1: Two supplying sequences of the modular two-phase SRM [10]

Each stator segment has three poles, two at its ends, with concentrated coils wound around, and one in the center, having double cross section and lacking windings. The two modules of the stator can be joined together either by prefabricated plastic molding or by a sleeve-type fixture. The SRM variant enables a very efficient use of the iron core, since the middle pole is passed thru all the time by magnetic flux, as it can be seen in the two supplying sequences shown in **Fig. 1** [10].

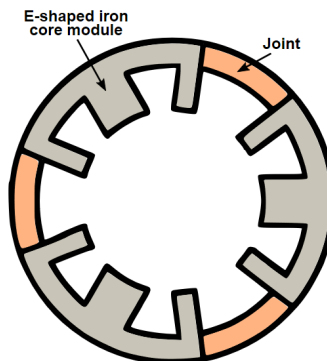


Fig. 2: 9/12 poles modular SRM [11]

The above presented structure was improved by H. Eskandari et al. by increasing the number of stator modules from two to three (as it can be seen in **Fig. 2**), mainly to increase the generated torque and the mechanical strength of the stator, and also to reduce its vibrations, an essential issue in automotive applications [11].

The segmented stator SRM can be built up also with external rotor. A such variant has 6, essentially E-shaped stator iron core modules, each with four poles, and a solid 22-poles outer rotor (as it can be seen in **Fig. 3**) [12]. It was demonstrated in the paper, that this SRM, designed for hybrid electrical vehicle applications, can produce over 20% higher torque as its classical SRM counterpart.

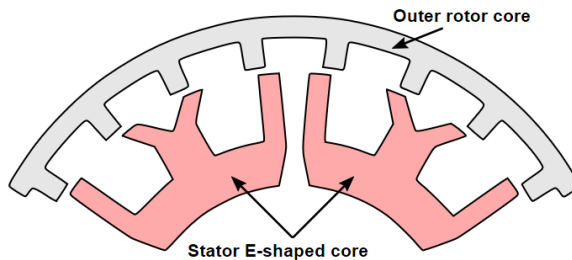


Fig. 3: Outer rotor segmented stator SRM topology [12]

A segmented stator SRM with 16 stator and 14 rotor poles given in **Fig. 4** was proposed by M. Ruba et al. [13], [14].

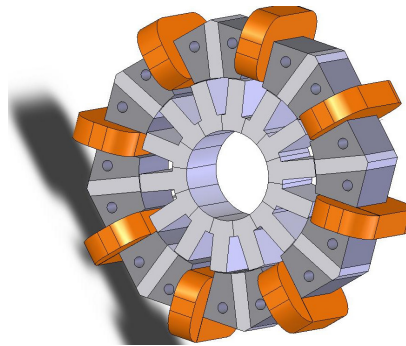


Fig. 4: The segmented stator SRM [13]

Its stator is built up of 8 U-shaped iron core modules, as that in **Fig. 5**. The coil is wound round the yoke. Two adjacent modules are separated by a non-magnetic spacer, which both assure the adequate shift of the modules, and a good magnetic separation. The rotor is a usual salient pole passive one.



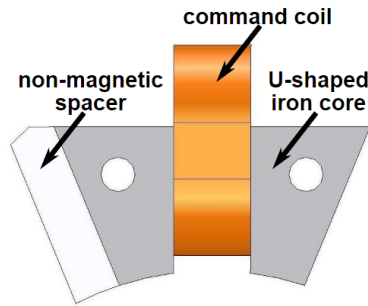


Fig. 5: A stator segment of the SRM given Fig. 4

The main advantages of this SRM developed for automotive applications are the easy and cheap manufacturing, high fault tolerance [15], less iron losses, and the opportunity of a fast on-site replacement of a damaged module in case of a coil failure.

### B. Segmental rotor approach

Several SRMs were developed with modular rotors. One of the first such constructions was patented by G.E. Horst [16]. The rotor of this two-phase unidirectional SRM is built up of independent iron core segments, as it can be seen in **Fig. 6**. The main advantage of this SRM variant is its great torque density.

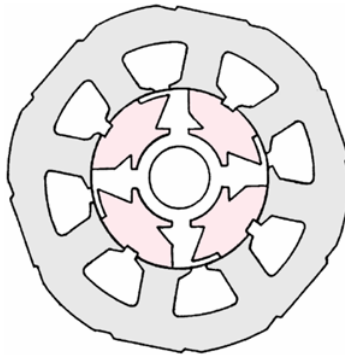


Fig. 6: The iron cores of a segmental rotor [16]

A newer, three-phase variant of the modular rotor SRM was proposed by D.C. Mecrow (see **Fig. 7**). The 8 rotor modules are attached to a non-magnetic steel shaft, which disables the circulation of the magnetic flux between the modules. The rotor segments require both circumferential location and retention against axial and radial forces, which is a common shortcoming of the segmental rotor constructions [17].

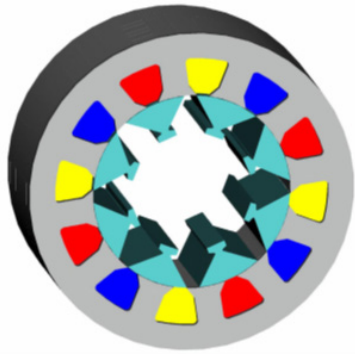


Fig. 7: Segmented rotor SRM [17]

This 12/8 poles SRM variant, as most of the modular rotor variants, has an important advantage over the classical design, that the flux path through the rotor is short. Each magnetic flux path only encloses a single stator slot, as it can be seen in **Fig. 8**. Thus, lower iron losses were achieved.

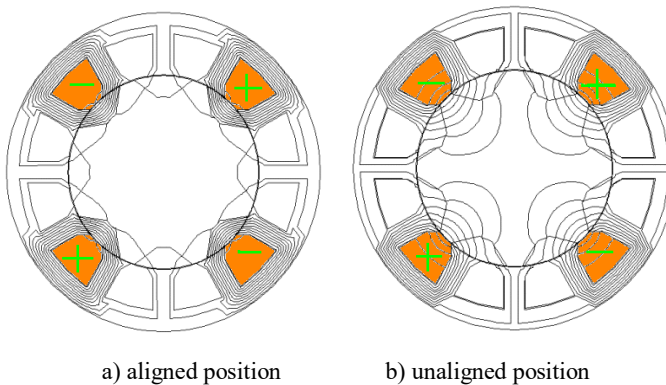


Fig. 8: Flux lines in the segmental rotor SRM [17]

In [17] the authors compared the SRM given in **Fig. 8** with both the axially laminated and the usual salient pole design. It was shown that higher torque per unit magnetic loading can be produced with the modular variant due to its better magnetic utilization. When one phase is supplied, 8 of the 12 stator poles are active (as compared with 4 in the case of a classical SRM). Hence the motor carries much more magnetic flux, more torque is generated.

J.D. Widmer et al. demonstrated in [18] that segmented rotor SRMs construction having a greater number of rotor segments than stator poles can lead to substantial performance increasing, mainly at low speeds and current densities. In the paper

also, useful relationships are given for the optimal calculation of the basic stator pole per rotor segment combinations, both for the SRM variants with fully-pitched and single-tooth windings.

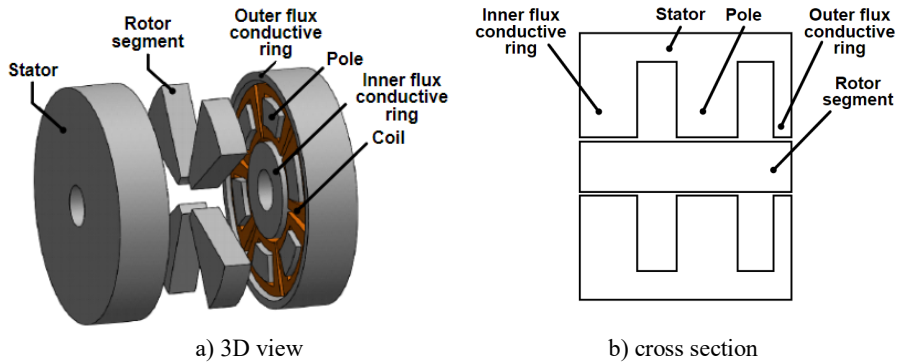


Fig. 9: Modular rotor axial flux SRM [19]

Also, the axial flux SRMs were developed with segmented rotor. Diverse such constructions are cited in the literature. An interesting variant was proposed by W. Sun et al. It has a closed cylindric construction [19]. The basis of both twin-stators, as it can be seen in **Fig. 9**, is an iron core disc having 6 poles on it. Each pole has a concentrated coil wound around. The magnetic fluxes generated are directed from one stator to another via the rotor by means of two conducting rings, one in the exterior of the stator and another in its interior. The rotor of the SRM comprises of 4 pie-shape cross section, equally shifted iron core segments. Due to this compact construction the SRM is very robust, its coils being totally enclosed inside the machine. Thus, they are well-protected, but their extra heating can be expected, too

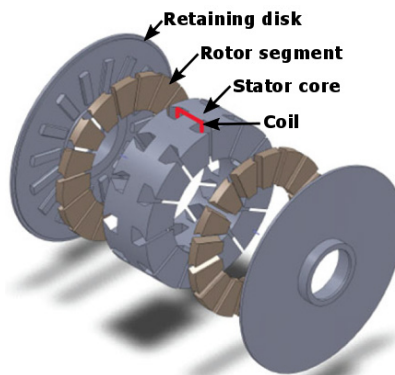


Fig. 10: Inner stator modular axial flux SRM [20]

A modular axial flux SRM with interior stator was proposed by R. Madhavan et al. As it can be seen in **Fig. 10**, the stator of the machine has poles on both of its faces, and the axis of the toroidal windings located on it are on the radial direction. The machine is closed on its both ends by two retaining disks. On the shaft, between these disks and the inner stator, are placed the two rotors comprising of a non-magnetic disc having embedded simple rotor iron core segments [20].

If the rotor segments of the axial flux SRM are fully inserted inside the non-magnetic material, high-speed applications are enabled. A simple such SRM with a single stator is proposed in [21]. Another specially constructed axial flux SRM variant was developed especially for automotive traction applications [22].

### C. Doubly segmented construction

A doubly segmented SRM, having both segmented stator and rotor, was proposed by M. Diko et al. (see it in **Fig. 11**) [23]. Its stator comprises of E-shaped modules with a concentrated coil on their yoke, like that given in **Fig. 5**. The rotor has segments as the SRM in **Fig. 7**.

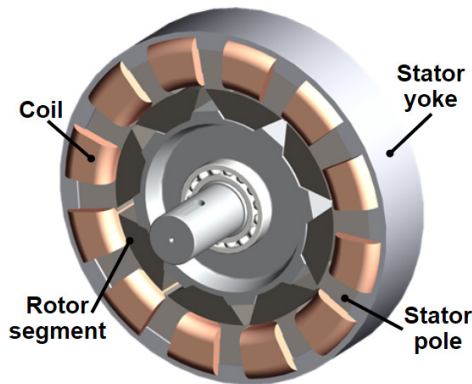


Fig. 11: Doubly segmented SRM [23]

The three-phase machine has a 12/8 poles structure. It is water-cooled by means of a spiral and is proposed to be used in an electric mini truck. It has very short magnetic flux paths and increased fault tolerance.

In [24] X. Xue et al. proposed an axial flux SRM segmented on both armatures, having a yokeless rotor (see it in **Fig. 12**). Its stator is built up of 8 C-shaped modules, each having two coils. The 10 rotor poles are connected to the shaft by simple support branches. Thus, the rotor had low mass and inertia, being well-suited for applications requiring good dynamic behavior, as also some of the automotive applications.

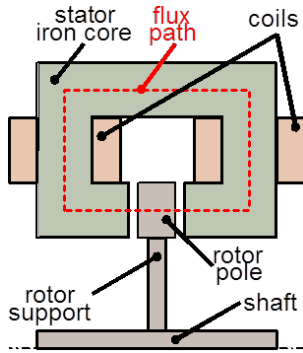


Fig. 12: Doubly segmented yokeless rotor SRM [24]

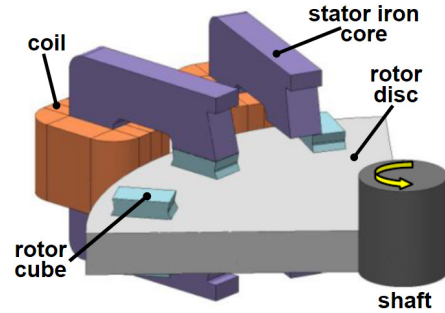


Fig. 13: The pancake shaped doubly modular SRM [25]

A. Labak and N.C. Kar developed a similar, but axial flux SRM. Its stator comprises of 16 C shaped iron core modules, each having a concentrated winding on it. The active parts of the rotor are the so-called cubes, embedded in an aluminum disc having the shaft in its middle, as it can be seen in **Fig. 13**. Due to its optimized flux paths, it has high efficiency, and thus it is proposed for electrical vehicle powertrain applications [25].

A very compact in wheel axial-flux segmented SRM was proposed by the research team lead by P. Andrada (see **Fig. 14**) [25].

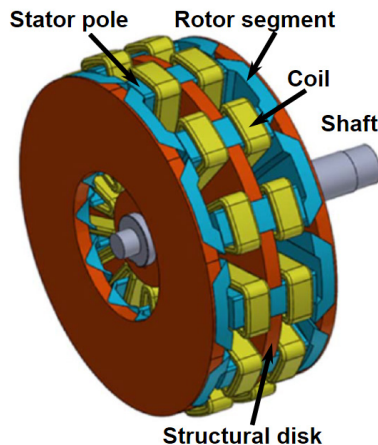


Fig. 14: The in wheel segmented rotor axial SRM [26]

As it can be seen in the figure, the stator is made of wedge-shaped iron core modules with concentrated coils wound round them. The segments are kept together

by a non-magnetic structural disk. The stator is sandwiched by two specially segmented rotors, also placed on non-magnetic support plates. The iron core segments are made of soft magnetic composite (SMC). The SRM has very short magnetic flux paths without flux reversal. It was particularly developed to direct drive light scooters or motorcycles.

An axial flux doubly segmented SRM was also developed by Z. Pan et al. [27]. Each of the 12 C-shaped stator modules, placed directly on the housing, have two together connected coils. The rotor comprises of 8 equally shifted active segment, as it can be seen in **Fig. 15**. The highly compact machine has good efficiency due to the low iron and copper losses.

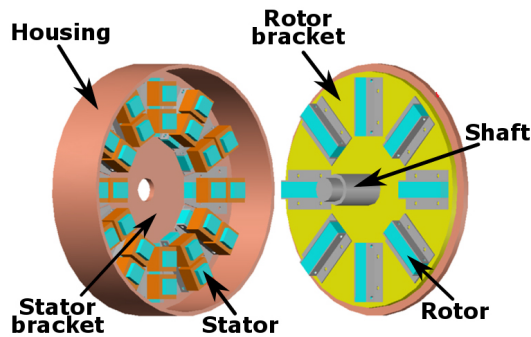


Fig. 15: Doubly segmented axial SRM [27]

Researchers at University of Oxford developed a two-phase, axial flux, high speed SRM with modular stator and twin segmented rotor [28]. The stator modules are of wedge-shape, and each one has wound round a concentrated coil. The segmental rotor is given in **Fig. 16**. All its iron core segments are made of SMC. As the machine can achieve high speed, it can be applied in hybrid electrical sport car traction application.

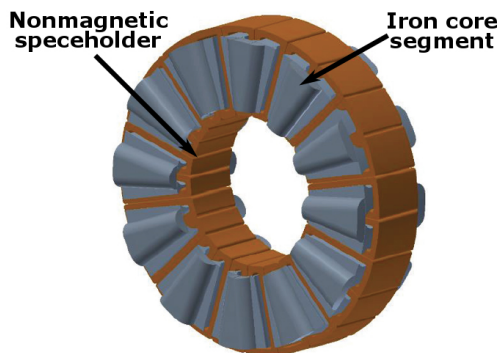


Fig. 16: The rotor of the high-speed axial flux doubly segmented SRM [28]

More complicated, having a lot of extra iron core, but probably more robust, is the SRM variant proposed by W. Ding in [29]. This axial flux doubly segmented SRM is a further development of that presented in [30], which had simpler E-shaped stator iron core modules. The SRM given in **Fig. 17** has 6 E-shaped stator segments, each with 2 concentrated coils wound on its yoke. The rotor is also segmented in a similar way as the stator, as the poles cross section concerns (the middle pole has double cross section area as those at the ends). In the paper, the proposed SRM was compared with a classical construction SRM and with a similar axial flux segmented stator variant but having non-segmented rotor. All of them had the same external diameter and axial length. The variant in discussion had the lowest iron mass, the highest torque, and the greatest power and torque density [29]. Therefore, it can be a very good competitor for the electrical machines used in automotive applications.

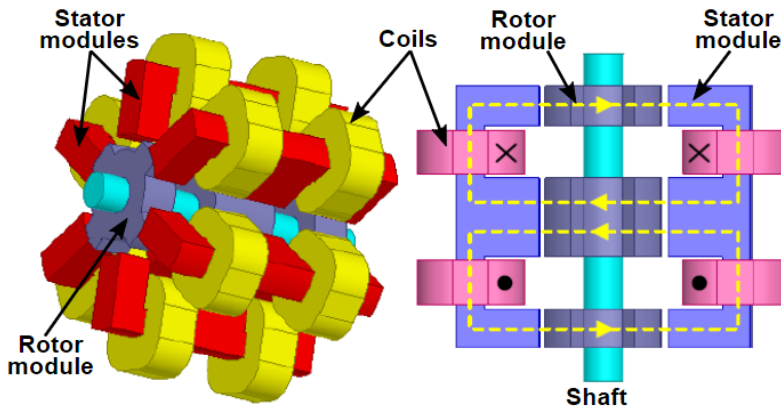


Fig. 17: The axial flux doubly segmented SRM [29]

This machine, as also that proposed in [30], can be extended on the axial direction by adding more poles or modules to fit the SRM to any power requirement.

#### D. Multilayer SRMs

Upon another approach, first proposed by E.S. Afjei et al., the segmentation of the SRM can be performed on the axial direction [31]. The suggested multilayer SRM has three magnetically independent modules (phases, or so-called layers), each of them being similar to a classical SRM. A specific feature is that the machine has identical number of poles (eight) on both armatures. All the coils on a module are connected together and form a phase of the machine. The rotor modules are shifted by  $15^\circ$  relatively to the neighbored modules (as it can be seen in **Fig. 18**).

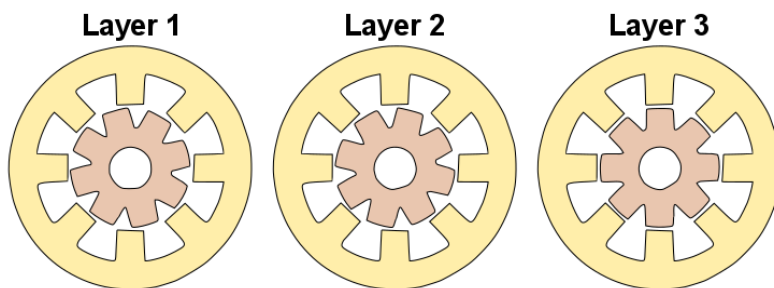


Fig. 18: The iron cores of the three-layer SRM

The torque ripple of the machine is significantly reduced due to the same effect as in the case of skewed rotor EMs [32]. Supplementary, due to the achieved phase independency, in its control larger phase advancements can be imposed, which are enabling a faster phase current rise up, an important issue in high-speed automotive applications.

Upon this approach, A. Salimi et al. developed a four-layer SRM [33]. Its stators are placed in line, while the rotor ones are shifted by  $11.25^\circ$ , as it can be observed in **Fig. 19**.

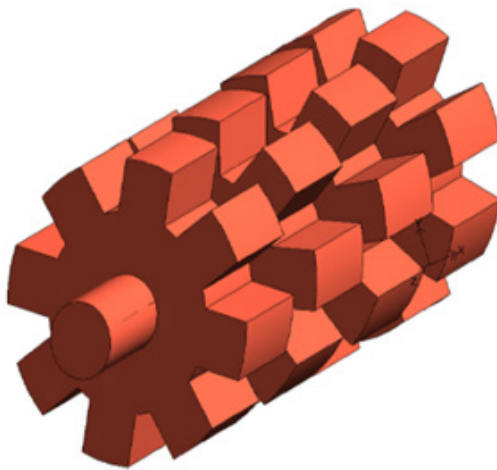


Fig. 19: The rotor of the four layers SRM [33]

In [34] a similar 3-phase, 7-layer SRM is proposed. Each 6-poles stator layers are also placed un-shifted, while the seven 4-poles rotor layers are shifted by  $12.7^\circ$ . Due to the great number of modules of this construction, at the same time three layers are active (having supplied coils).



### E. Hybrid modular SRMs

In the literature, there are several proposals to improve the performances of SRMs by inserting PMs, mainly in their stators. The hybrid SRMs having stator modules containing both coil and PM are combining the advantages of the PM excitation and the simplicity of the VRMs construction.

One of the simplest ways to perform this was by replacing the non-magnetic spacers from the modular SRM given in **Fig. 5** with ceramic PMs, as shown in **Fig. 20**.

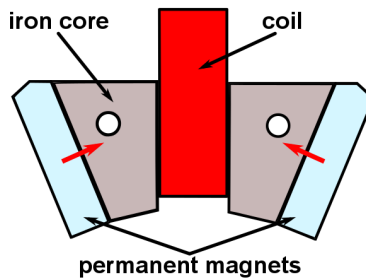


Fig. 20: The placement and magnetization of PMs [35]

As it can be seen in the figure, the PMs are magnetized alternatively, the magnetization direction being perpendicular to their face in contact with the poles of the stator segment. In [35] it was concluded, that the obtained mean torque of this SRM is greater by near 27% as in the case of the modular SRM considered as starting point (see **Fig. 4**). Unfortunately, also the torque ripples intensified with near 25% [35].

The stator segments in the hybrid SRM developed by P. Andrada et al. are containing two series connected concentrated coils wound round the poles and a PM between the pole legs, as it can be seen in **Fig. 21** [36]. The rotor of this SRM is a usual passive one.

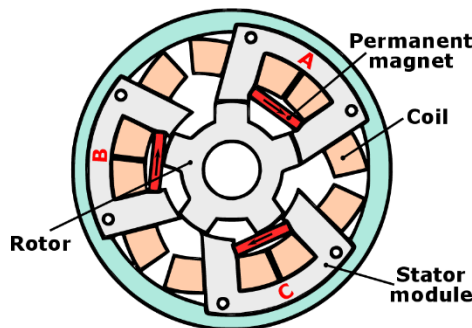


Fig. 21: The modular stator hybrid SRM [36]

The working principle can be understood from **Fig. 22**. When rotor poles are totally aligned with the poles of a stator module (as in the case of module A in **Fig. 16**), the magnetic flux generated by the PM is passing thru both the iron core and the rotor. When the rotor poles are in an un-aligned position, only a very small amount of the PM flux can pass thru the rotor due to the great magnetic reluctance. The magnetic flux generated by the coils can control the distribution of the PM flux in a way to put in movement the SRM.

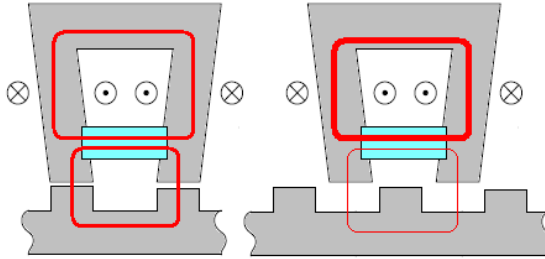


Fig. 22: Flux distribution in a modular stator hybrid SRM

Similar hybrid SRMs were also proposed by Ding et al. [37], [38].

Hybrid SRMs, beside their increased fault tolerance, have higher efficiency due to its PMs, and can be rated at higher power than conventional SRMs of the same size. Despite the PMs in their structure, such electrical machines lack cogging torque due to the placement of the PMs. All these make them attractive also for automotive applications [36].

### 4.3. Modular synchronous reluctance machines.

The synchronous reluctance machine (SyncRel) seem to be the most accepted VRM both by the manufacturers and users. Several companies (as ABB and Siemens) are series manufacturing such machines in a wide range of power. Their popularity is due to their numerous advantages, mostly common to all the VRMs, as cheap construction, high efficiency, good dynamics, low maintenance costs, etc. Therefore, several of their developments are targeting the automotive applications, too [39].

The stator of the SyncRel is identical with that of any usual three-phase a.c. machines. Therefore, the stator segmentation approaches used in the case of the PM synchronous machines (PMSMs) can be also applied for them.

A typical stator modularization of a three-phase a.c. machine (concretely proposed for a PMSM) is given in **Fig. 23** [40].

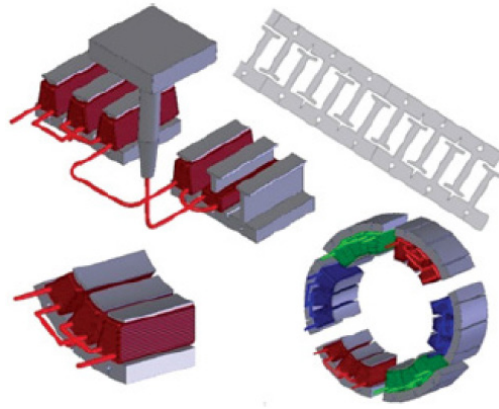


Fig. 23: Stator modules with concentrated windings of an a.c. machine [40]

The stator iron core is designed in a way as to minimize the scrap of laminated steel material, and to obtain large tooth width and small tooth tips. Three teeth with the concentrated coils around them comprise a module. By using six such modules a three phase 18-slot stator can be assembled. This segmented stator construction has diverse advantages, as that the concentrated windings are rigidly packed with a high slot fill factor. Supplementary, these a.c. windings have short end-coils, which makes them superior to the common distributed windings [40].

SyncRel stators can be also made of salient pole segments of one pole pitch length, having around non-overlapping fractional slot windings with significant fill factor and short end windings, as it is shown in **Fig. 24** [41]. This design contributes to an increased power density and efficiency, strongly compulsory in all the automotive applications.

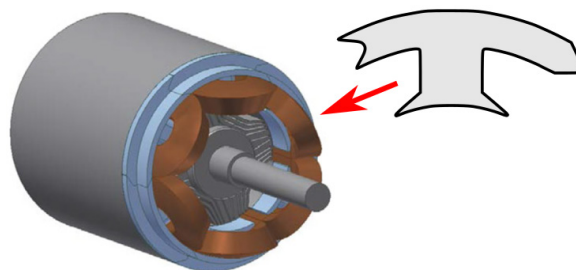


Fig. 24: Modular stator SyncRel [41]

The salient poles of the SyncRel, shown in **Fig. 25**, can be also made of SMC [42]

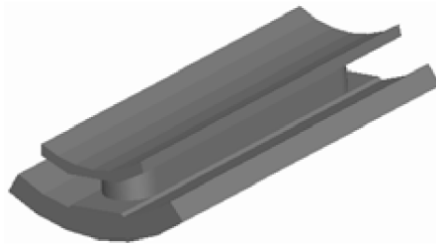


Fig. 25: Stator module made of SMC [42]

Since on each module a simple concentrated winding can be placed, its manufacturing is quite simple. This modular construction approach permits a high flexibility in phase number and control strategy selection, too. Due to the flexible SMC technology, special pole shoe and yoke shape designs can be applied. Also, a very good air-gap space usage can be achieved, which can lead to a high torque density, a basic requirement in automotive applications.

In the most widely spread variants of the SyncRels the laminations made rotor is passive and have a strong distributed anisotropy due to flux barriers and bridges, which must have optimized shapes for achieving high performances [4]. Even if their rotor is the most sensitive part from mechanical point of view, there are some developments considering the modular approach for them. As S. Taghavi and P. Pillay proposed in [43], the SyncRel rotor is comprising of single-pole laminations particularly bonded together as to have an adequate mechanical strength. The segments of the machine are asymmetrically designed, since the two sideway arms of the module do not have the same thickness (as it can be seen in **Fig. 26**). As a consequence of the overlapping neighbored layers, this design allows a strong lamination bonding.

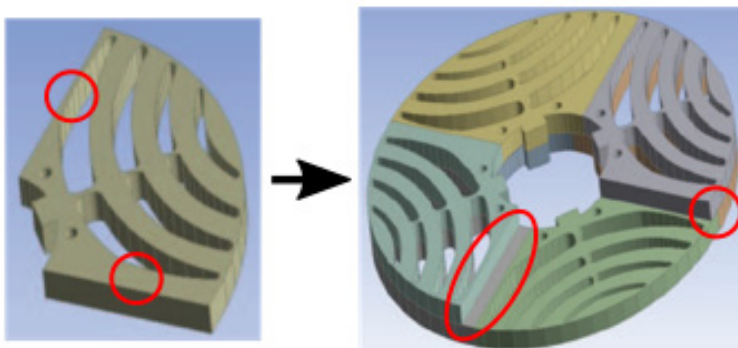


Fig. 26: Segmented rotor SyncRel [43]

#### 4.4. Other modular variable reluctance machines

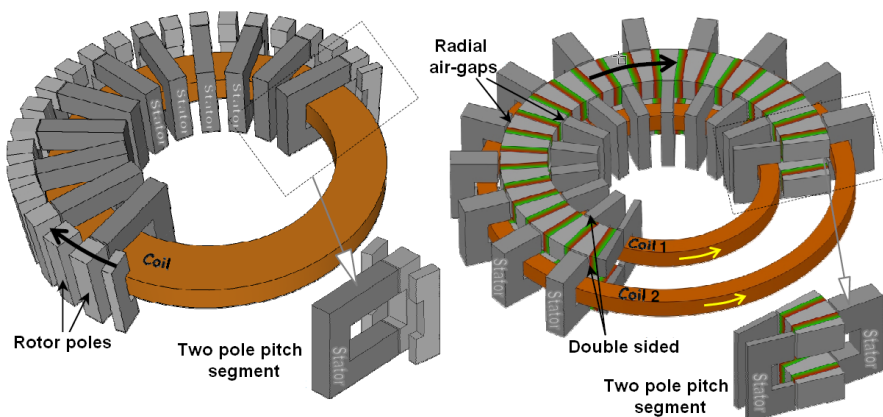
Several other VRMs must or can be built upon the modular construction approach. Next some such machines are taken into survey.

##### A. Transverse flux electrical machines

The basic features of the transverse flux machines (TFMs) are radically differing from those of usual electrical machines, due to the transverse direction of their flux paths and the homopolar magnetomotive force (mmf) generated by their ring-type coils. One of the major advantages of these machines is the high torque density. Supplementary, despite of their complicated construction and low power factor, the number of poles can be increased and meanwhile the synchronous speed diminished without reducing the mmf per pole [44]. All these features make the TFM a promising candidate for automotive (especially in-wheel) applications.

Fundamentally, these machines due to their complex three-dimensional magnetic flux path, can be constructed only upon the modular approach [45]. Usually their iron core segments are made of SMCs and are embedded in light non-magnetic materials, as glass or carbon fibre reinforced plastics, consequently reducing the overall mass of the machine and improving its dynamics [46].

The simplest TFMs, without any PMs, are of reluctance type, having less power density as those with PMs [47]. A typical such variant is given in **Fig. 27a**. The machine has U-shaped stator iron core segments, with the two poles of each module in the same plane. In the figure the ring-type armature winding, the segmented passive rotor, and the zoom of two pole pitch length segments can be easily observed, too.



a) reluctance type TFM

b) flux concentrating PM TFM

Fig. 27: Two modular TFM variants [48]

An example of the more typical, flux concentrating PM TFMs is shown in **Fig. 27b**. A phase of an armature winding is comprising of two ring-shape coils per phase. The armature flux direction has to be in accordance with the PM magnetic flux sense. Therefore, the two coils of the same phase are connected in series in a way as to have their magnetic fluxes added.

In both cases, for a three-phase TFM three correctly shifted units must be attached to a common shaft.

### B. Modular doubly salient variable reluctance machines

The double salient PM machines (DSPMMs) have salient poles on their both armatures. On their stator, beside the windings, also PMs are placed to improve their performances. Their rotors are usually passive, like those of the SRMs. DSPMM combine the advantages of the everlastingly available PM excitation and the simplicity of the VRM structures.

One of its most typical variants is the flux switching machine (FSM) shown in **Fig. 28**. The stator of the machine comprises of U-shaped iron core modules separated by alternatively magnetized PMs. The concentrated coils are placed around one leg of two adjacent modules and the PM placed between them [49].

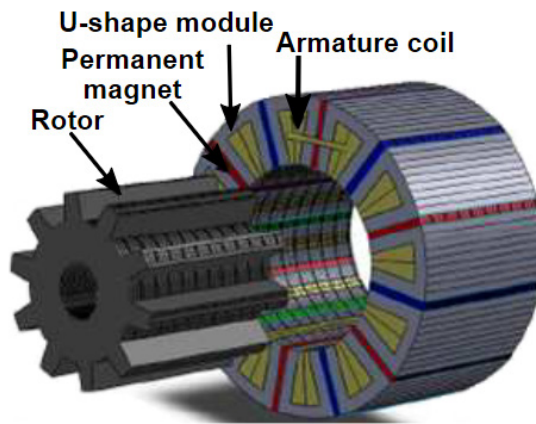


Fig. 28: Flux switching machine [49]

The FSM owns the advantages of the robustness and of having both mmf sources, the windings and the PMs, on its stator. Due to its very good magnetic flux concentration capability, the FSM can achieve high torque density. In addition, it has a passive, robust and easy to cool rotor [4].

Inappropriately, the high flux concentration and power density of the FSMs is supplemented by high iron core losses. These can be diminished without significant output torque decrease by segmenting also its rotor, as it was proposed by A. Thomas et al. in [50]. As it is shown in **Fig. 29**, the rotor modules are lamination stacks separated by flux barriers, made of non-magnetic material.

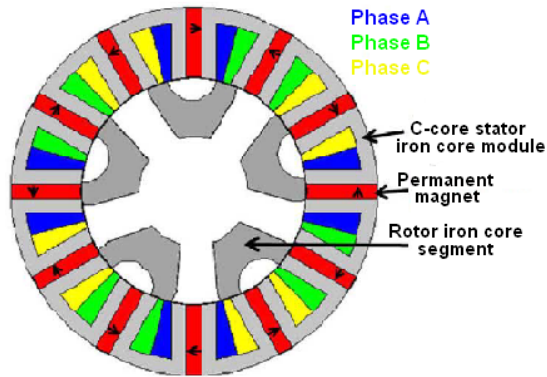


Fig. 29: Segmented rotor FSM [50]

The effect of the segmented rotor on the magnetic field distribution in FSM can be clearly seen in **Fig. 30**. If the rotor is segmented, the flux lines passing it are a little bit shorter than in the case of unsegmented rotor. As a consequence, better flux concentration and less iron core losses are achieved. Meanwhile, also the volume of the iron core is diminished.

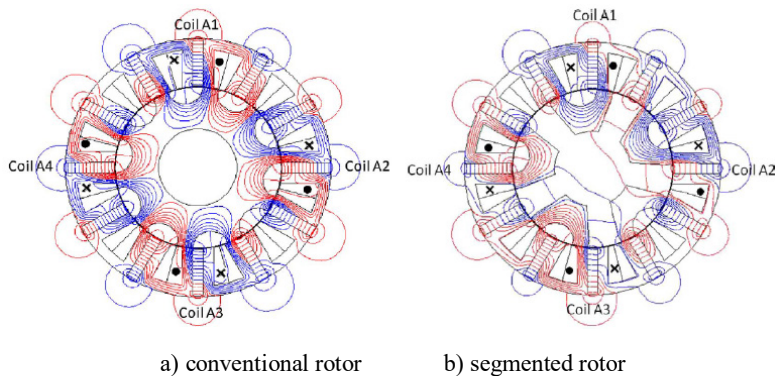


Fig. 30: Magnetic flux distribution in FSMs [50]

The FSMs can be also designed with an increased number of phases for better fault tolerance. These can be a promising candidate in safety-critical applications, as also the automotive ones [51].



In a similar way also other DSPMMs, as the flux reversal (FR) PM machines can be built up with segmented stators [52].

#### 4.5. Advancements in electrical machines brought by the modular approach

The developments of the modular construction of the electrical machines resulted in several enhancements in the field. Advancements had been achieved in the design, manufacturing, maintenance, efficiency and fault tolerance increase, etc. [6].

##### A. Design related advances

The modular approach permits an increased flexibility for the electrical machine designers. For example, more complex and efficient, even three-dimensional, magnetic flux paths can be applied. Consequently, the designers can easier shape the machines under development for any specific requirement imposed by the automotive applications.

The segmented iron core electrical machines, due to their optimized design, have iron core only where the magnetic flux must be directed. Therefore, significant iron core savings can be achieved, and as a result the machines will have less iron core losses.

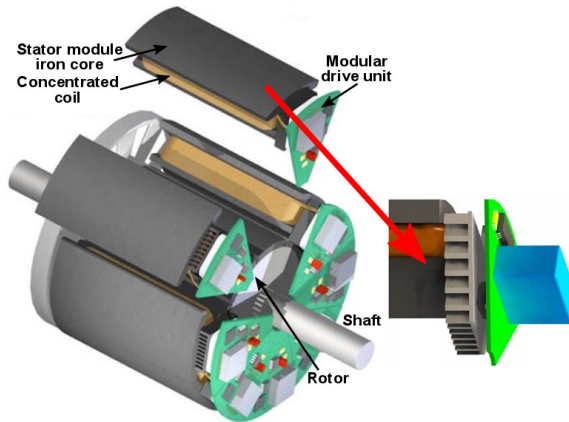


Fig. 31: The integrated modular motor drive (IMMD) concept [53]

The segmentally constructed electrical machines can be easily combined with similarly modular drive circuits. Upon the idea of N.R. Brown et al., within the so-called integrated modular motor drive (IMMD) concept (given in **Fig. 31**), the modules of the electrical machine and of the power converter can be integrated together into a single unit to increase the compactness and easy reparability of the machine-converter assembly [53].



## B. Advantages Connected to Manufacturing and Maintenance.

The segmented iron cores can be manufactured of bonded, ready to wound lamination stacks. This technology has various advantages, as high dimensional precision, great mechanical stiffness (which is permitting easy handling and further machining if required), very good electrical insulation between the laminations without any short cuts, no cushioning, less liquid absorption, etc. [54]. Supplementary, the stamping tools required by the manufacturing process are smaller and simpler, and accordingly they are much inexpensive.

By the iron core modularization, the magnetic material consumption is intensely decreased. The stator or rotor laminations are not stamped as one piece but divided into smaller segments. These modules can be stamped optimally from the raw material strip to reduce material losses (scraps), as in the example shown in **Fig. 32** [55].

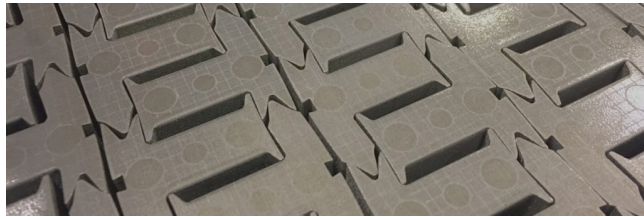


Fig. 32: The placement of iron core modules on the raw material strip [55]

Upon the modular iron core construction approach, the innovative bonding varnish technology can be applied for the efficient interconnection of the laminations. In contrast with the traditional technology of interlocking, this permits an easy to automate manufacturing of mechanically stiff iron core parts, made of evenly insulated sheets, as the poles of the electrical machines. Iron core segments produced by means of this technology can be seen in **Fig. 33** [56].

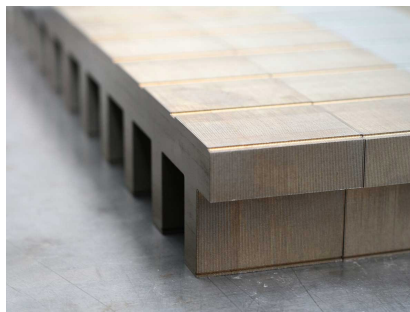


Fig. 33: Iron core modules manufactured via the bonding varnish technology [56]

As the iron core laminations of the stator and rotor can be manufactured separately, this technology also enables the fabrication of iron core stacks of the two armatures from different raw materials, if different properties, as mechanical strength, magnetizability, permeability, etc. are required for them [57].

The iron core modules can be also made of SMCs, which are ferromagnetic powder particles embedded in an insulating film coating [58]. Such modules can be formed of any three-dimensional shape and have very low eddy current losses [42], [58]. The net shape fabrication approach (for example the uniaxial pressing) can also lead to very low tolerances, and the material waste during manufacture is minimal. Due to the use of precisely fabricated iron core pieces, the air-gap length can be optimized, resulting in high torque density.

Iron cores made of SMC materials are very suitable mainly for the electrical machines working at high speeds [59]. As a wide range of SMCs are available on the market, the designers can select the most appropriate material for the given application, which can provide magnetic performances comparable to, or even surpassing that of the classical laminated sheets.

The segmentation of the iron cores is frequently in conjunction with the use of concentrated (non-overlapping) windings. The main reason is that they have shorter end winding as that of the distributed windings (see **Fig. 34**), thus enabling increased active length for the machine, in the case of automotive applications where often axial size limitations are imposed, as it can be. This way they are contributing to an increase of the power density of the electrical machine. It must be also mentioned, that concentrated windings also facilitate higher winding and filling factor [60].

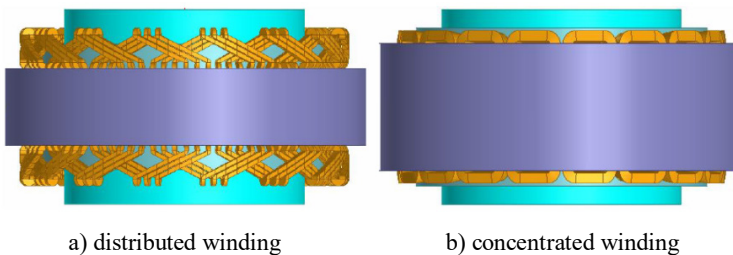


Fig. 34: Distributed vs. concentrated windings [60]

Another advantage of the non-overlapping windings is their straightforward manufacturing, which facilitates cheap high-series production. This advantage is multiplied by the simple winding of independent modules, as compared with that of non-segmented iron cores, due to the greater place having at disposal of the winding nozzle during winding, as it is shown in **Fig. 35** [61].

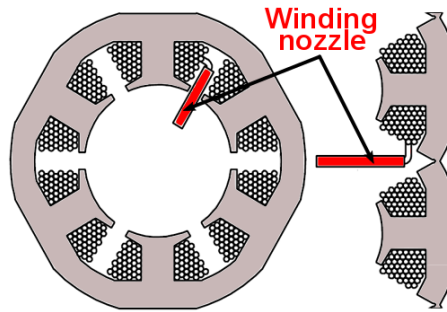


Fig. 35: Concentrated coils winding for different iron cores [61]

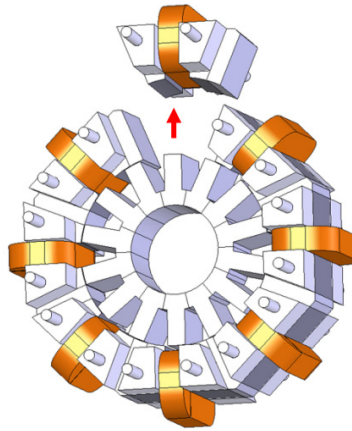


Fig. 36: Simple replacement of a faulted segment in a modular SRM [14]

The piece by piece assembly of the modular electrical machines also implies an easier maintenance. The short-circuited or opened coils can be more straightforwardly detected and replaced together with the iron core module round which are wound, as it can be seen in **Fig. 36**. In some cases, this can be performed without demounting the machine from the floor or pedestal [13].

The modular construction also facilitates a straightforward decommissioning and recycling due to the rapid and easy disassembly of the modular parts.

### C. Increased efficiency and lifetime.

As it was stated already, the iron cores segments of the modular electrical machines are designed in a way to have iron core only just where it is needed for optimally guiding the magnetic flux. This leads to an iron core mass and volume

reduction, which is beneficial for the power density increase. Supplementary, the optimized flux paths are much shorter than those in the classical variants of the electrical machines, resulting in diminished iron core losses.

Due to their shorter end windings, the concentrated windings contain less copper, and thus they have also less Joule losses. In addition, these windings are not so strongly surrounded by the iron core as the distributed ones, enabling this way an easier cooling. All these together contribute to the increase of efficiency. In addition, less heat is generated due to the smaller amount of losses, and the better cooling of the machine leads to an increased lifetime. These both are basic requirements in automotive applications.

#### D. Improved fault tolerance

One of the main advantages of the modular approach in the field of electrical machines is the opportunity to increase their fault tolerance, a decisive issue in safety and operationally critical applications, as those in automotive [62].

In most of the cases, one phase of the electrical machine comprises of one or more independent modules. Consequently, the operation of a phase has an insignificant influence on the other ones. If it is faulted, the other ones can continue to work in an unaltered way. The phase separation can be beneficially extended also to the power converter of the electrical machine [63], [64].

The iron core segmentation also makes easier the phase number increase of the electrical machines. As they have more phases, a fault of a single phase has less influence on the proper working of the machine. The phase separation can be best observed in the case of the modular SRMs. Their phases are inherently well-insulated, mainly because of the very small magnetic coupling between the stator coils [65]. By the SRM iron core segmentation the phase separation gets better [14].

#### E. Drawbacks of segmentation.

Unfortunately, the electrical machine segmentation has also some weaknesses. These mainly are due to rigidity issues resulted from replacing a single, stiff body by a structure made of more pieces. In many cases non-magnetic extra parts are needed to link the separate modules. This can cause extra technological problems and costs.

Because of the great electromagnetic forces acting on the less rigid iron core segments, a bending of the teeth or poles takes place (see **Fig. 37**).

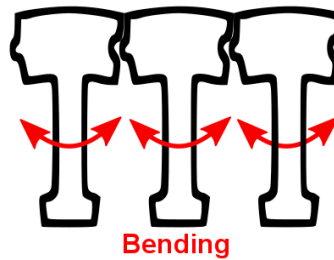


Fig. 37: Bending of the teeth in the case of a modular stator

The unsuppressed axial and radial forces can result in vibrations and noises, totally annoying phenomena in all the automotive many applications.

#### 4.6. Acknowledgement

This chapter was supported by the project "Advanced technologies for intelligent urban electric vehicles – URBIVEL - Contract no. 11/01.09.2016", project co-funded from the European Regional Development Fund through the Competitiveness Operational Program 2014-2020.

#### 4.7. References

- [1] K. Akatsu, N. Matsui, "New trend of motor technology for automobiles-Introduction and overview," in Proceedings of the ECCE Asia Downunder (ECCE Asia '2013), Melbourne (Australia), 2013, pp. 130-135.
- [2] Y. Kano, Y. Inoue, M. Sanada, "Current specifications of vehicle motors," in Proceedings of the ECCE Asia Downunder (ECCE Asia '2013), Melbourne (Australia), 2013, pp. 136-140.
- [3] I. Boldea, L.N. Tutelea, L. Parsa, D. Dorrell, "Automotive electric propulsion systems with reduced or no permanent magnets: An overview," IEEE Transactions on Industrial Electronics, vol. 61, no. 10, pp. 5696-5711, 2014.
- [4] G. Henneberger, I.A. Viorel, Variable Reluctance Electrical Machines. Aachen (Germany): Shaker Verlag, 2001.
- [5] L. Szabó, "A Survey on modular variable reluctance generators for small wind turbines," IEEE Transactions on Industry Applications, vol. 55, no. 3, pp. 2548-2557, 2019.
- [6] L. Szabó, "Novel variable reluctance generators used in small wind turbines. The modular approach," in Proceedings of the 19<sup>th</sup> International Carpathian Control Conference (ICCC '2018), Szilvásvárad (Hungary), 2018.

- [7] C.Y. Baldwin, K.B. Clark, *Design rules: The power of modularity*. Cambridge (USA): MIT Press, 2000.
- [8] I. Benția, M. Ruba, L. Szabó, "Modular electrical machines – A survey," in *Proceedings of the International Scientific Conference MicroCAD '2010*, Miskolc (Hungary), 2010, pp. 87-92.
- [9] C.R. Carison Jr, M.J. Hillyer, "Modular motor," US 4056749 A patent, 1977.
- [10] C. Lee, R. Krishnan, N. Lobo, "Novel two-phase switched reluctance machine using common-pole E-core structure: concept, analysis, and experimental verification," *IEEE Transactions on Industry Applications*, vol. 45, no. 2, pp. 703-711, 2009.
- [11] H. Eskandari, M. Mirsalim, "An improved 9/12 two-phase E-core switched reluctance machine," *IEEE Transactions on Energy Conversion*, vol. 28, no. 4, pp. 951-958, 2013.
- [12] S.R. Mousavi-Aghdam, M.R. Feyzi, N. Bianchi, M. Morandin, "Design and analysis of a novel high-torque stator-segmented SRM," *IEEE Transactions on Industrial Electronics*, vol. 63, no. 3, pp. 1458-1466, 2016.
- [13] M. Ruba, I.A. Viorel, L. Szabó, "Modular stator switched reluctance motor for fault tolerant drive systems," *IET Electric Power Applications*, vol. 7, no. 3, pp. 159-169, 2013.
- [14] L. Szabó, M. Ruba, "Segmental stator switched reluctance machine for safety-critical applications," *IEEE Transactions on Industry Applications*, vol. 48, no. 6, pp. 2223-2229, 2012.
- [15] M. Ruba, I. Benția, L. Szabó, "Novel modular switched reluctance machine for safety-critical applications," in *Proceedings of the 19<sup>th</sup> International Conference on Electrical Machines (ICEM '2010) Rome (Italy)*, 2010.
- [16] G.E. Horst, "Isolated Segmental Switch Reluctance Motor," US 5111096 patent, 1992.
- [17] B. Mecrow, J. Finch, E. El-Kharashi, A. Jack, "Switched reluctance motors with segmental rotors," *IEE Proceedings - Electric Power Applications*, vol. 149, no. 4, pp. 245-254, 2002.
- [18] J.D. Widmer, B.C. Mecrow, "Optimized segmental rotor switched reluctance machines with a greater number of rotor segments than stator slots," *IEEE Transactions on Industry Applications*, vol. 49, no. 4, pp. 1491-1498, 2013.
- [19] W. Sun, Q. Li, L.-L. Zhu, D. Xu, L. Li, "Adaptive Magnetic Equivalent Circuit of Rotor-Segmented Axial-Field Switched Reluctance Machine Incorporated with Finite-Element Method," in *Proceedings of the 21<sup>st</sup> International Conference on Electrical Machines and Systems (ICEMS '2018)*, Jeju (Korea), 2018, pp. 2709-2714.
- [20] R. Madhavan, B.G. Fernandes, "Axial flux segmented SRM with a higher number of rotor segments for electric vehicles," *IEEE Transactions on Energy Conversion*, vol. 28, no. 1, pp. 203-213, 2013.
- [21] B. Wang, D.-H. Lee, J.-W. Ahn, "Characteristic analysis of a novel segmental rotor axial field switched reluctance motor with single teeth winding," in *Proceedings of*

- the IEEE International Conference on Industrial Technology (ICIT '2014), Busan (South Korea), 2014, pp. 175-180.
- [22] J.D. Widmer, R. Martin, B.C. Mecrow, "Optimization of an 80kW segmental rotor switched reluctance machine for automotive traction," IEEE Transactions on Industry Applications, vol. 51, no. 4, pp. 2990-2999, 2015.
  - [23] M. Diko, P. Rafajdus, P. Makys, P. Dubravka, L. Szabó, M. Ruba, "A novel concept of short-flux path switched reluctance motor for electrical vehicles," Advances in Electrical and Electronic Engineering, vol. 13, no. 3, pp. 206-211, 2015.
  - [24] X. Xue, K. Cheng, Y. Bao, P. Leung, N. Cheung, "Switched reluctance generators with hybrid magnetic paths for wind power generation," IEEE Transactions on Magnetics, vol. 48, no. 11, pp. 3863-3866, 2012.
  - [25] A. Labak, N.C. Kar, "Designing and prototyping a novel five-phase pancake-shaped axial-flux SRM for electric vehicle application through dynamic FEA incorporating flux-tube modeling," IEEE Transactions on Industry Applications, vol. 49, no. 3, pp. 1276-1288, 2013.
  - [26] P. Andrada, E. Martínez, M. Torrent, B. Blanqué, J.I. Perat, "Novel in-wheel axial-flux segmented switched reluctance motor," in Proceedings of the 19th European Conference on Power Electronics and Applications (EPE '17 ECCE Europe), Warsaw (Poland), 2017.
  - [27] Z. Pan, S. Song, R. Ma, "A novel axial flux switched reluctance machine with segmented stator and rotor," in Proceedings of the 20<sup>th</sup> International Conference on Electrical Machines and Systems (ICEMS '2017), Sydney (Australia), 2017.
  - [28] J.H. Potgieter, F.J. Márquez-Fernández, A.G. Fraser, M.D. McCulloch, "Performance evaluation of a high speed segmented rotor axial flux switched reluctance traction motor," in Proceedings of the 22<sup>nd</sup> International Conference on Electrical Machines (ICEM '2016), 2016, pp. 531-537.
  - [29] W. Ding, Y. Hu, T. Wang, S. Yang, "Comprehensive research of modular E-core stator hybrid-flux switched reluctance motors with segmented and nonsegmented rotors," IEEE Transactions on Energy Conversion, vol. 32, no. 1, pp. 382-393, 2017.
  - [30] S.-H. Mao, M.-C. Tsai, "A novel switched reluctance motor with C-core stators," IEEE Transactions on Magnetics, vol. 41, no. 12, pp. 4413-4420, 2005.
  - [31] E.S. Afjei, H.A. Toliyat, "A novel multilayer switched reluctance motor," IEEE Transactions on Energy Conversion, vol. 17, no. 2, pp. 217-221, 2002.
  - [32] F. Daldaban, N. Ustkoyuncu, "Multi-layer switched reluctance motor to reduce torque ripple," Energy Conversion and Management, vol. 49, no. 5, pp. 974-979, 2008.
  - [33] A. Salimi, G. Rezazadeh, S. Nouroollah, N. Niassati, A. Hajihosseini, "A novel four layer switch reluctance generator," in Proceedings of the 15<sup>th</sup> International Power Electronics and Motion Control Conference (EPE-PEMC '2012), Novi Sad (Serbia), 2012.

- [34] E.S. Afjei, A. Siadatan, H. Torkaman, "Analytical design and FEM verification of a novel three-phase seven layers switched reluctance motor," *Progress In Electromagnetics Research*, vol. 140, pp. 131-146, 2013.
- [35] L. Szabó, "Permanent magnet boosted modular switched reluctance motor," *Journal of Computer Science and Control Systems*, vol. 9, no. 2, pp. 48-52, 2016.
- [36] P. Andrada, B. Blanque, E. Martinez, M. Torrent, "A novel type of hybrid reluctance motor drive," *IEEE Transactions on Industrial Electronics*, vol. 61, no. 8, pp. 4337-4345, 2014.
- [37] W. Ding, S. Yang, Y. Hu, S. Li, T. Wang, Z. Yin, "Design consideration and evaluation of a 12/8 high-torque modular-stator hybrid excitation switched reluctance machine for EV applications," *IEEE Transactions on Industrial Electronics*, vol. 64, no. 12, pp. 9221-9232, 2017.
- [38] W. Ding, S. Yang, Y. Hu, "Development and investigation on segmented-stator hybrid-excitation switched reluctance machines with different rotor pole numbers," *IEEE Transactions on Industrial Electronics*, vol. 65, no. 5, pp. 3784-3794, 2018.
- [39] S. Taghavi, P. Pillay, "A core analysis of the synchronous reluctance motor for automotive applications," in *Proceedings of the 21<sup>st</sup> International Conference on Electrical Machines (ICEM '2014)*, Berlin (Germany), 2014, pp. 961-967.
- [40] M. Rosu, P. Zhou, D. Lin, D.M. Ionel, M. Popescu, F. Blaabjerg, et al., *Multiphysics Simulation by Design for Electrical Machines, Power Electronics and Drives*. Hoboken (USA): John Wiley & Sons, 2017.
- [41] C.M. Spargo, B.C. Mecrow, J.D. Widmer, C. Morton, N. Baker, "Design and validation of a synchronous reluctance motor with single tooth windings," *IEEE Transactions on Energy Conversion*, vol. 30, no. 2, pp. 795-805, 2015.
- [42] W. Ouyang, S. Huang, A. Good, T. Lipo, "Modular permanent magnet machine based on soft magnetic composite," in *Proceedings of the 8<sup>th</sup> International Conference on Electrical Machines and Systems (ICEMS '2005)*, Nanjing (China), 2005, pp. 235-239.
- [43] S. Taghavi, P. Pillay, "A novel grain-oriented lamination rotor core assembly for a synchronous reluctance traction motor with a reduced torque ripple algorithm," *IEEE Transactions on Industry Applications*, vol. 52, no. 5, pp. 3729-3738, 2016.
- [44] I.A. Viorel, G. Henneberger, R. Blissenbach, L. Lövenstein, *Transverse Flux Machines. Their Behavior, Design, Control and Applications*. Cluj (Romania): Mediamira, 2003.
- [45] T. Husain, I. Hasan, Y. Sozer, I. Husain, E. Muljadi, "Design of a modular E-core flux concentrating transverse flux machine," *IEEE Transactions on Industry Applications*, vol. 54, no. 3, pp. 2115-2128, 2018.
- [46] J. Doering, G. Steinborn, W. Hofmann, "Torque, power, losses, and heat calculation of a transverse flux reluctance machine with soft magnetic composite materials and disk-shaped rotor," *IEEE Transactions on Industry Applications*, vol. 51, no. 2, pp. 1494-1504, 2015.



- [47] P. Bolognesi, "Design and manufacturing of an unconventional variable reluctance machine," in Proceedings of the 4<sup>th</sup> IET Conference on Power Electronics, Machines and Drives (PEMD '2008) York (UK), 2008, pp. 45-49.
- [48] S. Baserrah, "Theoretical and Experimental Investigations of a Permanent Magnet Excited Transverse Flux Machine with a Segmented Stator for In-Wheel Motor Applications," Ph.D. Thesis, University of Bremen, Bremen (Germany), 2014.
- [49] L. Someșan, E. Pădurariu, I.A. Viorel, L. Szabó, "Design of a permanent magnet flux-switching machine," in Proceedings of the 9th International Conference EL-EKTRO '2012, Žilina - Rajecské Teplice (Slovakia), 2012, pp. 256-259.
- [50] A. Thomas, Z. Zhu, L. Wu, "Novel modular-rotor switched-flux permanent magnet machines," IEEE Transactions on Industry Applications, vol. 48, no. 6, pp. 2249-2258, 2012.
- [51] A.S. Thomas, Z.-Q. Zhu, R.L. Owen, G.W. Jewell, D. Howe, "Multiphase flux-switching permanent-magnet brushless machine for aerospace application," IEEE Transactions on Industry Applications, vol. 45, no. 6, pp. 1971-1981, 2009.
- [52] B. Štumberger, G. Štumberger, M. Hadžiselimović, A. Hamler, V. Goričan, M. Jesenik, et al., "Performance comparison of three-phase flux reversal permanent magnet motors in BLDC and BLAC operation mode," Journal of Magnetism and Magnetic Materials, vol. 320, no. 20, pp. e896-e900, 2008.
- [53] N. Brown, T. Jahns, R. Lorenz, "Power converter design for an integrated modular motor drive," in Conference Record of the 2007 IEEE Industry Applications Conference & 42<sup>nd</sup> IAS Annual Meeting (IAS '2007), New Orleans (USA), 2007, pp. 1322-1328.
- [54] T. Stäuble. Lamination sheet, stack or assembly? (2018, March 27). Available: [http://www.swd-technology.com/wp-content/uploads/Fachbeitrag\\_Paketierung\\_ZWF\\_en1.pdf](http://www.swd-technology.com/wp-content/uploads/Fachbeitrag_Paketierung_ZWF_en1.pdf)
- [55] (2019, February 27). Stator segments with bonding varnish are competitive in large series productions! Available: <http://www.swd-technology.com/en/products/segmentierung-und-zahnsegmente/>
- [56] (2019, February 27). Bonding varnish in sample and small batch production. Available: <https://www.grau-stanzwerk.de/e/produkte/backlack.php>
- [57] S. Hara, S. Suga, S. Watanabe, M. Nakamura, "Variable valve actuation systems for environmentally friendly engines," Hitachi Review, vol. 58, no. 7, pp. 319-324, 2009.
- [58] L. Szabó, I.A. Viorel, V. Iancu, D.C. Popa, "Soft magnetic composites used in transverse flux machines," Oradea University Annals, Electrotechnical Fascicle, pp. 134-141, 2004.
- [59] S.P. Nikam, B.G. Fernandes, "Design of soft magnetic composite based modular four phase SRM for electric vehicle application," in Proceedings of the 21<sup>st</sup> International Conference on Electrical Machines (ICEM '2014), Berlin (Germany), 2014, pp. 112-116.

- [60] O. Moros, J. Richnow, D. Gerling, "New cost effective concentrated winding topology for induction machines," in Proceedings of the ANSYS Conference & 32<sup>nd</sup> CADFEM Users' Meeting, Nürnberg (Germany), 2014.
- [61] H. Akita, Y. Nakahara, N. Miyake, T. Oikawa, "New core structure and manufacturing method for high efficiency of permanent magnet motors," in Conference Record of the 2003 IEEE Industry Applications Conference & 38th IAS Annual Meeting (IAS '2003), Salt Lake City (USA), 2003, pp. 367-372.
- [62] L. Szabó. "Modular switched reluctance machines to be used in automotive applications," in Proceedings of the SRM Drives an Alternative for E-traction Workshop, Vilanova i la Geltrú (Spain), 2018.
- [63] A.G. Jack, B.C. Mecrow, J.A. Haylock, "A comparative study of permanent magnet and switched reluctance motors for high-performance fault-tolerant applications," IEEE Transactions on Industry Applications, vol. 32, no. 4, pp. 889-895, 1996.
- [64] G.-J. Su, J.W. McKeever, K.S. Samons, "Modular PM motor drives for automotive traction applications," in Proceedings of the 27<sup>th</sup> Annual Conference of the IEEE Industrial Electronics Society (IECON '2001), Denver (USA), 2001, pp. 119-124.
- [65] M. Ruba, L. Szabó, L. Strete, I.A. Viorel, "Study on fault tolerant switched reluctance machines," in Proceedings of the 18<sup>th</sup> International Conference on Electrical Machines (ICEM '2008), Vilamoura (Portugal), 2008.

# Double-Stator Switched Reluctance Motors

Hossein Torkaman and Majid Asgar

## 5.1. Introduction

The advances in power electronic devices, simulation software and manufacturing technology allow possibility of introducing SRMs as an attractive candidate for a wide range of industrial applications such as automotive and domestic appliances [1-3]. The main advantages of SRMs are simple structure, high efficiency, low maintenance cost, fault tolerance, high reliability, high torque-inertia and low price-performance ratios [4-6]. The structure of SRM has enough flexibility to produce distinctive characteristics for many required applications and intentions. Operating in saturation condition leads to have complex relationship and control in this machine. This reduces the total performance of the SRM and its drive in comparison with commonly used induction and permanent magnet machines [7]. Generally speaking, in SRM, the specific application determines the motor geometry, the power converter topology and the applied control method [8]. Hence, an enhancement in power density provides the opportunity to employ this machine in high-performance applications [9].

In an SRM (**Fig. 1**), rotation of the rotor is due to the resultant radial and tangential force vectors ( $F_R$  and  $F_T$ ), respectively. The structure of a rotary SRM dictates produced propulsion force on the rotating part by the interaction between stator and its corresponding coaxial rotor poles. The nonsymmetrical distribution of the mentioned forces lead to torque ripple production that can disturb positioning accuracy and thus causing vibrations. In this regard, monotonous distribution of forces could avoid additional ripple.

However, there are many different methods to decrease the motor ripple and increase the power and torque densities of SRM. These methods are categorized in improved control methods and optimum design of motor topology. In this regards, DSSRMs benefit from high torque density as well as low radial force level in comparison with the conventional SRMs [10, 11].

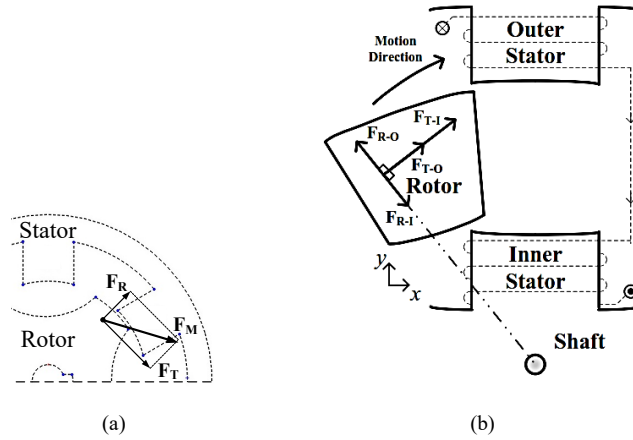


Fig. 1: The produced forces in: (a) SRM, (b) DSSRM

## 5.2. DSSRM structure

The concept of DSSRM comes from double-sided linear SRM (DLSRM). **Fig. 2** shows a DLSRM with segmented translator configuration.

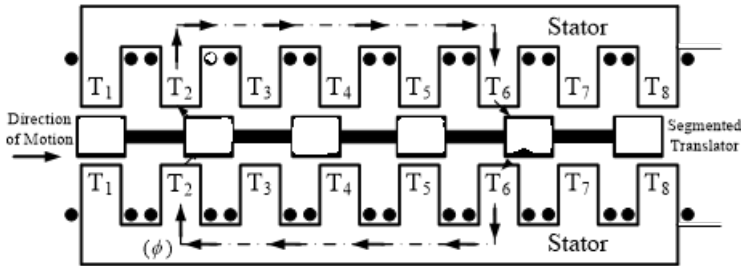


Fig. 2: DLSRM with segmented translator

Unlike single-side LSRMs, DLSRM does not have a lot of freedom in the air gap tolerance. One of the merits of DLSRM is high force density with lower inductance as it has four air gaps in its flux path. DSSRM improves the power/torque density and reduces the acoustic noise emission as compared with the conventional SRM. Advantages of the DSSRM in comparison with the conventional SRM are as follows [12]: 1) higher torque/power density; 2) higher force conversion efficiency; 3) higher motional force while lower radial force; 4) larger effective air gap reluctance at unaligned position.

In this type of machine, two inner and outer stators are employed (**Fig. 3**). These stators are made of laminated ferromagnetic material and windings are wrapped around each pole. The motor can be made in 3, 4 or 6 phases configurations.

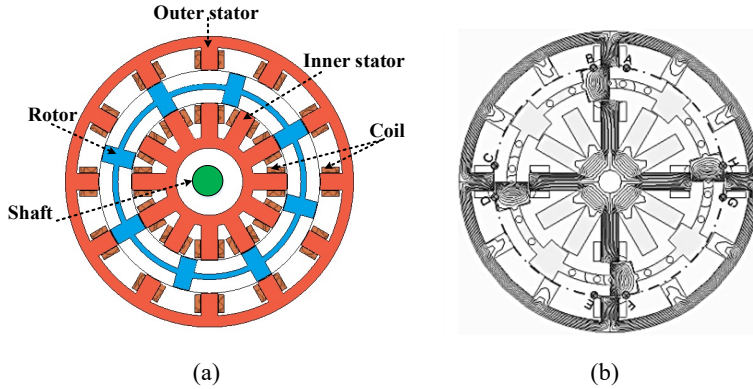


Fig. 3: (a) DSSRM, (b) Flux linkage path.

The rotor is located between the inner and outer stator. The rotor is formed by segments of laminated, which is hold together using a bridge (in one piece) or by a non-ferromagnetic cage (in segmented rotor). Because of position of the rotor it would be lighter than the rotor in SRM. It means that the rotor has a low moment of inertia and a fast response time. There are two narrow air gaps between rotor and two stators. There are different arrangements of the outer-stator/rotor/inner-stator poles in DSSRM, in which the common arrangements are 12/8/12, 12/10/12 and 8/6/, that are shown in **Fig.4**.

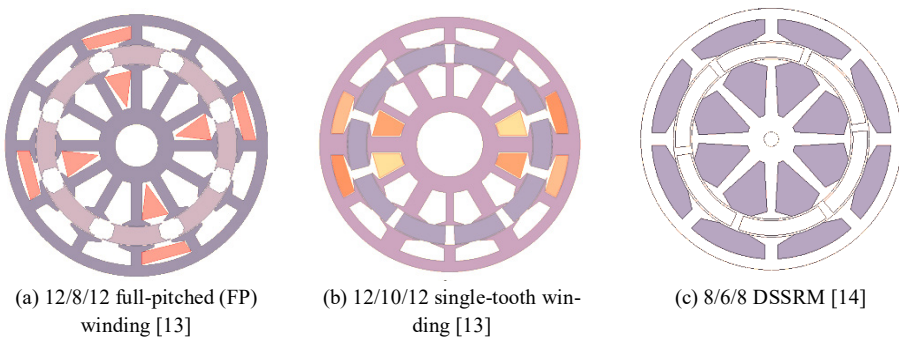


Fig. 4: Different arrangements of outer-stator/rotor/inner-stator poles

Based on the average torque equation ( $T_{av} \propto (L_a - L_u) / (\theta_a - \theta_u)$ ), the instantaneous torque profile of the motor depends on the phase inductance profile, which is heavily influenced by the equivalent air gap between stator and rotor at various rotor positions. Therefore, the modification of rotor geometry could potentially shape the torque profile of the DSSRM. Some of the rotor shapes are shown in **Fig. 5**. For comparison of this rotor shapes, the length, width, tips geometry, arc angle, thickness and number of steps should be optimized and then the motor characteristics would be evaluated.

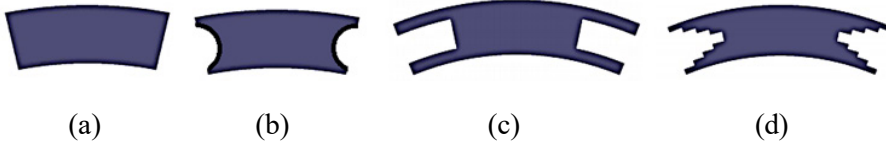


Fig 5: (a) Solid rotor, (b) Rotor with arc edge, (c) Rotor with tips, (d) Rotor with stepped layer [15]

The windings of the stators can be wrapped in form of single-tooth windings, short-pitched, full-pitched, concentrated winding and hybrid combination coil. The winding connections of the inner stator can be accessed through a hole placed in the shaft of the inner stator. Fig. 6 shows some typical winding configuration in DSSRM. The comparison among them does not result in a clear conclusion that designates one winding typology to be the better one. It is dependent on various factors, including the chosen application of the DSSRM, operating point and tolerable torque ripple. For fair comparison the copper, core and thermal losses, also current density, torque density, torque ripple, flux leakage should be evaluated for different configuration in each application. In addition to typical structure of DSSRM, there are different type of DSSRM topologies such as: Bearing less[16], linear[17, 18], yokeless linear[19], axial flux [20], that are used for various applications.

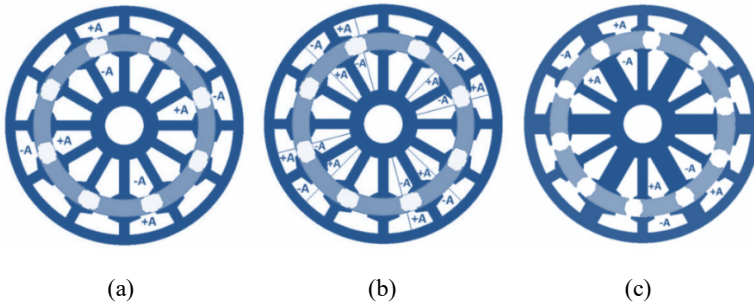


Fig. 6: (a) Full-pitched winding, (b) Concentrated windings-1, (c) Concentrated windings-2 [21]

The torque production of DSSRM is determined such as SRM by variation of co-energy versus rotor position or by the tendency of the magnetic circuit to minimize the reluctance of the flux path. Because of two excitation windings in inner stator and outer stator, the torque density would be higher in comparison to typical SRM with one excitation winding in. A counterclockwise excitation in stator phases leads a clockwise rotation of the rotor.

As mentioned before, the vibration and acoustic noises are the main disadvantage of SRMs, which overshadow their use in noise sensitive applications. DSSRMS can be considered as an alternative to this issue. In this regard, firstly, a structural analysis of the DSSRM should be done by multi-physic analysis, also FEM can be used to evaluate radial, axial and tangential forces at various parts of the machines. After that the acceleration, deformation, and velocity of the vibration should be assessed. In [14] compares structural analysis of a DSSRM and a conventional SRM with the same outer diameter, yoke thickness, and output power. It was shown that radial force is smaller in the DSSRM, and the force distribution in this machine tends to offer a lower vibration level and acoustic noise. Results show that the DSSRM machine experiences much lower vibration than the conventional SRM as shown in Table I.

TABLE I: VIBRATION COMPARISON OF SRM AND DSSRM IN TIME DOMAIN [14]

Parameter	12/8 SRM	8/6/8 DSSRM
Maximum acceleration (m/s <sup>2</sup> )	150	25
Maximum velocity (mm/s)	9	1
Maximum deformation (nm)	425	60

To better understanding the behavior of the machine, a DSSRM will be designed and different characteristics will be achieved and analyzed in the next section.

### 5.3. Design Procedure of the DSSRM

The design trend of the DSSRM is illustrated in **Fig.7**. Then the design of DSSRM is based on division structure into two SRMs (inner rotor SRM and outer rotor SRM). It should be considered that the same torque should be produced on the rotor by each of the inner and outer stators. In fact, balanced condition of the rotor is achieved by dividing the nominal torque of the DSSRM into two equal parts between two SRMs. Determining the  $D_{in}$  and  $D_{out}$  (of inner and outer stators diameters) should be achieved or determined by application. Also, the specific magnetic and electric loadings on two stators would create a balanced force on the middle rotor.

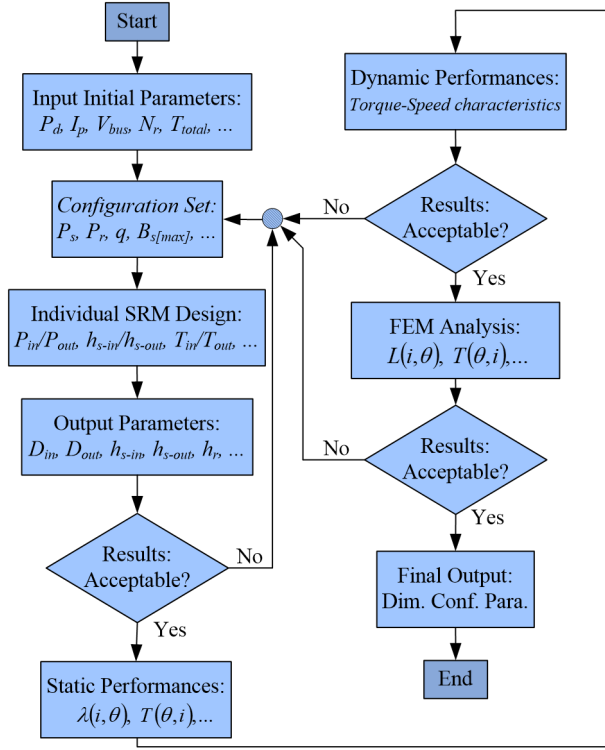


Fig. 7: Flowchart of design procedure of the DSSRM [10]

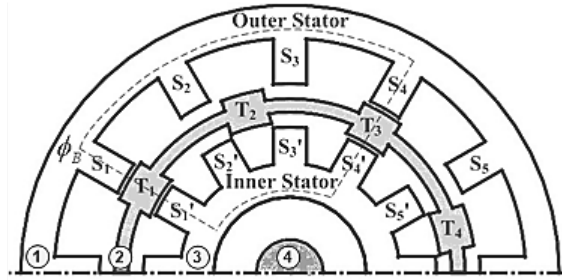


Fig. 8: Cross section view of the DSSRM with four parts: (1) Outer stator, (2) Rotor, (3) Inner-stator, (4) Shaft.

The torque produced by a DSSRM is the result of torque vectors formed by the inner and outer stators (Figure 8a). Therefore, by separating a DSSRM into two independent SRMs, some parts such as rotor and shaft are shared between two SRMs. The outer stator and shared rotor can form an independent interior rotor SRM and the inner stator and shared rotor can form an independent exterior rotor SRM. For design, the DSSRM is divided into four parts (**Fig. 8**). Parts 1, 2 and 4



form the interior rotor SRM and parts 2, 3 and 4 form the exterior rotor SRM. Therefore, parts 2 and 4 are common parts in the design of both SRMs

In this structure, the net centrifugal and centripetal forces on the rotor are the vector sum of the torque produced by the two stators. This force causes rotational motion that can be calculated as a function of rotating internal parameters:

$$F \cong m \times r \times \omega^2 \quad (5.1)$$

where  $m$  is the mass turning around with the shaft,  $r$  is the radius of outside of the stator and  $\omega$  is the angular speed [rad/s]. As explained in the previous section, to produce equivalent force on the rotor; due to inequality of the bore diameters, both stators are forced to produce unequal power. The power capacity of the DSSRM considering both inner and outer stators can be calculated as follows:

$$P_d = P_{in} + P_{out} = F \times v_m \quad (5.2)$$

$$\text{In DSSRM} \Rightarrow P_{in} \succ P_{out}$$

where  $v_m$  is maximum linear velocity [m/s]. Preceding the design of the SRM, initial parameters of the SRM configurations appropriate to the specific application are defined and listed in Table II. In this example, the  $D_0$  (outer diameter of the DSSRM) are considered as initial value with specific value, in design trend.

TABLE II. INITIAL PARAMETERS OF THE DSSRM.

Parameter	Description	Value
Ps	Number of Stator Poles	12 (dual)
Pr	Number of Rotor Poles	8
q	Number of Phases	3
D0	Stator Outside Diameter	260 mm
Pd	Total Output Power	1.2 kW
Vbus	Bus Voltage	80 V
IP	Peak Phase Current	20 A
$\beta s[\max]$	Maximum Stator Pole Arc	7.5 Deg.

### A. Inner rotor SRM design -Individually

The design variables considered for the analysis of inner rotor SRM are shown in **Fig. 9**. Due to the structure of proposed segmented DSSRM, the rotor yoke has been eliminated ( $b_{ry} = 0$ ).

As seen in **Fig. 9**, the outer diameter of the SRM is as follows:

$$D_0 = D_{sh} + 2b_{ry} + 2h_r + 2l_g + 2(h_{s-out} + b_{sy-out}) \quad (5.3)$$

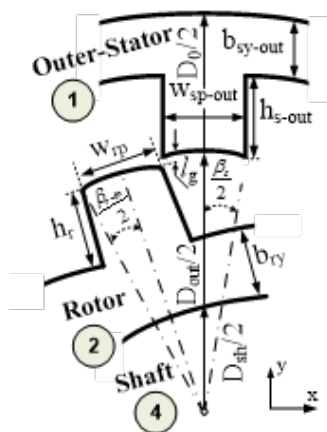


Fig. 9: Dimension parameters of an inner rotor SRM.

It should be noted that, the process of SRM design has some assumptions and constant coefficients which are detailed in Table III. The numerical value of the frame size factor is considered with respect to the design of an SRM.

TABLE III ASSUMPTION OF DSSRM DESIGN.

Parameter	Description	Value
$k$	Frame Size Factor	0.25
$k_1$	Constant Factor	0.08225
$k_2$	Constant Factor	0.7
$k_e$	Efficiency	40%
$k_d$	Duty Cycle	0.5
$B$	Flux Density	1.4 T
$D_{sh}$	Shaft Diameter	50 mm
$l_g$	Air Gap Length	0.5 mm
$M$	Lamination Material	M27 Steel
$\mu_0$	Magnetic Permeability of Space	$4\pi \times 10^{-7}$ H.m-1
$J$	Current Density	6 A/mm <sup>2</sup>

$k$  factor is the ratio between bore diameter and stack length which is called frame size factor.  $k_1$  is a constant factor which is equal with  $\pi^2/120$ .  $k_2$  is a constant factor that is related to the ratio of aligned and unaligned inductances.  $k_d$  is the ratio of the on-time of the switch to the time period which is called duty cycle. The bore diameter of an inner rotor SRM is obtained from the power output equation as

$$D_{out} = \sqrt[3]{\frac{P_{out}}{k_e k_d k_1 k_2 k B A_{S-out} N_r}} \quad (5.4)$$

The outer stator electric loading of the rotary SRM is given by:

$$A_{S-out} = \frac{2 \times i \times m \times T_{ph-out}}{\pi \times D_{out}} \quad (5.5)$$

The output torque of inner rotor SRM can be explained by:

$$T_{out} = k_d k_e k_2 k_3 (B \times A_{S-out}) D_{out}^2 \times L \quad (5.6)$$

The stator yoke thickness is found as:

$$b_{sy-out} = \frac{D_{out} \times \beta_s}{2} \quad (5.7)$$

The stator pole height is calculated as:

$$h_{s-out} = \frac{D_0}{2} - \frac{D_{out}}{2} - b_{sy-out} \quad (5.8)$$

The height of the rotor pole is defined as follows:

$$h_r = \frac{D_{out}}{2} - l_g - b_{ry} \quad (5.9)$$

The magnetic field intensity is given by:

$$H_{g-out} = \frac{D_{out}}{\mu_0} \quad (5.10)$$

The number of turns per phase for peak phase current is:

$$T_{PH-out} = \frac{H_{g-out} \times 2l_g}{I_p} \quad (5.11)$$

The area of cross-section of the conductor is calculated as:

$$ac = \frac{I_p}{J\sqrt{q}} \quad (5.12)$$

With calculating the number of coil winding turns completes the inner rotor SRM design. Geometrical and electrical parameters of the designed inner rotor SRM after required iterations are obtained and listed in Table IV.

TABLE IV GEOMETRICAL AND ELECTRICAL PARAMETERS OF THE DESIGNED INNER ROTOR SRM

Parameter	Description	Value
$P_{out}$	Outer Stator Power	483 W
$D_{out}$	Outer Stator Bore Diameter	200 mm
$L$	Stack Length	40 mm
$A_{s-out}$	Outer Stator Electric Loading	19100 A/m
$h_{s-out}$	Outer Stator Pole Height	20 mm
$h_r$	Rotor Pole Height	30 mm
$b_{sy-out}$	Outer Stator Yoke Thickness	10 mm
$b_{ry}$	Rotor Yoke Thickness	0 mm
$W_{sp}$	Outer Stator Pole Width	15 mm
$W_{rp-out}$	Inner Stator Pole Width	28 mm
$T_{ph-out}$	Outer Stator Coil Turns	75
$T_{out}$	Outer Stator Output Torque	5.88 Nm

### B. Outer rotor SRM design individually

The design variables that are considered for the analysis of outer rotor SRM are shown in **Fig.10**.

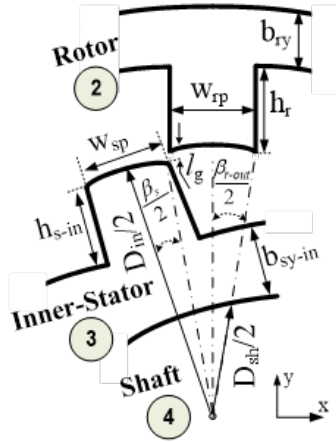


Fig.10: Dimension parameters of an outer rotor SRM.

The diameter of outer rotor SRM is obtained from the power output equation as:

$$D_{in} = \sqrt[3]{\frac{P_{in}}{k_e k_d k_1 k_2 k_B A_{S-in} N_r}} \quad (5.13)$$

The output torque of outer rotor SRM can be explained by:

$$T_{in} = k_d k_e k_2 k_3 (B \times A_{s-in}) D_{in}^2 \times L \quad (5.14)$$

The stator yoke thickness is found as:

$$b_{sy-in} = \frac{D_{in} \times \beta_s}{2} \quad (5.15)$$

The stator pole height is given by:

$$h_{s-in} = \frac{D_0}{2} - \frac{D_{in}}{2} - b_{sy-in} \quad (5.16)$$

The magnetic field intensity is defined as follows:

$$H_{g-in} = \frac{D_{in}}{\mu_0} \quad (5.17)$$

The number of turns per phase for peak phase current is:

$$T_{PH-in} = \frac{H_{g-in} \times 2l_g}{I_p} \quad (5.18)$$

TABLE V GEOMETRICAL AND ELECTRICAL PARAMETERS OF THE DESIGNED OUTER ROTOR SRM.

Parameter	Description	Value
Pin	Inner Stator Power	739 W
Din	Inner Stator Bore Diameter	140 mm
L	Stack Length	40 mm
As-in	Inner Stator Electric Loading	36380 A/m
hs-in	Inner Stator Pole Height	40 mm
hr	Rotor Pole Height	30 mm
bsy-in	Inner Stator Yoke Thickness	13 mm
bry	Rotor Yoke Thickness	0 mm
Wsp	Outer Stator Pole Width	15 mm
Wrp-in	Rotor Pole Width	17 mm
TPh	Inner Stator Coil Turns	100
Tin	Inner Stator Output Torque	5.4 Nm

Comparing Tables IV with V shows that the power received from DC-link to the inner stator is greater than the outer stator. Due to establish balancing condition in this motor that has two different stator diameters, the number of turns in inner

stator should be increased. Generally, in a double-stator motor, the following relationship is established ( $D_{out} > D_{in}$ ). Therefore, according to equations (6) and (14), due to inequality of the stators bore diameters, the calculated torque in the air gap between two stators and rotor poles, are not the same. In this case, the rotor pulls toward the outer stator. To prevent this issue, the number of turns in the inner stator windings increased to make the balancing condition. The results which are listed in Tables III and IV refers to this point ( $\alpha$  is inequality factor).

$$\begin{aligned}
 \text{In DSSRM: } D_{out} &= \alpha D_{in} \Rightarrow T_{ph-out} = \alpha^2 T_{ph-in} \\
 A_{S-in} &= \frac{2 \times i \times m \times \alpha T_{ph-out}}{\pi \times D_{out} / \alpha} = \alpha^2 A_{S-out} \\
 \Rightarrow P_{in} &> \alpha^2 P_{out} \Rightarrow T_{in} \cong T_{out}
 \end{aligned} \tag{5.19}$$

### C. Integration of the Designs

Based on the mentioned equations and specific application, the DSSRM has been designed analytically. The common variable parameters are illustrated in **Fig. 11**.

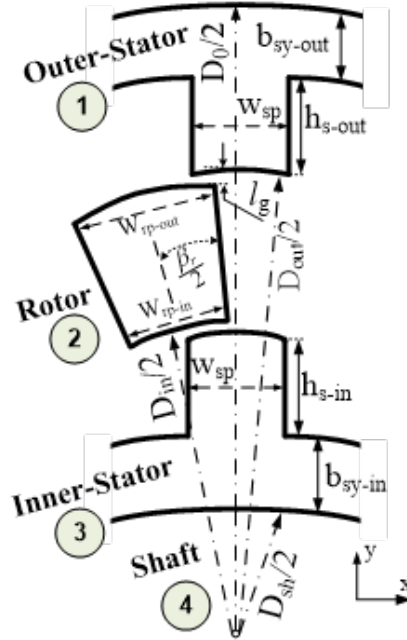


Fig. 11: Pole shaping of the segmented DSSRM.

TABLE VI GEOMETRICAL AND ELECTRICAL SPECIFICATIONS OF DESIGNED DSSRM.

Parameter	Description	Value
$P_d$	Developed Output Power	1.2 kW
$D_0$	Outer Diameter	260 mm
$L$	Stack Length	40 mm
$T_a$	Actual Output Torque	11.28 Nm
$A_{ST}$	Total Electric Loading	55480 A/m
$M_T$	Total Magnetic Loading	0.175 T

#### 5.4. Numerical Assessment of the Motor Characteristics

The overall performance of the designed DSSRM has been verified with static and transient finite element analysis (FEA). Having knowledge about the magnetic flux distribution in the motor for various rotor angles and excitation current is needed to predict motor efficiency. The 3D designed model using CAD package, is illustrated in **Fig. 12**. The designed DSSRM with the achieved dimensions (Table VI) includes two coaxial stators and one segmented rotor.

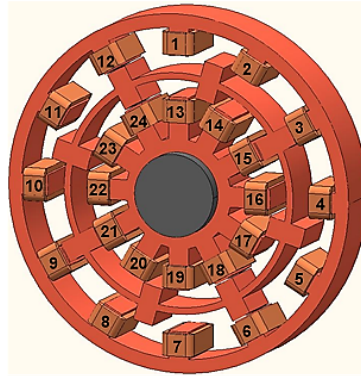


Fig. 12: The coil numbering of the 3D model in DSSRM.

The FEM is a useful tool to provide a complete analysis of the SRM, as it is able to model non-linear magnetic properties as well as static and dynamic studies. In DSSRM, the relevance between dimensions of inner and outer stators and the developed torque is not clear. Therefore, an adjustment of any device parameters demands a new computational analysis by FEM.

In order to analysis the actual performance of the DSSRM, rotor starts from unaligned position -15 Deg. toward aligned position 0 Deg., and then, moves from

aligned position 0 Deg. toward another unaligned position 15 Deg. in counter clockwise direction. In this states the constant excitation current of phase “A” is 8 A. The values of flux linkage at all discrete position of the rotor movements are computed. At aligned position, the magnetic flux density is obtained and shown in Figure 13. The maximum flux density ( $B_{\max}$ ) in 8 A excitation current is close to 1.43 T. As seen in **Fig. 13**, four stator pole pairs are participated for one phase energizing in DSSRM.

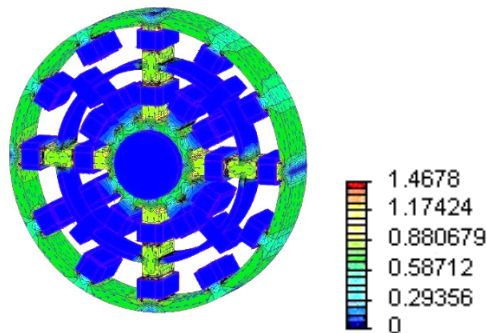


Fig. 13: Distribution of Flux density [Tesla].

Under 8A excitation current, the flux linkage vs. rotor position of the motor is calculated and shown in Figure 14. In the unaligned position, minimum flux is about 18.6 mWb and the peak flux in aligned position is 87 mWb. The inductance is defined as the ratio of flux-linking in active phase to the exciting current ( $L=\lambda/i$ ). It means, with considering constant current excitation in the simulation, the inductance shape is the same as flux-linkage that shown in **Fig.14**.

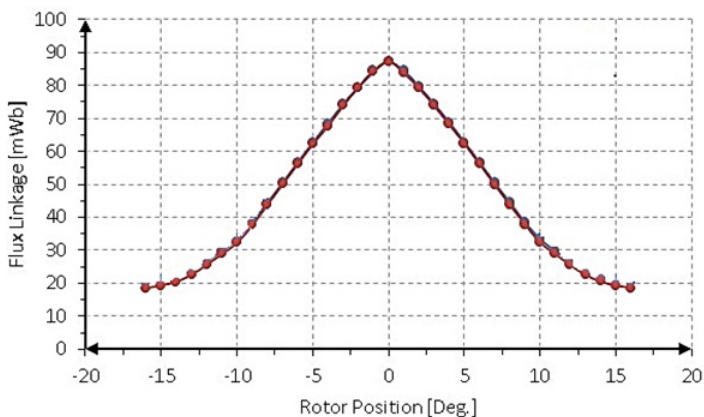


Fig. 14: Flux linkage profile.



As shown in **Fig.15**, the generated torque by DSSRM follows minimum reluctance path with the rotor rotation. The maximum values of the torque is obtained about 5.9 Nm at fully unaligned positions 7.5 Deg. under 8 A constant current.

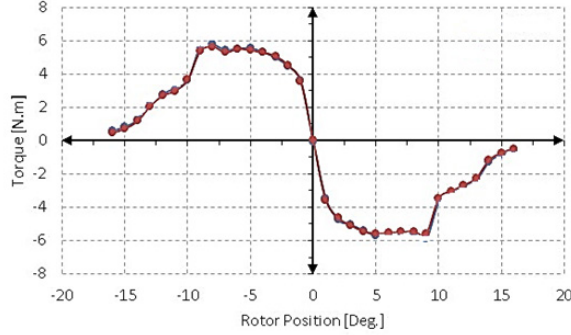


Fig. 15: Torque profile.

To verify the design strategy, the proposed flat-type DSSRM are fabricated. The different parts are shown in **Fig.16**. The depicted three-phase motor parts include a segmental rotor and two stators which the stators are located and centered inside the aluminum hollow cylinder and the rotor is placed on a thick aluminum frame. Also, the shaft is placed on one bearing that is ready to connect to the load. The main controller is designed by DSPIC microcontroller.

## 5.5. Manufacturing and Experimental Test

The first task to obtain the best dynamic performance of the machine is to compute turn ON/OFF angles at each current and speed working point. The main objective is to get the maximum torque possible at each current and speed reference point. It is also necessary to validate that the dynamic evolution of the phase currents is good. This is a key point to assure that the maximum peaks values do not go above the protection limits.

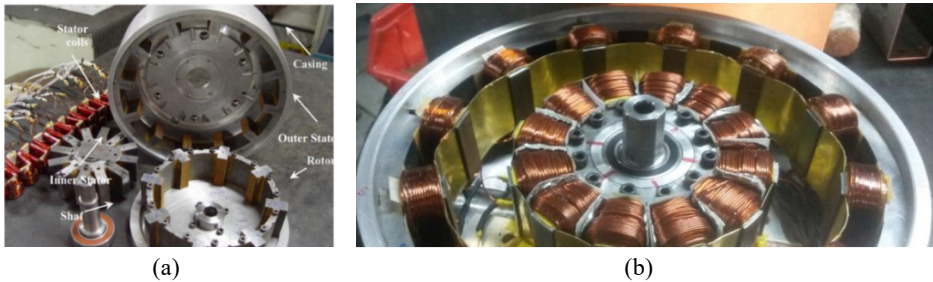


Fig. 16: (a) Different parts of motor, (b) Assembled stators of the motor

Different tests are done to verify the analytical results and FEM analysis [10]. The inductance values of the motor at aligned and unaligned positions are achieved and are shown in Table IV in comparison with the mentioned analysis. As seen in this table, the inductance value of aligned and unaligned positions are about 47 and 16 mH, respectively. The appropriate difference between values of these two positions proves the ideal operation of the motor in torque production. Also, the difference between analytical, FEM and experimental results in the unaligned position is 1 and 2 mH which are in the minimum value. However, in the aligned position, these differences are 5 and 1 mH.

TABLE IV. INDUCTANCE MAGNITUDE AT ALIGNED AND UNALIGNED POSITIONS.

Position	Analytical	FEM	Experimental
Aligned	43mH	48mH	47mH
Unaligned	13mH	14mH	16mH

The experimental torque-speed characteristic is obtained and shown in **Fig.17**. In low speeds (below the rated speeds) under 80 V DC-link power supply, the torque is limited by the motor current. At 1000 rpm speed, the generated torque is obtained about 8.5 Nm. At lower speeds (below 1200 rpm), the variation of the current rises almost instantly. These specifications adequate to use the proposed motor in special direct drive application.

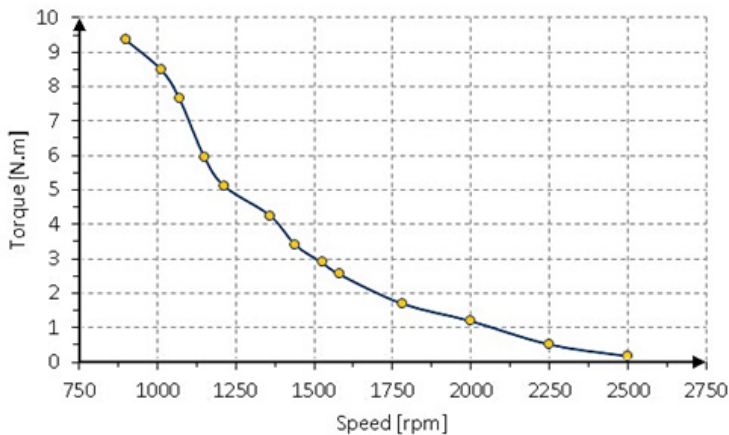


Fig. 17: Torque vs. Speed profile in open loop mode.

The efficiency of a DSSRM are shown in **Fig.18**. The maximum efficiency of the DSSRM is obtained about 78%. Also, in the medium and high speeds ranges, the efficiency of the DSSRM is better than the conventional SRM.

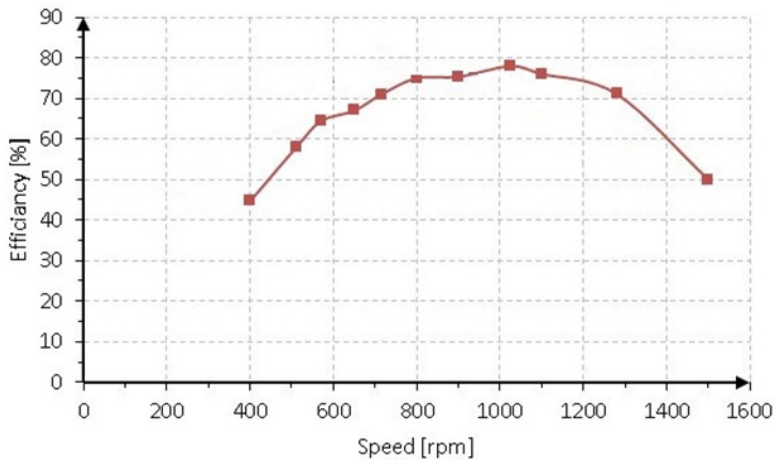


Fig. 18: Efficiency vs. Speed profile.

## 5.6. Conclusions

This chapter introduced DSSRM. In this regards motor structure, geometry, design, electromagnetics characteristics, prototyping and test presented. The motor characteristics show that the flux distribution, flux linkage, leakage inductance and torque profiles have normal behavior such as conventional SRM. This configuration can produce more torque and power density with lower radial force, vibration and acoustic noises. In which make it good candidate for direct drive applications. As a result, this analysis shows that this type of machine has potential to be used in different application such as electric vehicle, scooter, pump, fans, washing machine and flywheel.

## 5.7. References

- [1] H. Torkaman, A. Ghaheri, and A. Keyhani, "Axial flux switched reluctance machines: a comprehensive review of design and topologies," *IET Electric Power Applications*, vol. 13, no. 3, pp. 310-321, 2019.
- [2] O. Safdarzadeh, A. Mahmoudi, E. Afjei, and H. Torkaman, "Rotary-Linear Switched Reluctance Motor: Analytical and Finite-Element Modeling," *IEEE Transactions on Magnetics*, vol. 55, no. 5, pp. 1-10, 2019.

- [3] H. Torkaman, A. Ghaferi, and A. Keyhani, "Design of Rotor Excited Axial Flux-Switching Permanent Magnet Machine," *IEEE Transactions on Energy Conversion*, vol. 33, no. 3, pp. 1175-1183, 2018.
- [4] H. Torkaman, N. Faraji, and M. S. Toulabi, "Influence of Rotor Structure on Fault Diagnosis Indices in Two-Phase Switched Reluctance Motors," *IEEE Transactions on Magnetics*, vol. 50, no. 3, pp. 136-143, 2014.
- [5] H. Torkaman, "Rotor fault analysis and diagnosis in three-phase outer-rotor switched reluctance motor," in *4th Annual International Power Electronics, Drive Systems and Technologies Conference*, 2013, pp. 93-96.
- [6] A. Miremadi, H. Torkaman, and A. Siadatan, "Maximum current point tracking for stator winding short circuits diagnosis in Switched Reluctance Motor," in *4th Annual International Power Electronics, Drive Systems and Technologies Conference*, 2013, pp. 83-87.
- [7] O. Safdarzadeh, E. Afjei, and H. Torkaman, "Effective Magnetic Decoupling Control Realization for Rotary-Linear Switched Reluctance Motors utilized in Drilling Tools," *International Journal of Applied Electromagnetics and Mechanics*, vol. 57, no. 3, pp. 257-274, 2018.
- [8] H. Khanbabaie Gardeshi, and H. Torkaman, "Improved Control of Switched Reluctance Motor at High Speeds using Continuous Conduction Mode," *Tabriz Journal of Electrical Engineering*, vol. 47, no. 1, pp. 69-79, 2017.
- [9] H. Torkaman, R. Moradi, A. Hajihosseini, and M. S. Toulabi, "A comprehensive power loss evaluation for Switched Reluctance Motor in presence of rotor asymmetry rotation: Theory, numerical analysis and experiments," *Energy Conversion and Management*, vol. 77, pp. 773-783, 2014.
- [10] M. Asgar, E. Afjei, and H. Torkaman, "A New Strategy for Design and Analysis of a Double-Stator Switched Reluctance Motor: Electromagnetics, FEM, and Experiment," *IEEE Transactions on Magnetics*, vol. 51, no. 12, pp. 1-8, 2015.
- [11] M. Abbasian, M. Moallem, and B. Fahimi, "Double-Stator Switched Reluctance Machines (DSSRM): Fundamentals and Magnetic Force Analysis," *IEEE Transactions on Energy Conversion*, vol. 25, no. 3, pp. 589-597, 2010.
- [12] N. Arbab, W. Wang, C. Lin, J. Hearron, and B. Fahimi, "Thermal Modeling and Analysis of a Double-Stator Switched Reluctance Motor," *IEEE Transactions on Energy Conversion*, vol. 30, no. 3, pp. 1209-1217, 2015.
- [13] E. Cosoroaba, W. Wang, and B. Fahimi, "Comparative study of two winding configurations for a double stator switched reluctance machine," in *2014 International Conference on Electrical Machines (ICEM)*, 2014, pp. 1013-1017.
- [14] A. H. Isfahani, and B. Fahimi, "Comparison of Mechanical Vibration Between a Double-Stator Switched Reluctance Machine and a Conventional Switched Reluctance Machine," *IEEE Transactions on Magnetics*, vol. 50, no. 2, pp. 293-296, 2014.
- [15] W. Wang, M. Luo, E. Cosoroaba, B. Fahimi, and M. Kiani, "Rotor Shape Investigation and Optimization of Double Stator Switched Reluctance Machine," *IEEE Transactions on Magnetics*, vol. 51, no. 3, pp. 1-4, 2015.

- [16] Y. Sun, F. Yang, Y. Yuan, F. Yu, Q. Xiang, and Z. Zhu, "Analysis of a hybrid double stator bearingless switched reluctance motor," *Electronics Letters*, vol. 54, no. 24, pp. 1397-1399, 2018.
- [17] D. H. Wang, X. H. Wang, C. L. Shao, and Z. L. Wang, "Analysis and design of an annular winding dual side stator linear switch reluctance machine for ropless elevator driving system," in *2015 IEEE International Conference on Applied Superconductivity and Electromagnetic Devices (ASEMD)*, 2015, pp. 322-323.
- [18] D. Wang, X. Wang, and L. Xiong, "Performance analysis of a dual stator linear switch reluctance machine with rectangular segments considering force ripples for long stroke conveyor applications," in *2015 18th International Conference on Electrical Machines and Systems (ICEMS)*, 2015, pp. 295-298.
- [19] D. H. Wang, X. H. Wang, C. L. Shao, and L. X. Xiong, "Design aspects of a high thrust density dual stator yokeless Linear Switched Reluctance Machine for harsh conditions," in *2015 IEEE International Conference on Applied Superconductivity and Electromagnetic Devices (ASEMD)*, 2015, pp. 468-469.
- [20] H. Goto, "Double Stator Axial-Flux Switched Reluctance Motor for Electric City Commuters," in *2018 International Power Electronics Conference (IPEC-Niigata 2018 -ECCE Asia)*, 2018, pp. 3192-3196.
- [21] E. Cosoroaba, E. Bostanci, Y. Li, W. Wang, and B. Fahimi, "Comparison of winding configurations in double-stator switched reluctance machines," *IET Electric Power Applications*, vol. 11, no. 8, pp. 1407-1415, 2017.



# Definition of a Strategy for an Axial Flux Switched Reluctance Machine Torque Control

Aritz Egea, Gaizka Ugalde, Javier Poza

## 6.1. Introduction

In the transition towards a new era of low-carbon society and climate resilient economy, one of the European Union's key policy objectives for the upcoming decades is cutting 60% of CO<sub>2</sub> emissions from transport, where fossil fuel dependence is around 96%. Electric vehicles (EV) are considered to be the most plausible alternative to fossil fuel-based road transport. There is a source of uncertainty related to the availability of reliable and diversified supply of metals to produce the necessary permanent magnets (PM) to assure high efficiency and high-power density electrical motors. The shift from a fossil fuel dependence scenario to a permanent-magnet dependence scenario (even more critical as they can only be found under single source monopolies) could limit significantly the large-scale introduction of EVs as PM based motors could not be supplied in adequate volumes at a competitive cost.

In this context, the development of high efficiency motors using magnet-free motor designs is crucial. A promising option for this new generation of electric motors could be reluctance technology: this kind of motors stands out for its wide constant power capability, reliability and security. However, it has been left out of the first line up to now due to its lower power density when compared to PM motors.

On the other hand, the use of axial-flux configurations has proved recently in PM motors that power density can be increased in a relatively cost-effective way.

VENUS European project Consortium is working in a design that combines both approaches, reluctance motors in axial-flux configuration, Axial Flux Switched Reluctance Motor (AFSR). The topology selected was first presented by Labak [1, 2] and the designed motor for VENUS project will be constructed and integrated in an electric vehicle in the future.

Even if some authors proposed different analytical models for switched reluctance machines [3, 4], the intrinsic nonlinearity of this type of machines makes use of finite element almost unavoidable [5, 6]. Once the machine is characterized by FEM tools may be simulated using Matlab Simulink [7, 8].

The SRM machines by nature present a quite high torque ripple bringing a challenge for the definition of the control strategy in applications where this ripple may be critical. Different strategies have been proposed in the literature. For example, Dong-Hee Lee [9] presents an extended work about SRM control while Husain [10], gives a general view of SRM machine torque ripple minimization. Peter [11] and Lee [12] also give some notes for reduction of the torque ripple.

In this chapter, the torque control strategy for the designed machine is presented [14]. This control is separated in two different actions, one for low speed operation and the other for higher speed operation. The aim of using two different actions is to improve the driving experience but reducing the computational load of the control board.

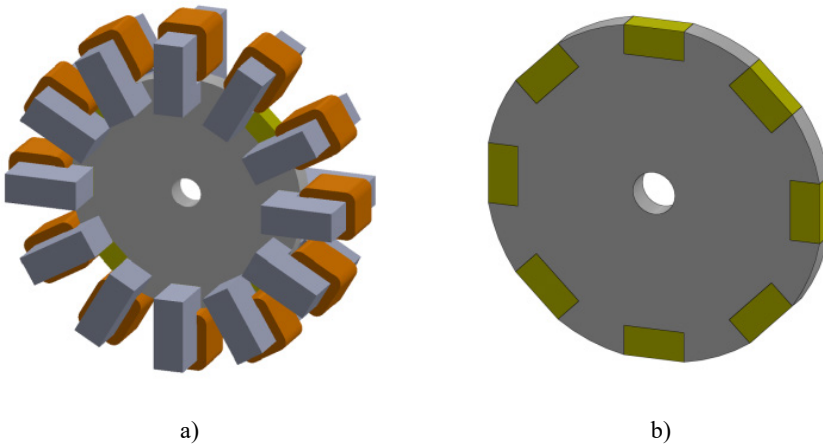


Fig.1: a) Rotor and stator arrangement by using axial-flux configuration and b) rotor detail [13]

## 6.2. Axial-Flux Switched Reluctant Motor model

### A. Axial-Flux Switched Reluctant Motor

**Fig.1** shows the geometry of the AFSRM used in this work. The motor comprises a rotor disc carrying 8 rotor poles and 12 stator coil assemblies placed on the periphery of the rotor disc.



## B. Electrical Equations

Usually a simplified model of the SRM motor is used, as assuming the non-linearity of the inductance is not so easy analytically. The main electrical equation of a SRM machine is the one described in (6.1) expression.

$$V(t) = R_{ph}i(t) + \frac{d\psi(\theta, i)}{dt} \quad (6.1)$$

The voltage in each phase (V) is the sum of the voltage drop in the phase resistance  $R_{ph}$  and the flux linkage derivative as a function of the position and the current. Due to the non-linearity of the inductance, a simple mathematical expression cannot describe the current trajectory. Therefore, the flux linkage derivative can be split into two terms:

$$\frac{d\psi(\theta, i)}{dt} = \frac{d\psi(\theta, i)}{di} \frac{di}{dt} + \frac{d\psi(\theta, i)}{d\theta} \frac{d\theta}{dt} \quad (6.2)$$

The first term in (6.2) assumes the current time derivative and the inductance that is a function of the position and the current:

$$\frac{d\psi(\theta, i)}{di} \frac{di}{dt} = L(\theta, i) \frac{di}{dt} \quad (6.3)$$

The second term in (6.2) is also known as the back emf. This emf is a function of the rotational speed, the current and the inductance change:

$$emf = \frac{d\psi(\theta, i)}{d\theta} \frac{d\theta}{dt} = \frac{dL(\theta, i)}{d\theta} \omega i(t) \quad (6.4)$$

So, expression (6.1) can be rewritten as follows:

$$V(t) = R_{ph}i(t) + L(\theta, i) \frac{di}{dt} + \frac{dL(\theta, i)}{d\theta} \omega i(t) \quad (6.5)$$

Equation (6.5) shows clearly that a mathematical model of a SRM machine is not easy to develop. The evolution of the current is not an easy task to describe and neither the inductance value, as it is dependent of the current and the position.

## C. Torque production

In case of a linear machine, the inductance value has a trapezoidal shape as shown in **Fig. 2**. Depending on the current activation moment, the machine may work at motoring or regeneration. Ideally, the current is established instantaneously. If the current is activated while the inductance is increasing, so when the rotor pole is getting closer to the stator pole, the generated torque is positive. On contrary,

when the rotor pole is moving from aligned to unaligned position the torque is negative.

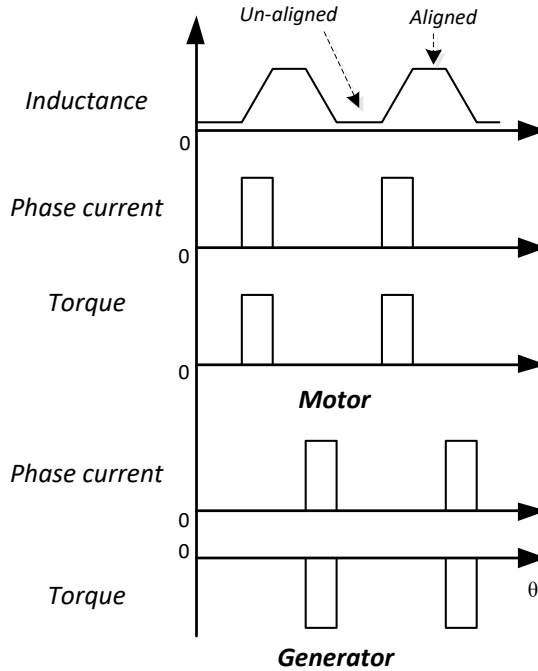


Fig.2: Inductance and torque profile [11]

This figure makes clear the importance of the current activation time. The maximum torque per phase is obtained if the current is activated just when the inductance starts increasing (unaligned position) and deactivated at maximum value of inductance (aligned position). In any other case, the average torque will be decreased. If the current activation time is shorter, the torque will decrease, while if it is longer negative torque will be produced. This all shows the importance of switching on and switching off the current at the right moment.

In case of a linear SRM machine, the electromagnetic torque,  $T_e$ , can be expressed as:

$$T_e = \frac{1}{2} i^2 \frac{dL}{d\theta} \quad (6.6)$$

This expression is only valid with a linear inductance. A general expression valid also in case of a non-linear inductance is when the electromagnetic torque is obtained from the co-energy,  $W'$ :

$$T_e(t) = \frac{dW'}{dt} \quad (6.7)$$

The co-energy is the integration of the flux linkage along the current:

$$W'(I, t) = \int_0^i \Psi(i, t) di \quad (6.8)$$

In **Fig. 3** the energy and co-energy concept is explained in a graphical way. The shown flux linkage follows a non-linear behavior, which results in a higher mechanical energy than the energy storage in the inductance. In case of a linear inductance (flux linkage) both energies are equal making the expression (6.7) valid.

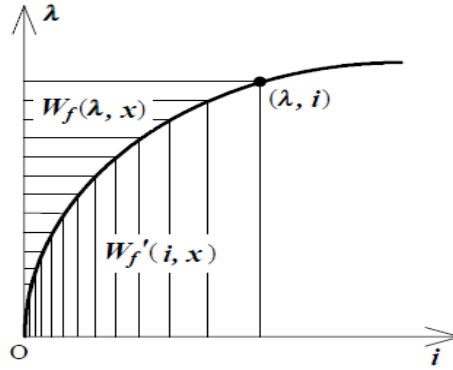


Fig.3: Energy and co-energy

#### D. Non-Linear model

At the proposed SRM model, the input of the machine is the stator voltage, while the outputs are the torque, position and speed. Integrating the input voltage, the flux in each phase is obtained. Having this flux and the rotor position, it is possible to get the instantaneous current in each phase from tables calibrated previously with FEM simulation, analytical model or experimental result. A torque characteristic as function of the current and the rotor position must be also obtained. The electromagnetic torque is the input of the mechanical model from where the mechanical torque, speed and position are obtained.

In this project, the non-linear model is implemented in Matlab /Simulink. The electromagnetic model is based in a torque and current map. FEM-3D simulations are needed to get these torque vs. current and position, and current vs. flux and position maps. Then including this maps in the electromagnetic model shown in **Fig. 4** it is possible to have a SRM machine model assuming the non-linearity.

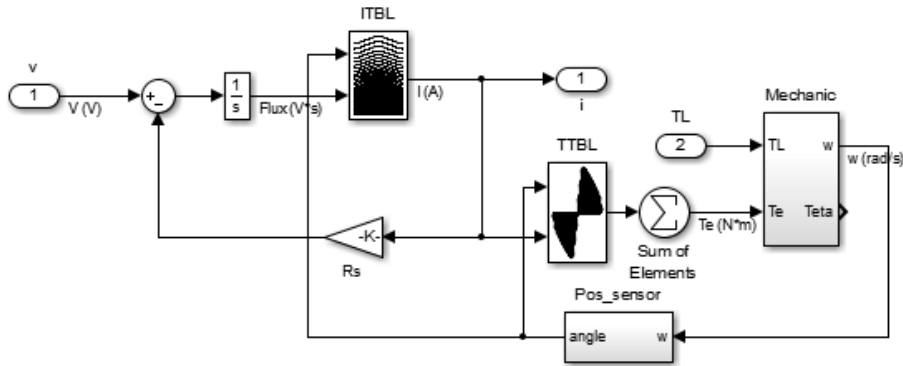


Fig.4: SRM Matlab-Simulink model [13]

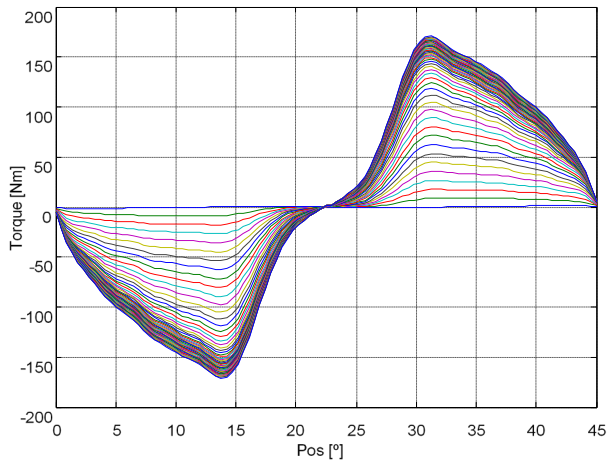


Fig.5: Torque vs. Current and position curves (Each curve corresponds to a current level, starting at 0A and reaching 910A) [13]

The modularity of this motor topology makes phases to be magnetically decoupled, thus motor performance can be extrapolated from the analysis of one pole pair and considering the number of active phases and poles. As the motor has three-phases, only one of them should be simultaneously active to generate torque in one direction. With 12 stator poles in the motor, there are 4 poles per phase. Therefore, motor parameters (torque, losses, etc.) are 4 times higher than in one pole.

FEM-3D simulations get accurate curves of switched reluctance motor's characteristic (flux vs. current, and torque vs. position). In these FEM-3D magneto static simulations a unique C-core together with three rotor poles is simulated. Three rotor poles are simulated so the influence of the adjacent poles in the flux lines

can be considered. The coil in the C-core is fed with different current levels and a movement from  $0^\circ$  to  $45^\circ$  is performed to take a complete torque cycle. From these simulations torque (**Fig. 5**) and flux linkage curves are obtained so then dynamic simulations may be performed in Matlab Simulink software.

### 6.3. Torque Control Strategy

The general view of the system is shown in **Fig. 6**. The control is based on two main loops, the current and torque loops

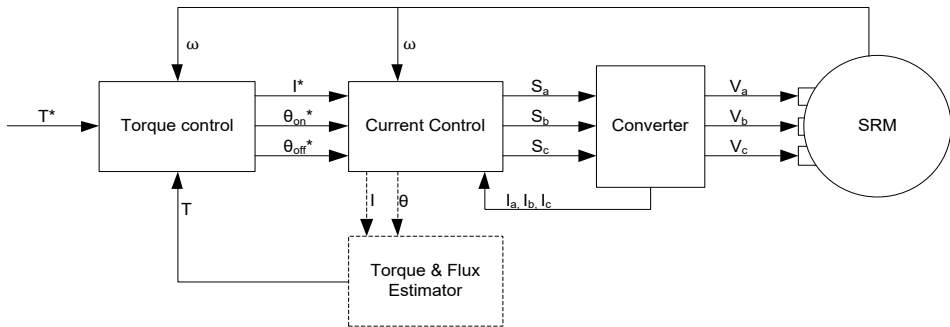


Fig. 6: Controlled SRM flow diagram [13].

The current loop gives gate signals to the converter considering the current consign the actual current and the activation/deactivation angles. A simple on/off control proves to be sufficient for the current loop.

The torque control generates the signals for the current control depending on the rotational speed, the torque consigns and the torque estimator. The proposed torque control strategy includes a direct torque control for higher speeds and a PI control for the lower speeds as shown in **Fig.7**. The direct torque control is based in a previous characterization of the machine to get a characteristic function, which gives the current consign depending on the speed and the torque consign. This control will give a constant current consign with which a main torque equal to the consign torque will be generated. However, the torque ripple is not controlled this way, and it could be quite dangerous when starting the vehicle in a slope. Due to the ripple, a negative momentary negative torque may occur making the vehicle move in reverse direction. To avoid this problem along with uncomfortable vibrations a PI controller may be use at low speeds. The PI controller generates a current consign from the error between the torque consign and the real torque. As a torque sensor is not used the actual torque must be estimated

using a torque estimator. This estimator is obtained when characterizing the machine. The torque is represented as a function of the currents and the position (**Fig.5**).

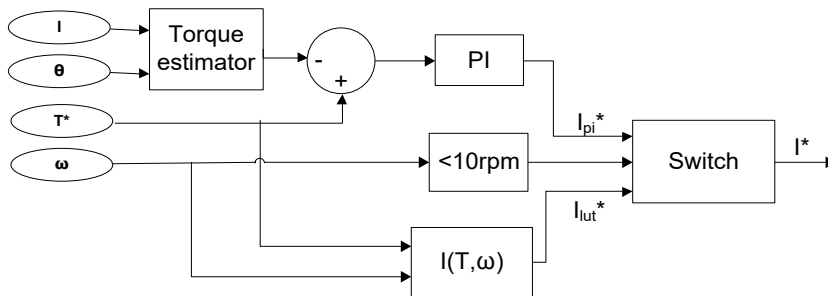


Fig. 7: Torque control strategy [13].

As explained before due to the impossibility to set the current instantaneously the dynamic performance of the AFSRM varies from the static one.

In static mode or with ideal square form current the maximum torque is obtained when the phase is activated from  $22.5^\circ$  to  $45^\circ$ . However, the current needs some time to be established. The activation and deactivation signals must be given in advance, so the maximum possible torque is given. In Table I and Table II the optimal activation and deactivation angles are shown.

TABLE I: PHASE ACTIVATION ANGLE DEPENDING ON THE SPEED AND CURRENT

A/rpm	0	1000	2000	3000	4000	5000	6000	7000
50	22,5	22,0	21,6	21,1	20,6	20,2	19,7	19,2
150	22,5	21,0	19,5	18,0	16,5	15,0	13,5	12,0
250	22,5	19,9	17,3	14,6	12,0	12,0	12,0	12,0
350	22,5	19,5	16,5	13,5	12,0	12,0	12,0	12,0
450	22,5	19,0	15,5	12,0	12,0	12,0	12,0	12,0

TABLE II: PHASE DEACTIVATION ANGLE DEPENDING ON THE SPEED AND CURRENT

A/rpm	0	1000	2000	3000	4000	5000	6000	7000
50	45,0	44,2	43,4	42,6	41,8	41,0	40,2	39,4
150	45,0	43,2	41,4	39,6	37,8	36,0	36,0	36,0
250	45,0	42,8	40,5	38,3	36,0	36,0	36,0	36,0
350	45,0	42,4	39,9	37,3	36,0	36,0	36,0	36,0
450	45,0	42,0	39,0	36,0	36,0	36,0	36,0	36,0

As it can be deduced the higher the speed and the current are, more critical this phenomenon is. In **Fig. 8** the maximum torque the machine gives depending on the speed and the current is shown. The torque generated by the machine is reduced markedly with increasing speed.

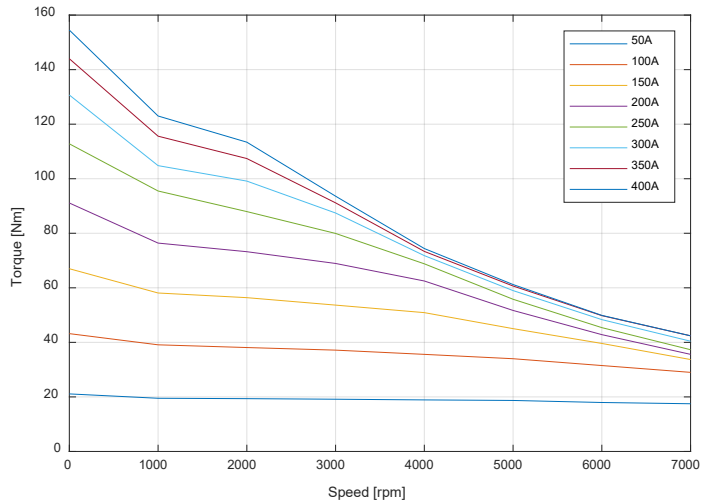


Fig. 8: Dynamic torque performance [13]

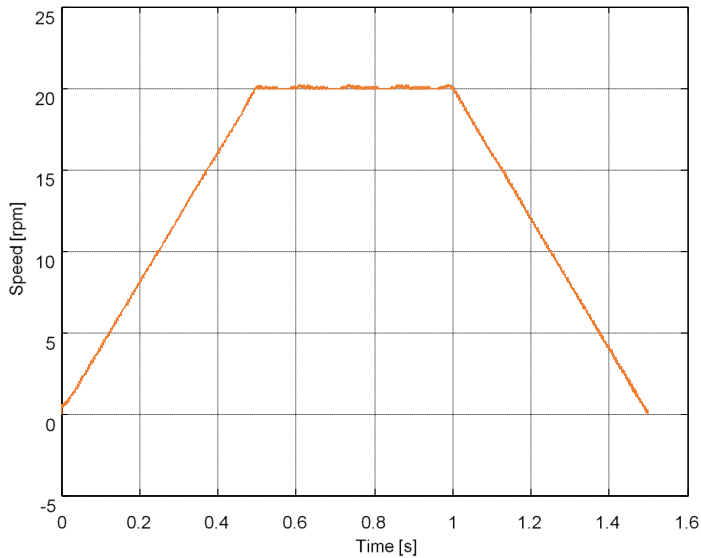


Fig.9: Acceleration-deceleration speed profile [13]

## 6.4. Machine Performance

### A. Simulations

To check the validity of the proposed method by simulations the machine is rotated at between 0 and 20 rpm speed as defined in **Fig. 9** while a constant torque consign of 48Nm is set. When the rotational speed is less than 10 rpm a PI torque control is performed, while over this threshold the direct torque control is working obtaining the torque evolution shown in **Fig. 10**. It is easily noticeable how the torque ripple of  $\pm 10\text{Nm}$  is eliminated when using the PI controller. This happens because the current consign is changing all the time when the PI is activated, while a constant current consign is generated with the direct torque controller as may be seen in **Fig. 11**.

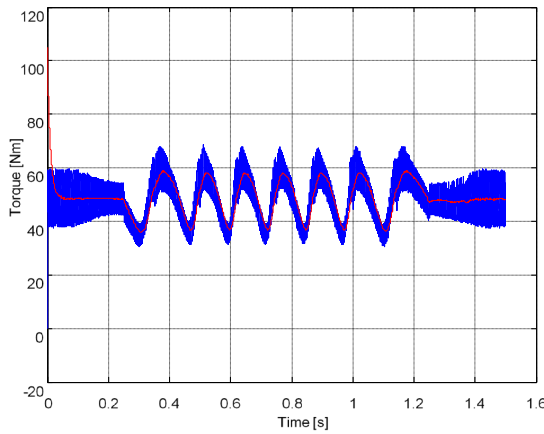


Fig. 10: Torque time waveform [13]

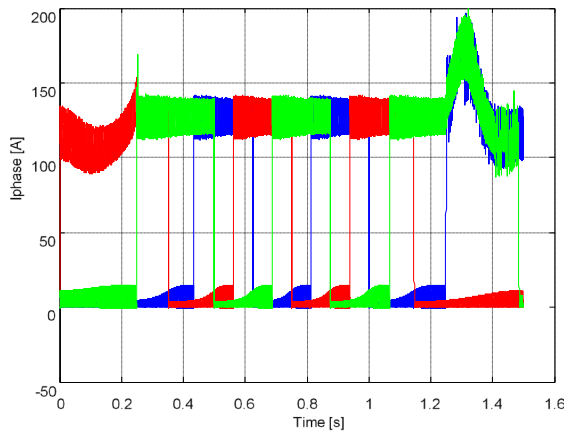


Fig. 11: Three phase current waveforms [13]



The PI controller presents better performance in terms of torque ripple minimization and even following the torque consign. However, this is very dependent on the current reading sample time capability and the needs of the control board. Furthermore, using a PI controller the torque capability is reduced. Therefore, the combination of control methods proposed in this work is considered a good option, where accuracy, behavior and computational speed are combined.

## B. Test Bench

After simulation, and once having the motor prototype experimental tests were carried on in the test bench shown in **Fig. 12**. First stall or static characteristic of the machine was obtained supplying the machine with a DC current supply. Then dynamic tests were done so both the machine dynamic performance and the control strategy were validated.

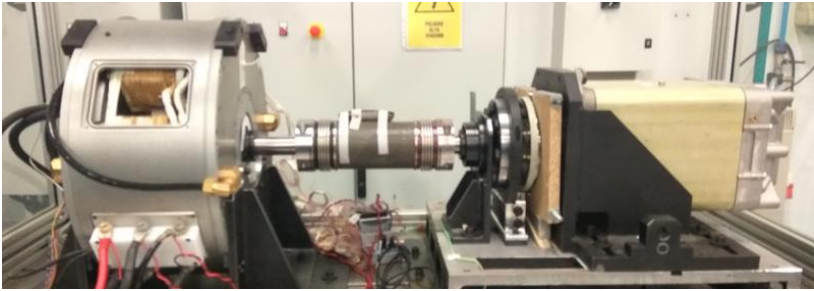


Fig. 12: Test Bench

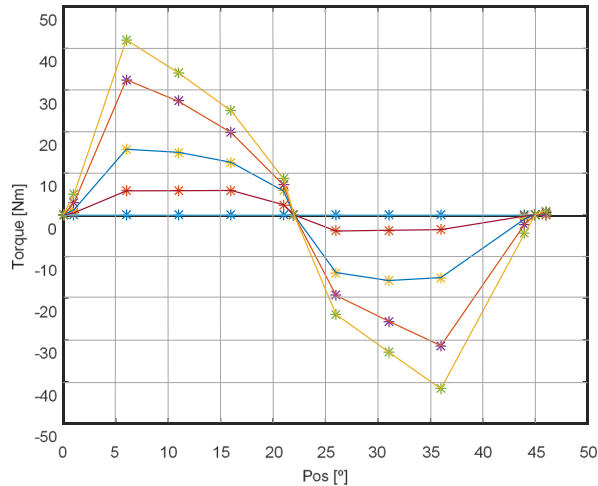


Fig. 13: Experimental points of Torque VS current static characteristic (Phase maximum current 130 A DC)

**Fig. 13** shows the experimental test points of the Torque Vs current static characteristic of the VENUS motor. Due to the power limits of the DC current supply equipment, the maximum testing current level has been established at 130A.

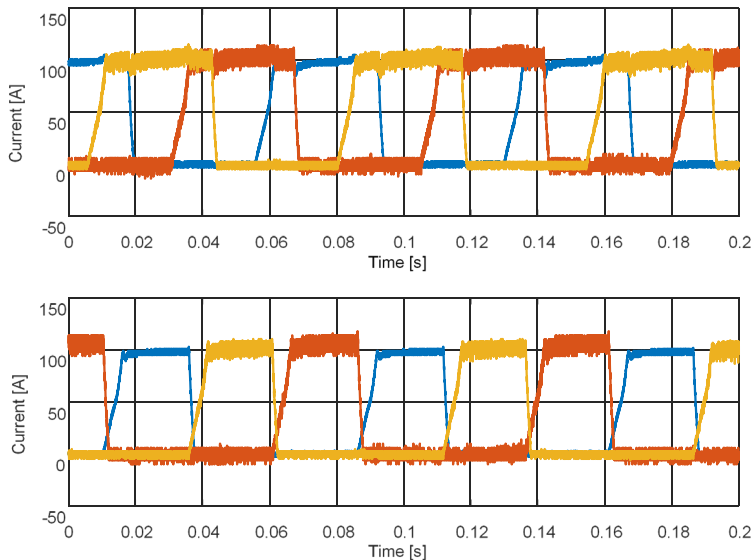


Fig. 14: Resulting currents of each phase for the case of 100 A controlled at both control modes, overlapping (up) and none overlapping (down)

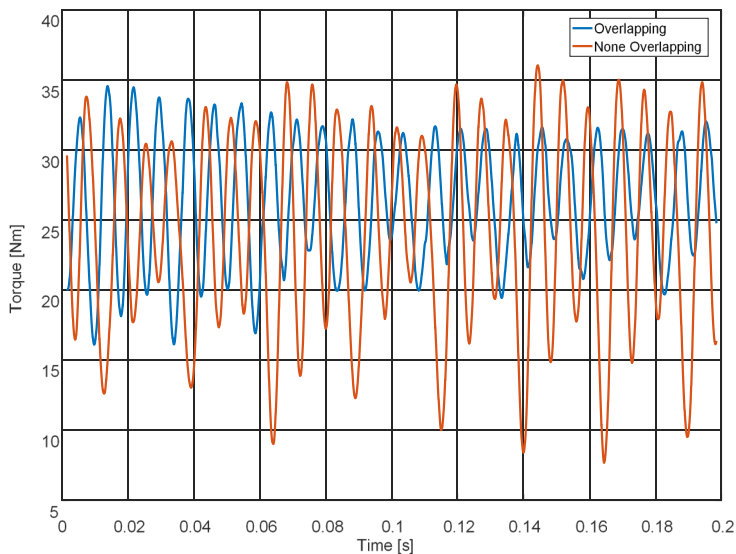


Fig. 15: Torque @100A, Overlapping and none overlapping

The first task to obtain the best dynamic performance of the machine is to compute turn ON/OFF angles at each current and speed working point. The main objective is to get the maximum torque possible at each current and speed reference point. It is also necessary to validate that the dynamic evolution of the phase currents is good. This is a key point to assure that the maximum peaks values do not go above the protection limits.

The optimization has been done for the two operation mode strategies, **Fig. 14** and **Fig. 15**:

1. No overlapping Strategy: The phase currents do not have a common area of constant current value at top set point level.
2. Overlapping Strategy: The phase currents have a common area of constant current value at top set point level.

The optimization of the ON/OFF angles is based in an iterative process, for each strategy (overlapping and no overlapping) and speed and current level:

1. The control is test with the theoretical ON/OFF values obtained from the simulations of the control design task.
2. An iterative adjustment of the ON/OFF angles is done around the initial values searching the maximum torque value per ampere.
3. The current waveform is checked. In case of high currents peaks, these angles are discarded going back to point 2.

Next, some examples of the current shape with the optimized points for the non-overlapping strategy are shown in **Fig. 16** and **Fig. 17**. For the overlapping strategy, similar dynamic performances are obtained.

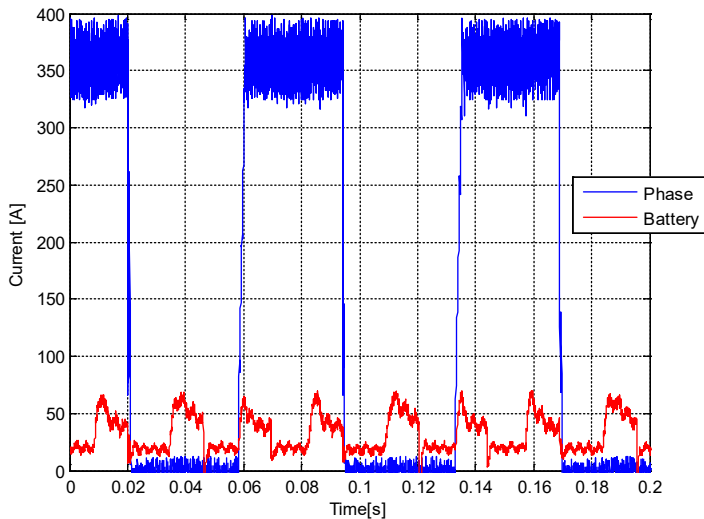


Fig. 16: Phase current waveform & battery current waveform (@Torque 1pu & Speed 100rpm)

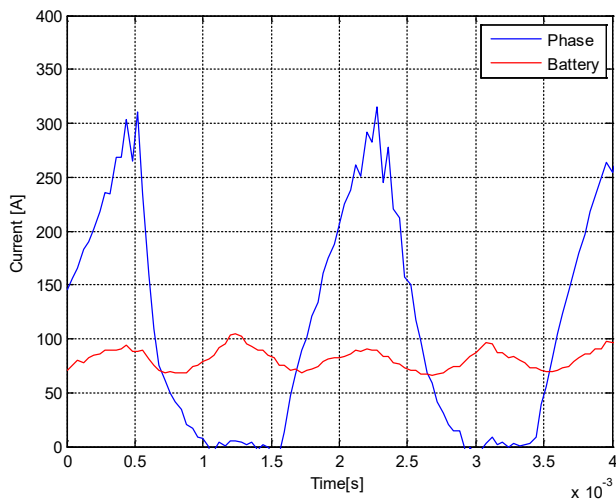


Fig. 17: Phase current waveform & battery current waveform (@Torque 0.6pu & Speed 4000rpm)

Once the on/off angles are optimized and the PI controller is set for low speeds, the dynamic performance of the machine is obtained as shown in Table III. At low speed / low torque demand, the system is able to give the desired torque but, at higher speeds and torque demand the given torque is reduced as predicted.

TABLE III: MEASURED TORQUE (PU) AT DIFFERENT TORQUE REFERENCE SET-POINTS

PU\rpm	100	1000	2000	3000	4000
<b>0.2</b>	0.21	0.21	0.20	0.20	0.2
<b>0.6</b>	0.62	0.61	0.61	0.6	0.6
<b>1</b>	1	0.98	0.90	0.78	0.6

## 6.5. Conclusions

The results of the proposed torque control strategy, which combines a torque feedback control for low speeds and a direct current, consign generator for higher speeds show its validity.

At lower speeds where torque ripple may be critical, mostly when accelerating from zero speed a prominent ripple can lead to an uncomfortable driving experience due to vibrations. Even more critical may be when starting in a slope; the vehicle may go in reverse direction due to a negative torque caused by the ripple. This all is avoided as shown in the results using a PI control at low speeds.

At higher speeds, the ripple vibration is not so noticeable by the vehicle occupants as the inertia may absorb it, so a direct current consign generation show to be enough.

The main difficulty of this control is that the characterization of the electrical machine will define the effectivity of the control. However, his work has shown that obtaining the torque and inductance characteristic of the machine is an easy task, leading to a proper control.

The optimal on/off switching angles calculated in simulation give a good reference for the experimental setting of the actual optimal switching points. However, these points must be slightly changed so the torque per ampere ratio is maximized.

## 6.6. References

- [1] Labak and N. C. Kar, "A Novel Five-Phase Pancake Shaped Switched Reluctance Motor for Hybrid Electric Vehicles," Vehicle Power and Propulsion Conference, 2009. VPPC '09. IEEE, Dearborn, MI, 2009, pp. 494-499.
- [2] A. Labak and N. C. Kar, "Designing and Prototyping a Novel Five-Phase Pancake-Shaped Axial-Flux SRM for Electric Vehicle Application Through Dynamic FEA Incorporating Flux-Tube Modeling," IEEE Transactions On Industry Applications, Vol. 49, No. 3, pp. 1276-1288, May-June 2013.
- [3] Horacio Vasquez, Joey K Parker, "A New Simplified Mathematical Model for a Switched Reluctance Motor in a Variable Speed Pumping Application". Mechatronics, Volume 14, Issue 9, November 2004, Pages 1055-1068, ISSN 0957-4158
- [4] S. Smaka, S. Masica and M. Cosovic, "Fast Analytical Model of Switched Reluctance Machine," Power Electronics Conference (IPEc-Hiroshima 2014 - Ecce-Asia), 2014 International, Hiroshima, 2014, pp. 1148-1154.
- [5] P. Lobato, S. Rafael, P. Santos and A. J. Pires, "Magnetic Characteristics Modelling for Regular Switched Reluctance Machines: Analytical and FEM Approaches," Power Engineering, Energy and Electrical Drives, 2009. POWERENG '09. International Conference on, Lisbon, 2009, pp 60-65.
- [6] B. Parreira, S. Rafael, A. J. Pires And P. J. C. Branco, "Obtaining The Magnetic Characteristics of an 8/6 Switched Reluctance Machine: from FEM Analysis to the Experimental Tests," IEEE Transactions On Industrial Electronics, Vol. 52, No. 6, pp. 1635-1643, Dec. 2005. DOI: 10.1109/Tie.2005.858709
- [7] H. Le-Huy and P. Brunelle, "A Versatile Nonlinear Switched Reluctance Motor Model in Simulink using Realistic and Analytical Magnetization Characteristics," Industrial Electronics Society, 2005. IECON 2005. 31st Annual Conference of IEEE, 2005.

- [8] F. Soares and P. J. Costa Branco, "Simulation of a 6/4 Switched Reluctance Motor Based on Matlab/Simulink Environment," IEEE Transactions On Aerospace And Electronic Systems, Vol. 37, No. 3, Pp. 989-1009, Jul 2001.
- [9] Dong-Hee Lee (2011). "Advanced Torque Control Scheme for the High Speed Switched Reluctance Motor". Advances in Motor Torque Control, Dr. Mukhtar Ahmad (Ed.), ISBN: 978-953-307-686-7, INTECH, DOI: 10.5772/20701.
- [10] I. Husain, "Minimization of Torque Ripple in SRM Drives". IEEE Transactions on Industrial Electronics, Vol. 49, No. 1, pp. 28-39, Feb 2002.
- [11] J. Peter, "Modeling & Torque Ripple Minimization of Switched Reluctance Motor for High Speed Applications" International Journal of Science and Modern Engineering (IJISMe) ISSN: 2319-6386, Volume-1, Issue-10, September 2013
- [12] Jin Woo Lee, Hong Seok Kim, Byung Il Kwon And Byung Taek Kim, "New Rotor Shape Design for Minimum Torque Ripple of SRM Using FEM". IEEE Transactions on Magnetics, Vol. 40, No. 2, pp. 754-757, March 2004.
- [13] A. Egea, G. Ugalde and J. Poza, "Torque Control Strategy for an Axial Flux Switched Reluctance Machine," 2016 XXII International Conference on Electrical Machines (ICEM), Lausanne, 2016, pp. 1215-1220.  
DOI: 10.1109/Icelmach.2016.7732679
- [14] A.Egea, G. Ugalde, J.Poza. "Torque control strategy for an axial flux switched reluctance machine". Workshop on SRM drives an alternative for E-Traction. February 2, 2018. Vilanova I la Geltrú (Spain)

# Novel In-Wheel Double Rotor Axial-Flux SRM Drive for Light Electric Traction

Pere Andrada, Balduí Blanqué, Eusebi Martínez,  
José I. Perat, José A. Sánchez, Marcel Torrent

## 7.1. Introduction

Light electric vehicles (LEVs) can be categorized as L vehicles in accordance with Directive 2007/46 /EC of the European Union (EU) [1]. This category of vehicles comprises two-, three- and four-wheeled vehicles with limited weight (maximum 550 kg) and power (maximum 15 kW). Light electric vehicles contribute to improving mobility and reducing the emissions of pollution and greenhouse gases, which is desired by both government authorities and citizens. These vehicles are generally more affordable than cars and, given their smaller size, they can be parked in small spaces while also helping to reduce traffic congestion. As a result of these advantages, LEVs currently lead in global electric vehicle sales, a market that is expected to grow from 9.3 trillion dollars in 2017 to 23.9 trillion dollars in 2025. China and especially other countries in Asia (Indonesia, Vietnam, Japan and India) are the markets where the highest growth is expected [2]. More moderate growth is anticipated for Europe and the USA, and it will depend not only on more attractive models emerging, but also the enactment of government policies that will restrict the use of internal combustion vehicles. LEVs are powered by an electric drive (motor + electronic power converter + control) that ranges between 2-10 kW of power and they are supplied by means of a battery pack (Pb-Acid, Li-Ion) with voltages of between 36 and 100 V. There are two different types of electric drives for LEVs: direct drives, in which the motors are located inside the wheel or wheels (in-wheel motor or hub motors) and drives with a mechanical transmission (gears, toothed belts or chains) between the motor shaft and the wheel [3]. Although in-wheel motor drives have some drawbacks, such as an increase in unsprung mass that

deteriorates ride comfort, some of their advantages are the elimination of a mechanical transmission and the provision of more useful space in the vehicle.

Nowadays, the most usual in-wheel motors are brushless DC motors and permanent magnet synchronous motors with external rotors. Nevertheless, switched reluctance motors constitute a promising alternative because of their rugged construction and lack of permanent magnets. Rotary switched reluctance machines (SRM) are usually radial flux machines in which the air-gap flux flows mainly in the radial direction relative to the axis of rotation. This type of SRM usually has a cylindrical shape with a stator and rotor that are most commonly internal but can also be external. Less common among rotary switched reluctance machines is the axial flux SRM, in which the air-gap flux flows mostly parallel to the axis of rotation. The stator and rotor are arranged in parallel plates perpendicular to the axis of rotation. Some studies on axial flux switched reluctance motors demonstrate that this type of machine can obtain higher torque density than radial flux switched reluctance machines. These superior features of the axial flux switched reluctance machine are due to the increase in air-gap area, which depends on the diameter of the machine; whereas the air-gap area in radial type machines depends on the machine's length.

The first axial-flux variable reluctance motor was reported by Unnewher and Koch in 1973 [4], while in recent years some authors have made important contributions to developing axial-flux switched reluctance machines. Arihara et al. have presented the basic design methodology for the axial counterpart of the classic rotary SRM [5]. Murakami et al. have studied the optimization of an axial-flux 18/12 SRM [6]. Madhavan et al. have contributed to developing the axial counterpart to a rotor segment SRM in a machine comprising two rotors and a stator with toroidal type winding [7]. Labak et al. have proposed a novel multiphase pancake shaped SRM with a stator composed of a series of C-cores, each with an individually wound coil, perpendicularly disposed to an aluminum rotor, in which a suitable number of cubes, the rotor poles, of high permeability material have been added. Torque is produced in this machine by the tendency of these cubes to align with the two poles of an energized C-core [8]. Some authors have detailed the manufacturing problems of these machines and proposed building its magnetic circuit with different materials such as grain oriented electrical steel (Ma et al. [9]), soft magnetic composites (Kellerer et al. [10]) and sintered lamellar soft magnetic composites (Lambert et al. [11]).

This chapter presents a summary of the authors' work [12-15, 19] on a new axial-flux switched reluctance machine (AFSRM) using a particular distribution of stator and rotor poles, which results in short flux paths without flux reversal and an electronic power controller specially intended for the propulsion of LEVs.



## 7.2. Description of the proposed AFSRM

### A. Basic considerations

In this chapter a novel axial-flux SRM (AFSRM) with a stator sandwiched between two rotors has been designed for LEVs. It is a particular case of a three-phase machine, with multiplicity equal to two, of the family of axial-flux SRMs presented in [12]. **Fig.1** provides a schematic view of the proposed AFSRM. The stator and rotors are arranged in parallel planes that are perpendicular to the rotation axis. Each rotor is separated from the stator by an air-gap. Both rotors are formed by a number of poles,  $N_R$ , that are all joined together on the opposite side of the air-gap by means of a flat annular piece. The rotor poles and flat annular piece are made of ferromagnetic material. The stator is formed by a number of poles,  $N_S$ , protruding and with the same length at both ends of a supporting disk that is attached to a hollow shaft. The cross section of the stator pole is triangular, although other shapes are possible. The poles are made of ferromagnetic material and the structural disk of a nonmagnetic material.

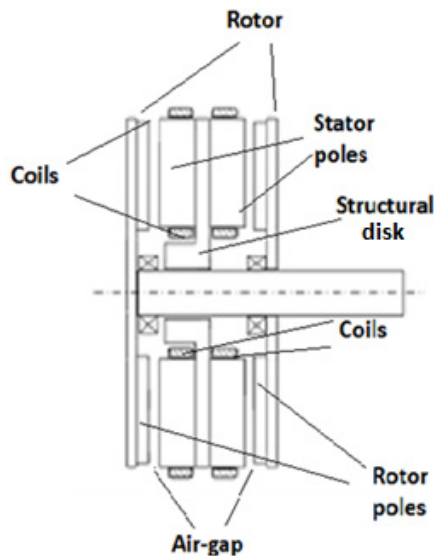


Fig.1: Schematic view of AFSRM

Two coils are wound around the opposite ends of the stator poles and are connected in series. The coils of two adjacent stator poles are also connected in series forming a double electromagnet,  $Z$ . The numbers of double electromagnets, stators and rotor poles will be given according to the number of phases of the machine,  $m$ , in agreement with the following relationships:

$$Z = k m \quad (7.1)$$

where  $k$  is an integer denominating multiplicity, that is, the number of working stator pole pairs. In the case of  $k > 1$ , the phase windings are obtained by properly connecting the  $k$  different double electromagnets of each phase. In any case, the terminals of the phase windings are led through the hollow shaft and out of the machine.

The number of stator poles,  $N_s$ , is given by:

$$N_s = 2Z = 2km \quad (7.2)$$

Both rotors have a number of rotor poles,  $N_R$ , that have to accomplish the following rule:

$$N_R = k(2m - 1) \quad (7.3)$$

The angle,  $\gamma$ , between the axes of two consecutive double electromagnets in the stator is given by:

$$\gamma = \frac{360^\circ}{Z} \quad (7.4)$$

And the angle,  $\alpha$ , between two rotor poles is equal to:

$$\alpha = \frac{360^\circ}{N_R} \quad (7.5)$$

Therefore the angle,  $\delta$ , between the axes of the stator poles of two consecutive double electromagnets is:

$$\delta = \gamma - \alpha = \frac{360^\circ \cdot (N_R - (k \cdot m))}{k \cdot m \cdot N_R} \quad (7.6)$$

In **Fig. 2**, the disposition of the aforementioned angles ( $\alpha$ ,  $\gamma$  and  $\delta$ ) in the stator and rotor is depicted.

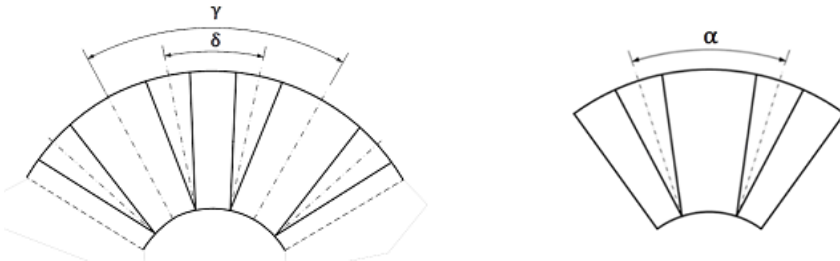


Fig. 2: Disposition of the double electromagnets in the proposed AFSRM: stator (left), rotor (right)

**Fig. 3** shows the flux path when a current flows through the coils of a double electromagnet. The flux lines link the stator poles of both sides with the poles of the two rotors, thus forcing the alignment of these poles without flux reversal.

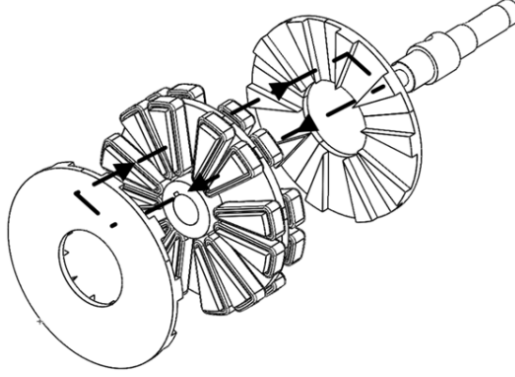


Fig. 3: View of the flux path in one double electromagnet

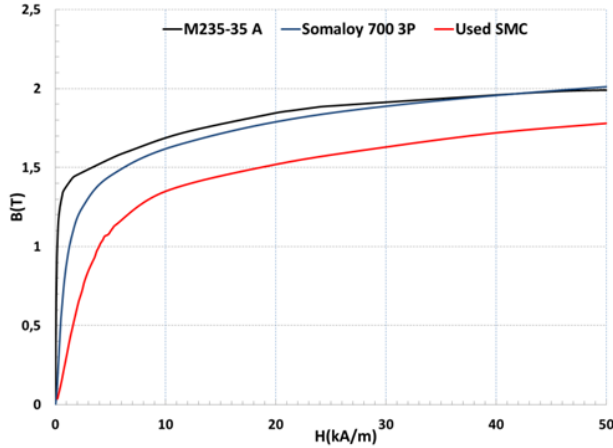


Fig. 4: Comparison of B-H curves between M235-35A, Somaloy 700 3P and the SMC used in this study.

## B. Magnetic material considerations

The proposed AFSRM's magnetic circuit is difficult to construct using silicon iron laminations, which is why this machine's magnetic parts for the stator and rotors were made of SMC (Soft Magnetic Composites) [16-18]. SMC are iron powder particles separated by an electrically insulated layer. The benefits of SMC are: a unique combination of magnetic saturation; low eddy current losses; 3D-flux-carrying capability; and cost-efficient production of 3D-net-shaped components due to the powder metallurgy process. However, SMC has low

induction of saturation and higher specific losses than the silicon iron steels that are commonly used in high-performance electric machines, such as the M235-35A. Somaloy 700 3 P was our first choice, due to its high magnetic characteristics. However, in the end, practical and economic factors informed our decision to manufacture the stator and rotor pole pieces of the AFSRM by tooling pre-fabricated SMC blanks with lower magnetic characteristics than Somaloy 700 3 P. Here, we refer to this material as "used SMC". **Fig. 4** compares the B-H curves of both SMC materials with the B-H curve of M235-35 A.

### C. Description of the AFSRM prototype

A prototype of an in-wheel AFSRM with natural cooling was designed with the goal of propelling a direct traction light electric scooter with 13-inch wheels and no transmission. It required a maximum torque of 80 Nm between 0 to 30 km/h ( $\sim 334$  rpm) and a constant power of 2.8 kW between 30 km/h to 18 km/h ( $\sim 1200$  rpm). Due to the machine being placed inside a 13-inch wheel, the maximum external dimensions equal the motor frame's diameter of 308 mm and an axial length of 116 mm. **Fig.5** shows an exploded view of the prototype: a two-rotor three-phase AFSRM with multiplicity two, 12 stator poles and 10 rotor poles.

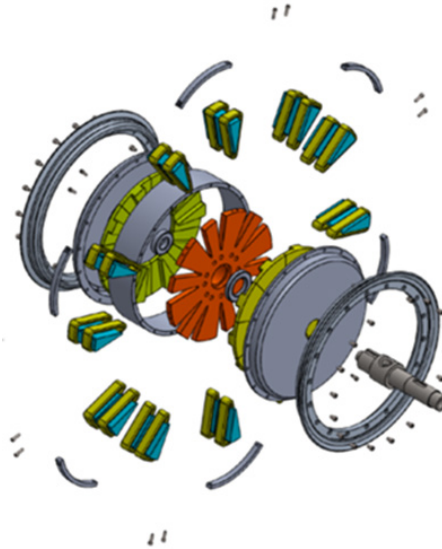


Fig. 5: Exploded view of the AFSRM prototype

The stator poles were made of SMC and inserted into the supporting disk (shown in red in **Fig. 5**). Moreover, the rotor poles and flat annular support were built by a set of 10 independent SMC pieces glued to both covers of the machine. The covers and supporting disk were made of aluminum. **Fig. 6** shows photographs of the stator and rotor pole pieces. A rated voltage of 96 V was

chosen to avoid high current values. Two different alternatives were considered for the winding of the AFSRM prototype, both of which using insulation of thermal class 180°C. First, opposite double electromagnets were connected in series (**Fig. 7**), with  $N_c$  turns per coil and each conductor having two subconductors in parallel each with diameter  $d$ . Second, opposite double electromagnets were connected in parallel (**Fig. 8**), with  $2N_c$  turns per coil and each conductor having a diameter  $d$ . Finally, in order to facilitate the construction of the winding, we chose the second alternative. Each coil was wound with 32 turns and rectangular rather than round wire was used ( $2 \times 2.39 \text{ mm}^2$ ). This solution resulted in a very low skin factor, since the maximum expected frequency of the currents in the machine is 250 Hz (corresponding to a maximum speed of 1500 rpm). Furthermore, this provided a filling factor of 56.4%. **Fig. 9** shows photographs of the stator and the stator poles inserted into the supporting disk, with the disposition of two adjacent pre-wound coils. The measured total phase resistance (20°C) of the winding and the output cable (AWG7) was 60 mΩ.

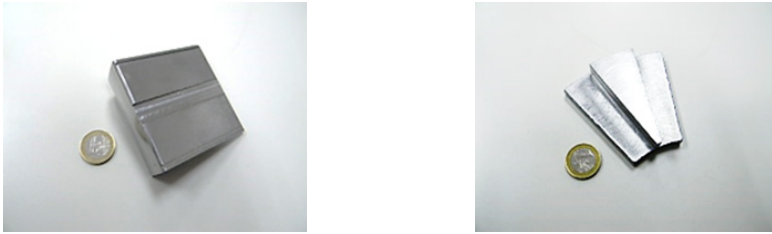


Fig. 6: Stator pole (left) and rotor pole pieces (right), made of SMC

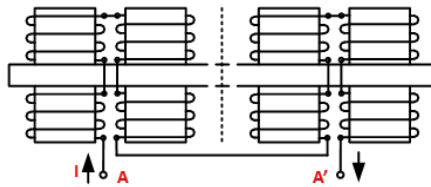


Fig. 7: Schematic drawing of one phase of the AFSRM showing the coil arrangement and the series connection of the double electromagnets that are diametrically opposed

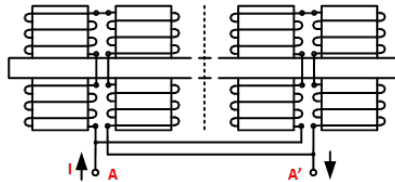


Fig. 8: Schematic drawing of one phase of the AFSRM showing the coil arrangement and parallel connection of the double electromagnets that are diametrically opposed.

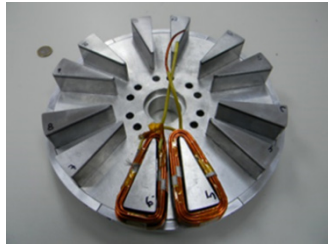
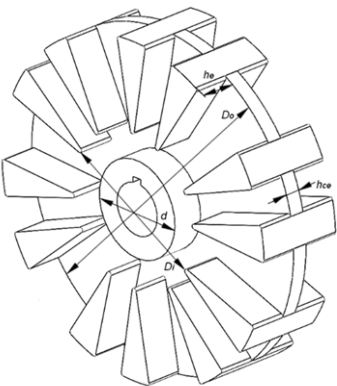


Fig. 9: Stator showing the inserted pole pieces and the disposition of two adjacent coils



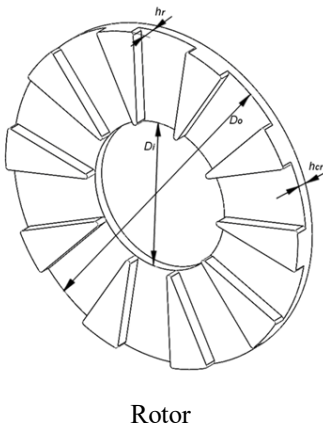
Fig.10: Stator and two motor covers: the central part the SMC rotor pieces glued onto the cover (left); the fully assembled AFSRM prototype (right).

TABLE I. MAIN DIMENSIONS OF THE AFSRM PROTOTYPE



Stator

Parameter	Symbol	Values
Number of phases	m	3
Number of double electromagnets	Z	6
Number of stator poles	N <sub>s</sub>	12
Number of rotor poles	N <sub>R</sub>	10
Angle between rotor poles	$\alpha$	36
Angle between axes of stator poles in the two consecutive double electromagnets	$\delta$	24°
Angle between axes of consecutive double electromagnets	$\gamma$	60°
Output stator/ rotor diameter	D <sub>o</sub>	260 mm



Parameter	Symbol	Values
Inner rotor diameter	$D_i$	117.9 mm
Inner stator diameter	$d$	50 mm
Air-gap	$g$	0.5 mm
Height of protruding stator pole	$h_e$	28.9 mm
Thickness of supporting disk	$h_{ce}$	12 mm
Height of rotor pole	$h_r$	10 mm
Thickness of rotor yoke	$h_{cr}$	8 mm

**Fig.10** provides a view of the complete stator, including the winding and the two covers with the glued rotor pole pieces. Table I indicates the main dimensions of the prototype: a three-phase AFSRM with multiplicity two.

### 7.3. Electronic power controller

Currently, no commercial electronic power controllers exist for light electric traction SRMs. This is one of the causes slowing down the use of SRM as a power traction unit for light electric traction vehicles. In order to overcome this drawback an SRM controller for light electric vehicles was designed and built. Specifically, this controller was conceived for powering any type of low voltage three-phase SRM designed for propelling light electric vehicles [19]. **Fig. 11** depicts a wiring diagram of the SRM controller showing the connection of the power components (battery pack, SRM), of the sensors (speed/position, temperature) and of the driving functions of the vehicle (key switch, throttle, brake, forward/reverse). The controller must handle input voltages of between 36 V up to 100 V from a pack of batteries and should be able to work with a peak current of 400 A for 2 minutes and 150 A RMS for 60 minutes. It has to manage the signals from the SRM sensors (speed/position, current and temperature) and the control inputs/outputs, thus requiring that special attention be paid to communications. It should allow installing external software for controlling the SRM and even connecting it to a HIL (hardware in the loop) platform. In addition, it should be small, compact, safe and ready to work on board a light electric vehicle; therefore, all pertinent regulations should be taken into account. The entire controller should be encased in housing that guarantees IP66 protection.

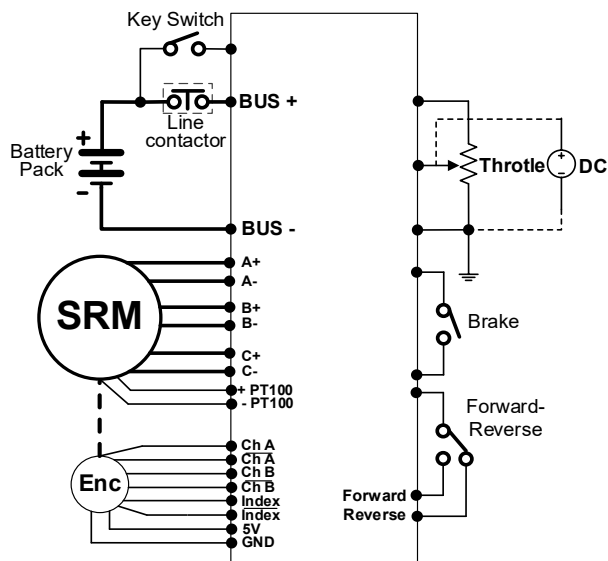


Fig.11: SRM controller wiring diagram.

In order to accomplish the abovementioned specifications, the controller's architecture was designed according to the block diagram shown in Fig.12. In the following sections describe the different parts: electronic power converter, capacitor bank, ancillary parts, printed circuit board, DSP controller and HIL platform.

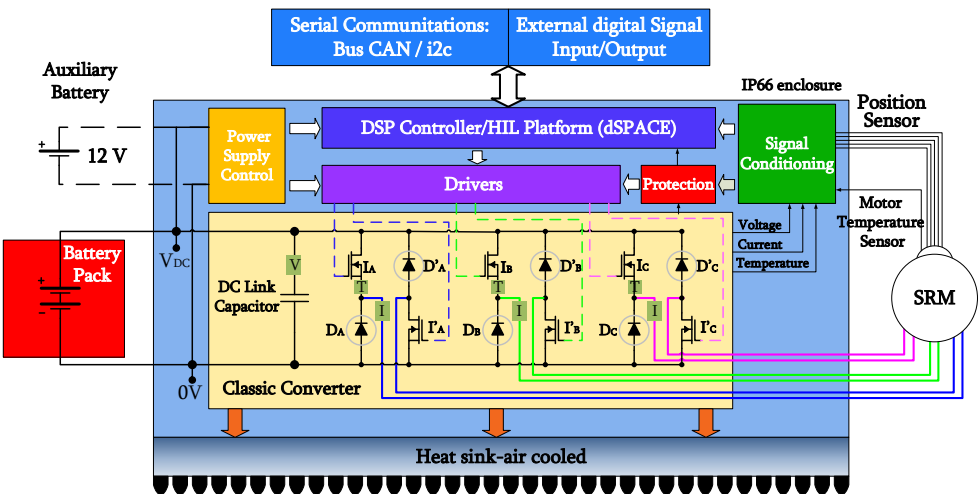


Fig.12: Block diagram of the SRM controller



### A. Electronic power converter

The electronic power converter is the core of the controller. Even though a number of phases greater than three can be a good choice for an SRM drive, as this reduces torque ripple and increases fault tolerance. When minimizing the number of power components, the best and most advisable option is usually a three-phase SRM drive, as a consequence the number of phases of the power converter is set to three. Although some efforts have been made to use common three-phase inverters for AC machines (IM and PMSM), they are not entirely suitable for SRM drives [20, 21] because the torque in SRM drives is independent of the current sign and therefore requires unipolar converters. There are several types of power converters for SRM [22], but in this case we chose a classical asymmetric power converter with two power switches and two diodes per phase (**Fig.12**), because this ensures independence of phases and provides fault tolerance.

Commercial phase-leg modules containing solid state power switches can be used in SRM power converters, but they require twice as many modules as an inverter does for alternating current machines (when they really uses only half of the components in each module), implying a significantly higher cost for the electronic power converter. In the case under study, the high electric requirements resulted in the choice of discrete components for the power switches and diodes, which were, respectively: power MOSFETs and high voltage Schottky diodes.

Taking into account the maximum voltage that the converter needs to work (112 V for a 100 V battery pack), the power semiconductors were chosen with a voltage margin that was at least 30% higher in order to ensure that the voltage peaks caused by switching transients did not damage the power semiconductors. The power MOSFET selected was Ixys IXFN360N15T2, because of its low  $R_{DS,on}$ , and the chosen diode was Microsemi APT2X101S20J (which includes two diodes in parallel). Both with SOT-227 package due to its ability to electrically isolate active parts and thus requires no additional insulation film between the case and heat sink, i.e., thermal resistance is reduced. In addition, this package allows for semiconductors to be simply screwed onto a standard flat extruded heat sink. Finally, as a result of many simulations, each switch and diode in **Fig. 12** was built with, respectively, 4 Ixys IXFN360N15T2 modules in parallel and 2 Microsemi APT2X101S20J modules in parallel.

### B. Capacitor bank

The design of the capacitor bank took into account: the maximum voltage ripple (7 V peak to peak), the resistance of the battery and connection cables (10 m $\Omega$ ); and the worst-case current conditions (150 A RMS). Furthermore, we sought to minimize the surface area occupied by the capacitors and found the most compact solution to be 66 cylindrical capacitors (Rubycon .160BXW820MEFR18X50: 82

$\mu\text{F}$ , 160 V), which occupied a surface area of approximately  $210\text{ cm}^2$  (each capacitor had a diameter of 18 mm and a height of 50 mm), with a total capacity of 54 mF.

### C. Ancillary parts

Other important parts of the SRM controller that we have denominated "ancillary parts" are: the control power supplies, the signal conditioning and the gate drivers. The controller's electronics were powered by a 12 V rail that required an external supply. This 12 V rail generated three other auxiliary voltages for internal usage and supplied optional external elements: -12 V for the negative supply of current sensors and conditioning the analog circuit; plus 3.3 V and 5 V for supplying other digital components. These auxiliary voltage supplies were implemented with non-isolated step-down converters.

For measuring the current, we used four open loop Hall effect current sensors (LEM HAS 300-P): one for each of the three phases and another for the DC bus current. The measurement gain can be configured in two ways: by making one or two turns with the power cable around the sensor or by choosing one of two possible gains from the analog circuitry. For the DC bus voltage measurement, a voltage divider was used with an analog adaptation circuit. This measurement was also configurable with two possible gains.

The signal conditioning was implemented in two stages. The first adjusted the range to within 0-10 V when the measurement is unipolar, or  $\pm 10\text{ V}$  when it is bipolar. After this first stage, the signal is branched into two paths: the first one to the dSPACE; and the second one to another analog stage that adapts to the 0-3 V range required by the DSC analog-to-digital acquisition.

Each of the 4 parallel power MOSFETs were driven by a single gate-driver, which was isolated in order to avoid high frequency interference between power and control. The integrated circuit chosen for this purpose was the ADUM3223BRZ and employed one for each of the 6 channels. The floating secondary sides were supplied with 9 V by means of 6 standard isolated power supplies (MTE1S1209MC).

### D. Printed circuit board

Regarding the power converter, the capacitor bank, the isolated gate drives, the voltage, current and temperature sensors, the signal conditioning, the control power supplies, the power connectors and the input/output connectors: all of these were incorporated onto a printed circuit board (PCB) of 6 layers with a total of  $70\text{ }\mu\text{m}$  copper thickness. The semiconductors (MOSFETs and diodes) were mounted on an aluminum heat sink. The great challenge we faced in designing the power part of the PCB was obtaining good thermal performance in light of the high currents it had to handle. By correctly placing the components and adequately routing the tracks and conduction planes, the current path's re-

sistance and inductance are minimized, which helps in two ways: first, the Joule conduction losses are reduced, and this facilitates thermal handling; second, it reduces ringing due to the switching of high currents. The layout of the power part was designed in order to minimize the current loops of the 6 switching cells (formed by the capacitor, the MOSFET and the diode of each leg). This layout allows the DC bus to be implemented with 4 continuous copper layers along the 6 legs (2 layers for positive and 2 for negative), thus minimizing the DC bus inductance and enhancing the heat dissipation. The midpoints of each arm, which are also the motor outputs, were routed across only the bottom layer for contact with the power semiconductors and across the top layer, where they were reinforced with copper bars that were screwed onto the PCB. To improve the flow of the currents from the battery to the PCB (400 A during 2 min), additional copper bars were implemented to connect the legs of the 3 phases (see bottom of **Fig. 13**).

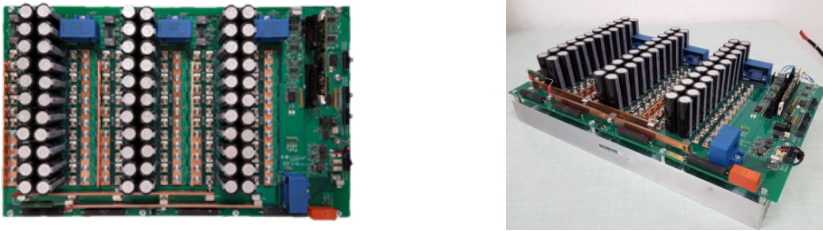


Fig.13: Plan (left) and side (right) views of the controller for SRM.

### E. DSP Controller and HIL Platform

The SRM controller included a DSP, TMS320F28335 control CARD from Texas Instruments attached to the main PCB, denominated DSC. The SRM controller was designed to also allow for control of the converter by means of an external HIL platform, if required. **Fig. 14** shows how the converter can be controlled and monitored by both DSC and by an HIL platform, which in this case is dSPACE.

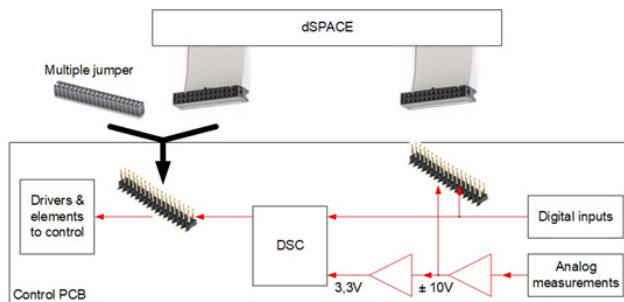


Fig.14: Control of the power converter by DSC or by dSPACE.

## 7.4. Performance evaluation of the proposed AFSRM drive

Once the AFSRM and the controller were built, the drive was tested in a test rig in order to assess its performance.

### A. Test rig description

The AFSRM was mounted and coupled through a torque-meter (Kistler 4550A500S10N1KA0 500 Nm) to a DC motor brake (DC LOAD). In addition, it was connected to a DC source that was variable in voltage and current (APS DPS 100-450) by means of the electronic power controller described in section 7.3 and controlled by a HIL platform (dSPACE ACE 1006). The measurements of torque, speed and power were monitored by means of testing power analyzer system (eDrive package GEN2tA-6ch-2Ms/s, from HBM). **Fig. 15** shows a photograph of the complete test layout.

### B. AFSRM drive control

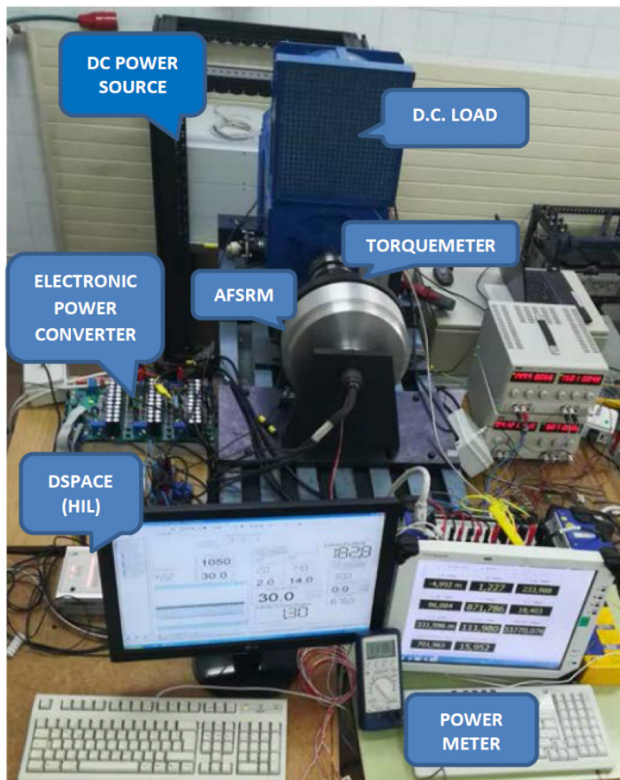


Fig. 15: AFSRM drive test rig

In order to meet the drive's requirements (Section 7.2), the control strategy for the proposed AFSRM drive used: hysteresis control with variable turn-on and turn-off angles at low and medium speeds; and a single pulse with variable turn-on and turn-off angles for high values of speed. The values of reference current and of the turn-on and turn-off angles for each operating point were determined after many performed with Matlab-Simulink using the results of finite element analysis on the AFSRM [12-13].

### C. Experimental results of the AFSRM drive

The test rig enabled us to determine the experimental torque-speed curves. **Fig. 16** shows these curves, including power isolines, which allows for better comparison with the drive's requirements. We also consider the behavior of the drive at different operating points under the aforementioned control strategy. **Fig.17** shows: the waveforms of phase current, phase voltage and bus current for 500 rpm, 60 Nm with hysteresis control ( $\theta_{ON} = -4^\circ$ ,  $\theta_{OFF} = 12^\circ$ ). **Fig. 18** depicts the waveforms of phase current, phase voltage and bus current for 900 rpm, 30 Nm with hysteresis control ( $\theta_{ON} = -7^\circ$ ,  $\theta_{OFF} = 8^\circ$ ). **Fig. 19** shows the waveforms of phase current, phase voltage and bus current for 1400 rpm, 20 Nm with single pulse control ( $\theta_{ON} = -7^\circ$ ,  $\theta_{OFF} = 8^\circ$ ).

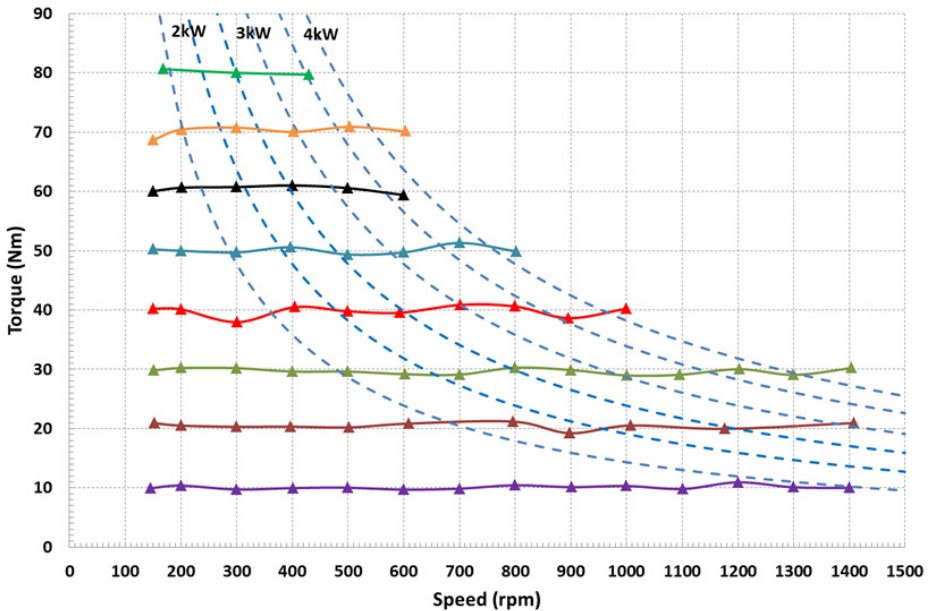


Fig.16: Torque-speed curves experimentally obtained on the test rig.

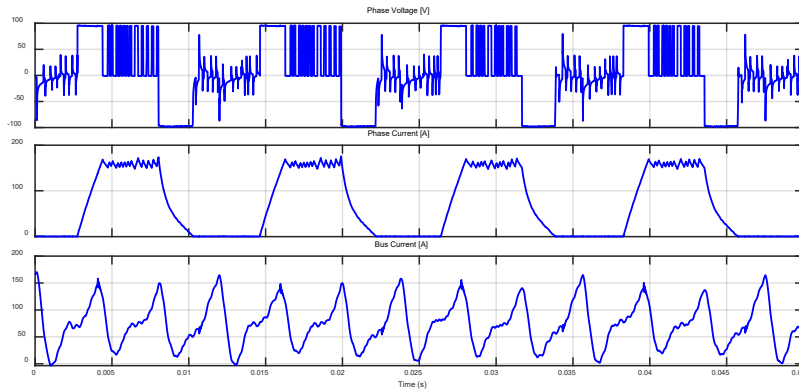


Fig. 17: Waveforms of phase current, phase voltage and bus current for 500 rpm, 60 Nm with hysteresis control  $\theta_{ON} = -4^\circ$ ,  $\theta_{OFF} = 12^\circ$ .

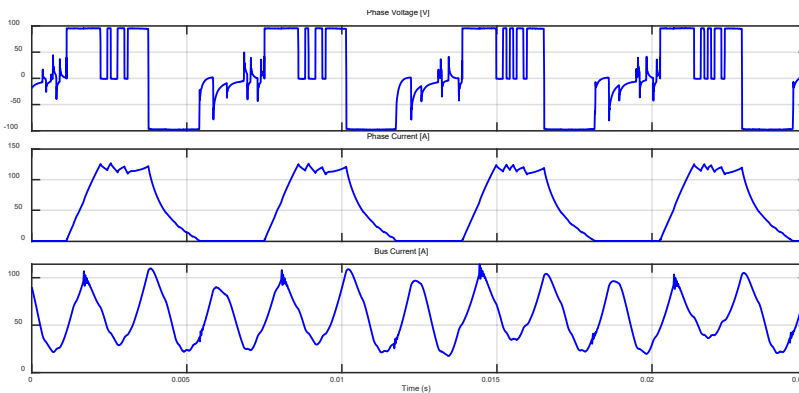


Fig. 18: Waveforms of phase current, phase voltage and bus current for 900 rpm, 30 Nm with hysteresis control  $\theta_{ON} = -7^\circ$ ,  $\theta_{OFF} = 8^\circ$ .

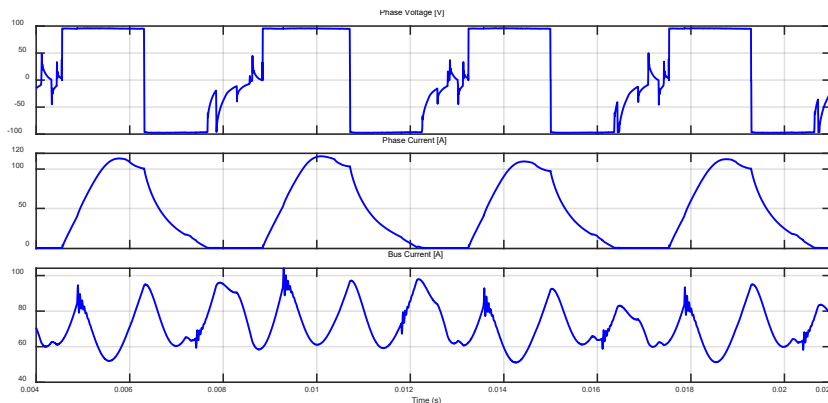


Fig. 19: Waveforms of phase current, phase voltage and bus current for 1400 rpm, 20 Nm with single pulse control  $\theta_{ON} = -7^\circ$ ,  $\theta_{OFF} = 8^\circ$ .

## 7.5. Conclusions

This chapter has presented a new in-wheel axial-flux switched reluctance motor (AFSRM) drive designed especially for the propulsion of light electrical vehicles. This motor comprises a stator sandwiched by two rotors, and the particular arrangement of the stator and rotor poles generates short flux paths without flux reversal. Due to the difficulty in manufacturing the magnetic circuit with laminated silicon iron was made of soft magnetic composites. The complete electromagnetic analysis of the prototype was performed using 3D-FEA, and the results obtained were used by Matlab-Simulink for the simulation of the whole drive, taking into account the AFSRM, the power converter and the control strategies. Simulations show that the performance of the drive matches very well with the requirements of LEVs.

## 7.6. Acknowledgements

This research was supported by the Spanish Ministry of Economy and Competitiveness (DPI 2014-57086-R) and Feder funds. The electronic power controller was built by CITCEA. The authors would like to thank AMES S.A. for providing the SMC pieces, especially for the support given by Dr. Mark Dougan, Chief Metallurgist in the Dept. of R&D AMES S.A., and Dr. José Antonio Calero, R&D Manager of AMES S.A..

## 7.7. References

- [1] Directive 2007/46/EC, consolidated version of 31 March 2018 (contains amendments and corrections up to and including Commission Regulation 2017/2400).
- [2] Navigant Research. Executive Summary: "Light Electric vehicles, Low speed/Neighborhood EVs, Electrical Motorcycles, and Electric Scooters: Global Market Analysis and Forecasts". Published 1Q 2017.
- [3] Y. Tang, J. J. H. Paulides, I. J. M. Besselink, F. Gardner, E. A. Lomonova. "Indirect Drive In-Wheel System for HEV/EV Traction". EVS27 Barcelona, Spain, November 17 - 20, 2013, pp. 1-9.
- [4] L. E. Unnewehr and W.H. Koch. "An axial air-gap reluctance motor for variable speed applications", January/February 1974, IEEE Transactions on Power Apparatus and Systems.
- [5] Arihara and K. Akatsu. "Basic properties of an axial-type switched reluctance motor". IEEE Transactions on Industry Applications, Vol 49, No 1, January/February 2013, pp. 59-65.



- [6] Murakami, H. Goto, O. Ichinokura. "A study about optimum stator pole design of axial-gap switched reluctance motor". ICEM 2014, 2-5 September, Berlin, pp. 975-980.
- [7] R. Madhavan, B.G. Fernandes. "Axial flux segmented SRM with a higher number of rotor segments for electric vehicle". IEEE Transactions on Energy Conversion, Vol. 28, No 1, March 2013, pp.203-213.
- [8] Labak, N.C. Kar. "Designing and prototyping a novel five-phase pancake-shaped axial flux SRM for electric vehicle application through dynamic FEA incorporating flux-tube modeling". IEEE Transactions on Industry Applications, Vol. 49, No 3, May/June 2013, pp.1276-1288.
- [9] Ma, R. Qu, J. Li. "Optimal design of an axial flux switched reluctance motor with grain oriented electrical steel". 18th International Conference on Electrical Machines and Systems (ICEMs), 25-28 October 2015, Pattaya City, Thailand 2015, pp. 2071-2077.
- [10] T. Kellerer, O. Radler, T. Sattel, S. Purfürst. "Axial type switched reluctance motor of soft magnetic composite". Innovative Small Drives and Micro-Motor Systems, 19-20 September 2013, Nuremberg, Germany, pp.29-34.
- [11] T. Lambert, M. Biglarbegian, S. Mahmud. "A novel approach to the design of axial-flux switched reluctance motors". Machines 2015, 3, 27-54.
- [12] P. Andrada, E. Martínez, B. Blanqué, M. Torrent, J.I. Perat, J.A. Sánchez. "New axial-flux switched reluctance motor for E-scooter". ESARS ITEC Toulouse, 2-4 November 2016.
- [13] P. Andrada, E. Martínez, M. Torrent, B. Blanqué. "Electromagnetic evaluation of an in-wheel double rotor axial-flux switched reluctance motor for electric traction" REPQJ. Vol 1, No 15, April 2017. pp. 671-675.
- [14] P. Andrada, B. Blanqué, E. Martínez, J.A. Sánchez, M. Torrent. "In wheel-axial-flux SRM drive for light electric vehicles". Workshop on SRM an alternative for E-traction. Vilanova i la Geltrú Barcelona Spain. February 2, 2018, pp. 39-46.
- [15] PCT/EP2017/076976, "An axial flux switched reluctance machine and an electric vehicle comprising the machine".
- [16] A.Kringe, A.Boglietti, A.Cavagnino, S.Sprague. "Soft magnetic material status and trends in electric machines". IEEE Transactions on Industrial Electronics, Vol 64, No 3, March 2017, pp 2404-2414.
- [17] A.Schoppa, P.Delarbe. "Soft magnetic powder composites and potential applications in modern electric machines and devices". IEEE Transactions on Magnetics, Vol 50, No 4, April 2014.
- [18] M.J.Dougan. "An introduction to powder metallurgy soft magnetic components: materials and applications". Powder Metallurgy Review, Autumn/Fall 2015, pp 41-49.



- [19] P. Andrada, B. Blanqué, M. Capó, G. Gross, D. Montesinos. "Switched reluctance motor controller for light electric vehicles". 20th European Conference on Power Electronics and Applications (EPE'18 ECCE Europe), 2018. P1-P11.
- [20] A.C. Clothier and B.C.Mecrow. "The use of three phase bridge inverter with SR drives". Eight Int. Conference on Electric Machines and Drives 1997, pp. 351-355.
- [21] T. Celik. Segmental rotor switched reluctance drives. Phd Thesis. University of Newcastle upon Tyne. School of Electrical, Electronic and Computer Engineering. August 2011.
- [22] S. Vukosavic and V.R. Stefanovic. "SRM inverter topologies: a comparative evaluation". IEEE Transactions on Industry Applications, vol 27, No 6, 1991, pp. 1034-1047.



# Axial-Flux Twin-Rotor Segmented-Stator High-Speed SRM for High-Performance Traction Applications

Francisco J. Márquez-Fernández; Johannes H. J. Potgieter, Malcolm D. McCulloch, Alexander G. Fraser

## 8.1. Introduction

The following chapter presents a summary of the work carried out by the authors within the project M2SRM at the Energy and Power Group, Department of Engineering Science, University of Oxford, UK, and McLaren Automotive Ltd, Woking, UK. This summary was first presented at the workshop "SRM drives - an alternative for E-Traction", organized by the Department of Electrical Engineering at the Polytechnic University of Catalonia (UPC) in February 2018 [1]. The original publications as well as numerous supporting references can be found in [2 – 8].

Electric and Hybrid-Electric powertrains are now common in the market and nowadays virtually all OEMs (Original Equipment Manufacturers or vehicle manufacturers) offer one or several of such models. The motivations for electrification differ across the different vehicle segments. While for small passenger cars the main motivation is the reduction in fuel consumption and emissions, in the higher performance vehicle class electric traction machines are used for their superior dynamic response and higher power density. High performance turbocharged combustion engines suffer from “turbo-lag”, a phenomenon that drastically slows the response of the engine to step increases in torque demand, especially at low rpm until the turbocharger kicks in. In contrast, an electric drive provides almost instantaneous changes in torque. Combining both in a hybrid powertrain results in a vehicle with increased performance and driveability that is ultimately much more fun to drive.

Most of the commercial EV and HEV solutions sport some form of PMSM (Permanent Magnet Synchronous Machine) mostly due to their higher power and torque density. However, PMSMs also bring in a number of disadvantages: over

80% of the rare earth material needed for the fabrication of the permanent magnets used in traction machines (neodymium and dysprosium mostly) is concentrated in China; thus the market price of these materials is somewhat volatile and a change in trade policy by the Chinese government could have a large impact in the supply chain of the EV and HEV industry. Moreover, in a PMSM the magnetizing field cannot be switched off, hence field weakening currents need to be applied whenever the machine is operating above its base speed even if no torque is being produced. This field weakening currents result in increased winding losses, reducing the overall energy efficiency of the PMSM.

SRMs (Switched Reluctance Machines) do not rely on permanent magnets, which can be seen as an advantage for the aforementioned reasons, while retaining relatively high torque and power density in comparison with other topologies such as the synchronous reluctance machine and the induction machine. The higher levels of noise and vibrations associated with SRM operation could be problematic, especially in a pure EV, but they are not considered a hinder in a hybrid sport application as the one in this study, since the ICE (Internal Combustion Engine) will expectedly create much stronger noise and vibrations.

In order to reduce cost and increase performance levels, there is a large drive to increase the torque and power density of traction motors. By increasing the rotational speed, the power density can be increased, although care must be taken to preserve the mechanical integrity of the rotating parts. In addition, the high speed needed for high power density, together with the high pole count needed to keep the magnetic paths as short as possible while boosting the torque density result in high frequency operation. This, in turn, leads to magnetic losses both in the iron core of the machine (iron losses) and in the copper windings (proximity losses), potentially reducing the energy efficiency of the machine. Moreover, the lack of permanent magnets leads to higher current levels in order to produce the desired torque. For all these reasons, the thermal management of this kind of machines is not trivial, and it will determine to a large extent the success of any particular machine design.

## 8.2. Topology Selection and Description

### A. Topology selection process

In order to find the optimal topology for the application, an extensive design space was explored. All machine concepts considered in this process were based on reluctance torque production and therefore permanent magnet free. The aim was to maximize power and torque density. Besides, the machine concept selected should preferably be multi-rotor, since this was considered a good feature increasing both torque density and reliability in the initial project proposal. **Fig. 1** shows some of the geometries considered.

All the machines were analyzed using 3D FEA (Finite Element Analysis) to obtain the basic electromagnetic characteristics, and those that seemed interesting were investigated further. The outcome of this selection process is the machine topology described in this work.

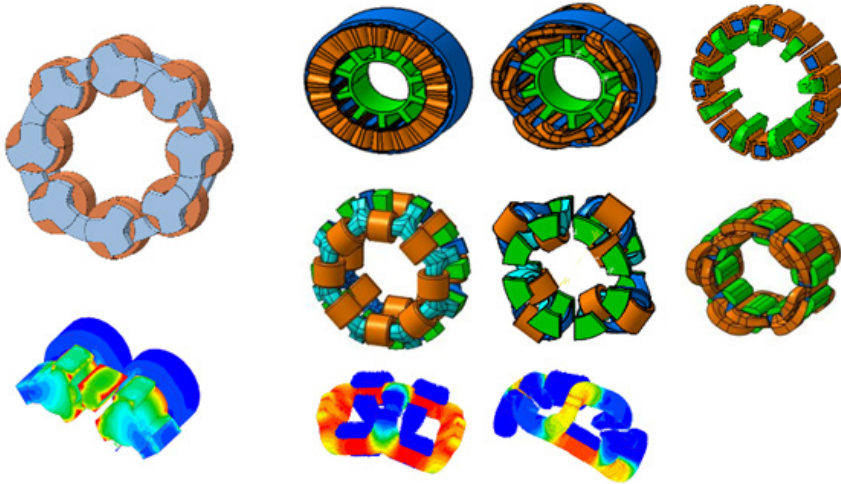


Fig. 1: Some of the machine concepts in the design space considered

## B. Description of the SRM topology

The selection process described in the previous section resulted in the following electrical machine topology: 2-phase, axial flux, segmented twin rotors, segmented stator SRM. The stator features individual poles made of SMC (Soft Magnetic Composite) to achieve the complex geometric shapes and reduce magnetic losses. These poles are wound independently and then assembled together as shown in **Fig. 2** for the first prototype [5,6,8].

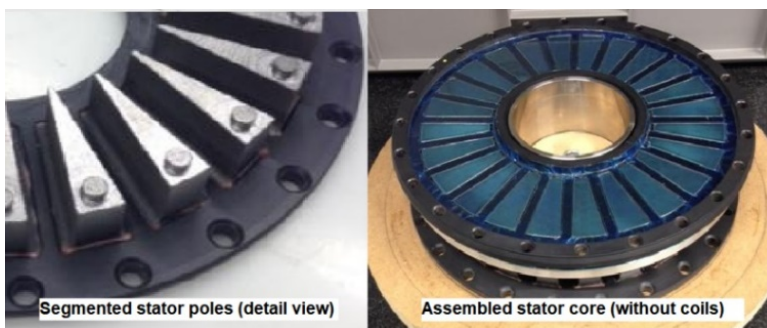


Fig. 2: Stator of the first prototype machine. Figure based on [6].

The stator coils are pre-wound and vacuum-impregnated in a high thermal conductivity epoxy prior to assembly. Due to the specific requirements of the cooling concept - presented in a later section - the coils must be structurally stable, able to retain their shape when mounted on the stator poles. In addition, the high electrical frequency during operation requires the use of litz wire. For all these reasons, the manufacturing of the coils has proved to be significantly more challenging than initially expected. **Fig. 3** shows a coil under manufacturing and a terminated coil [6].



Fig. 3: Fully finished coil (left) and bespoke tool for coil manufacturing (right). Figure based on [6].

The twin-rotors are also segmented, consisting of triangular SMC poles mounted together in a structure that ensures the rotor's mechanical integrity at the maximum rotational speed. A CAD (Computer Aided Design) model of the described SRM topology can be seen in **Fig. 4**, where only the active parts of the machine are shown. A list of the most relevant target specifications for the design of the SRM traction machine is compiled in Table I.

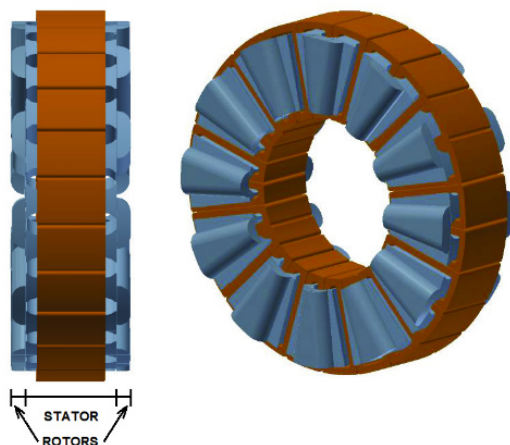


Fig. 4: CAD model of the proposed SRM topology. Based on [5].

TABLE I. MAIN DESIGN PARAMETERS FOR THE SRM

Parameter	Value
Rated power	60 – 80 kW
Maximum rotational speed	20 000 rpm
Base rotational speed	10 000 rpm
Maximum fundamental electrical frequency	4 kHz
Maximum outer diameter	254 mm
Maximum axial length	170 mm
Decoupled deceleration	> 10 000 rpm/s
Rotor pole outer pressure limit	< 125/353 MPa
Maximum winding temperature	180 C
Maximum SMC temperature	250 C
Maximum coolant outlet temperature	125 C

### C. Cooling concept

Due to the high current levels in the winding, high frequency and magnetic saturation during operation, the losses in the proposed SRM stator are not concentrated in either the coils or the stator poles, but rather evenly distributed among them [6]. For this reason, a cooling concept in which the temperatures of the winding coils and iron poles are decoupled is highly desirable.

This thermal decoupling is achieved by circulating a liquid coolant, preferably water based, through cooling channels formed between the winding and the stator poles as shown in **Fig. 5**. In this way, the cooling effect will be approximately the same for both parts and the only thermal coupling besides the coolant temperature is due to the plastic spacers used to mount the winding coils onto the iron cores [3].

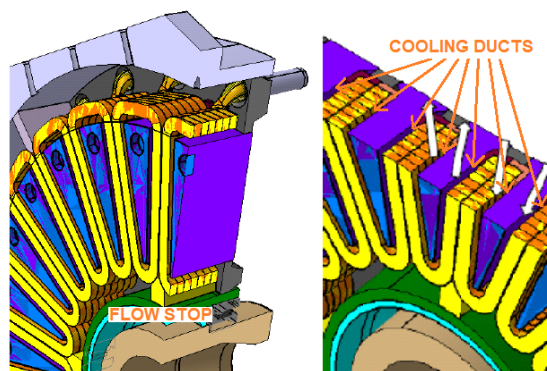


Fig. 5: Cooling ducts between the winding coils and the stator poles. Based on [4].

### 8.3. Topology Optimization

#### A. Optimization process description

In this section, a brief description of the optimization of the selected SRM topology is presented. The optimization scheme used couples FE electromagnetic analysis and a lumped parameter thermal model in order to evaluate the impact of the different design parameters in the performance of the machine [3].

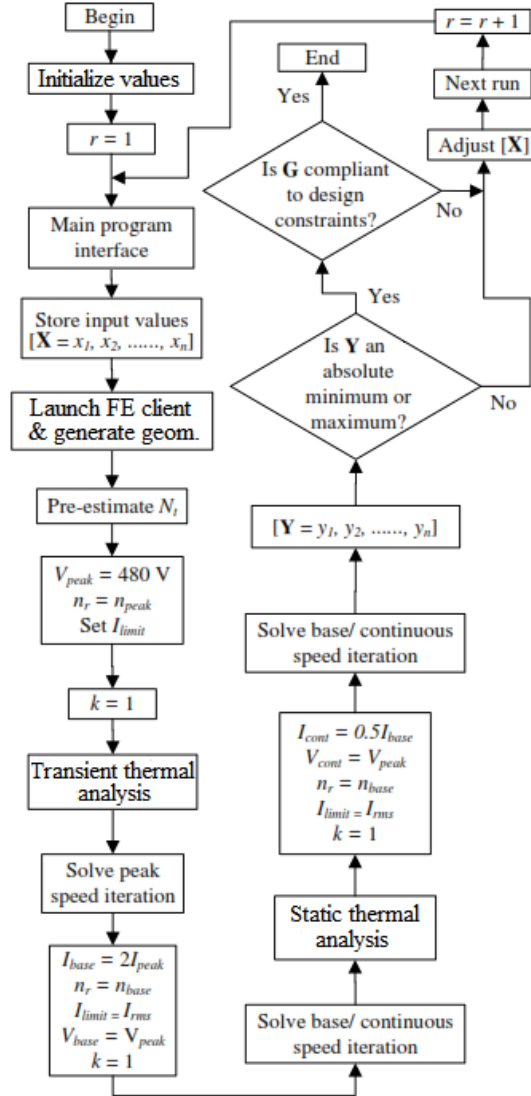


Fig. 6: Optimization process flow diagram. Figure based on [3].



Each machine geometry considered is analyzed according to the following procedure: first, all main parameters of the machine are set. Then, the algorithm proceeds with the peak speed iteration, finding the optimal number of turns for the stator coils such that at peak speed and full voltage the winding current is maximized without exceeding the maximum temperature threshold. In this iteration, a transient thermal model considering only the thermal masses of the components and excluding all cooling actions is used, ensuring that the peak power can be sustained for at least 10 seconds.

Then, the continuous power iteration is carried out. First, the current is reduced to half of the current obtained in the peak speed iteration, the speed is set to base speed and the algorithm checks whether the current can be controlled to the specified value or a fixed pulse voltage excitation should be used. Subsequently, the algorithm iterates again in order to find the current level that can be sustained indefinitely without exceeding the thermal limits. In this case a steady state thermal model is used, taking into account the direct cooling of both winding coils and stator poles.

Finally, the optimizer evaluates the objective function for the analyzed geometry and checks if it corresponds to a minimum point, in which case the optimization is finished. Otherwise, the next parameter set is proposed and the whole process is repeated for the corresponding new geometry.

## B. Electromagnetic modelling

Both a 3D FE model and a 2D FE linearized model have been developed to evaluate the performance of the machine. During the optimization process, the 2D model is used due to its lower computational cost. Once a good machine candidate is identified, a more exhaustive FE simulation is conducted using the 3D model [3,5].

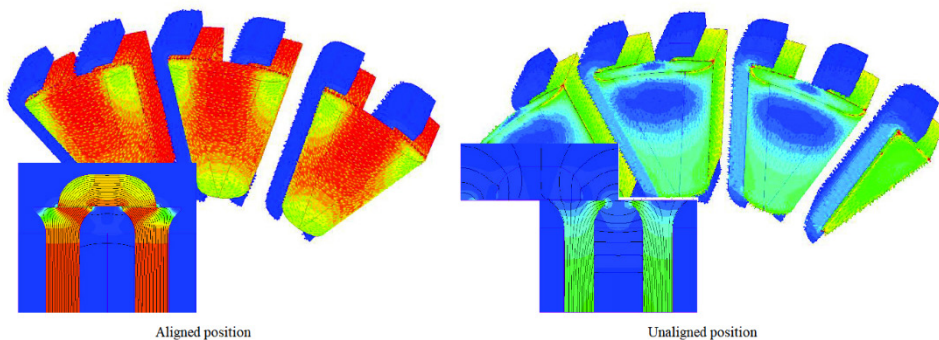


Fig. 7: 3D and 2D linearized FE models in the aligned (left) and unaligned (right) position. Figure based on [5].

### C. Coolant flow and thermal modelling

In order to assess the thermal performance of the machine for the different loading cases two models are created: a coolant flow model to estimate the coolant flow distribution, heat transfer coefficients and pressure drop in the cooling channels, and a thermal model to estimate the temperature in the different parts of the machine. Both models are lumped parameter models because of the need for fast execution [4].

The coolant flow model estimates the flow distribution in the different cooling paths by calculating the pressure drop based on the Darcy-Weisbach equation and experimental correlations for the different bends and fittings.

The thermal model uses the convection coefficients from the coolant flow model and the losses from the FE analysis in order to estimate the temperature of the coils and the stator poles. The thermal model of the coil (shown in Fig. 8) models each turn individually with four nodes, and takes into account not only heat conduction along the wires, but also axial heat conduction between consecutive turns [8].

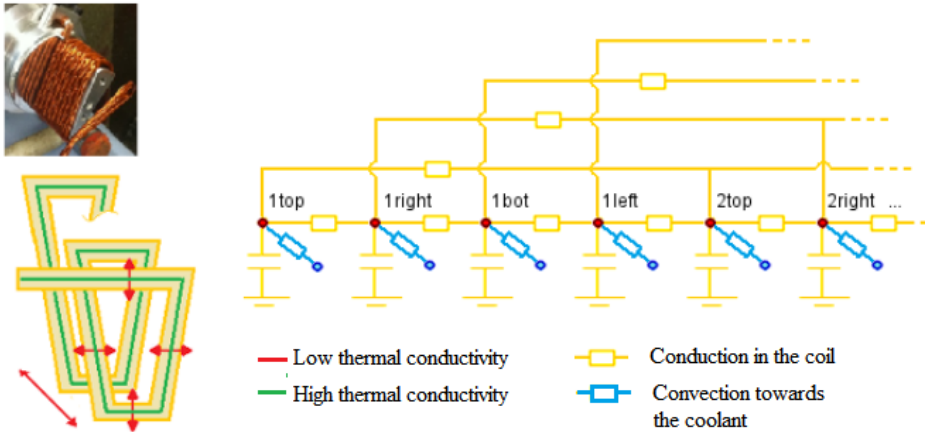


Fig. 8: Lumped parameter thermal model of a coil. Based on [8].

### 8.4. Experimental results

The degree of novelty in the proposed topology resulted in a number of unexpected delays during manufacturing – particularly of the winding coils – and also during the testing phase that could not be addressed completely within the project time scope. For these reasons, only two types of tests were successfully carried out: thermal tests of purposely designed motorettes and static tests of the first version of the machine prototype. Some relevant experimental results are presented in this section.

## A. Thermal experiments

In order to validate the performance of the proposed cooling approach and to calibrate the thermal models developed, motorettes comprising one stator tooth and one coil have been manufactured (see Fig. 9) [6,8].

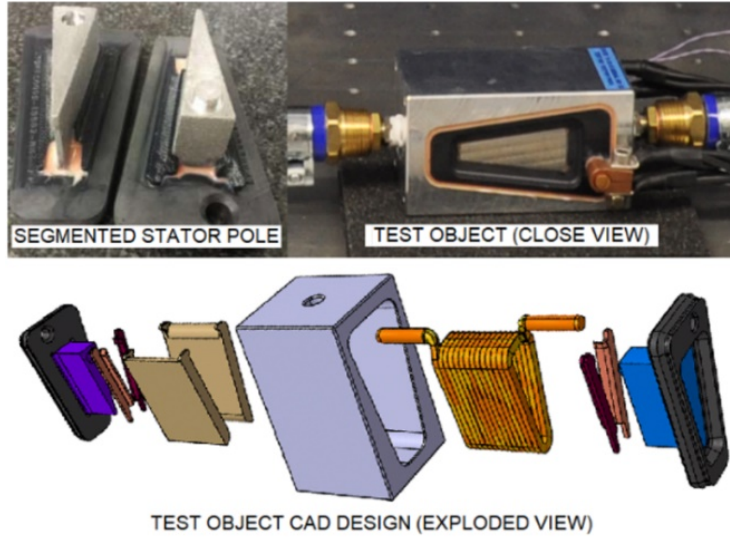


Fig. 9: Single core test motorette. Figure based on [6].

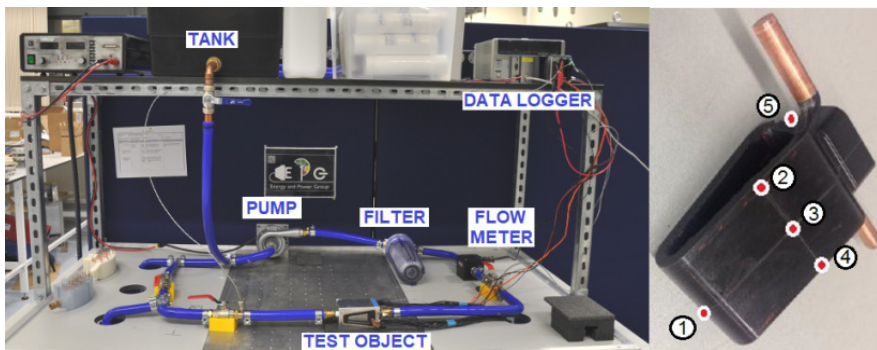


Fig. 10: Experimental setup (left). Location of the thermistors in a coil (right). Figure based on [6].

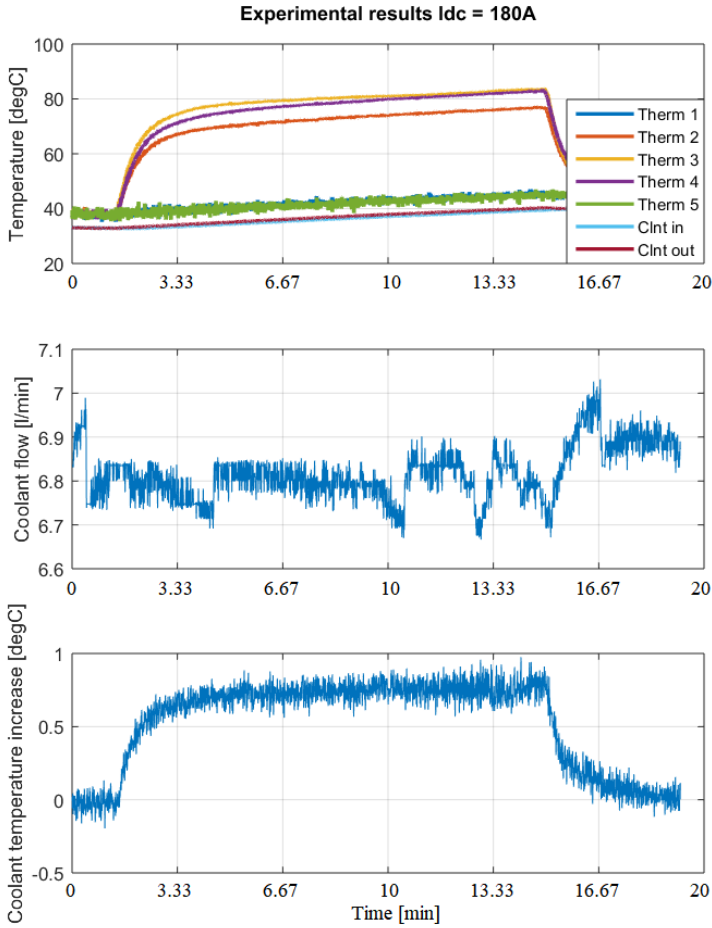


Fig. 11: Logged temperatures (top), coolant flow rate (middle) and coolant temperature increase (bottom) for 180 A. Figure based on [8].

Five miniaturized thermistors installed in different locations over the winding allow to characterize the temperature distribution over the coil. One motorette is placed in the test bench shown in Fig. 10, supplied by a 5 kW DC power supply capable of delivering 25 V and 200 A. An electric pump circulates the coolant fluid (distilled water in these experiments) through the circuit. The coolant flow as well as the inlet and outlet coolant temperatures are also recorded.

## B. Static mechanical tests

The machine prototype was installed in a test-bench in the lab and static torque measurements were performed locking the rotor at certain predefined positions. The figures in this section show some of the measurement results obtained from these tests and their comparison to FE results when relevant [5].

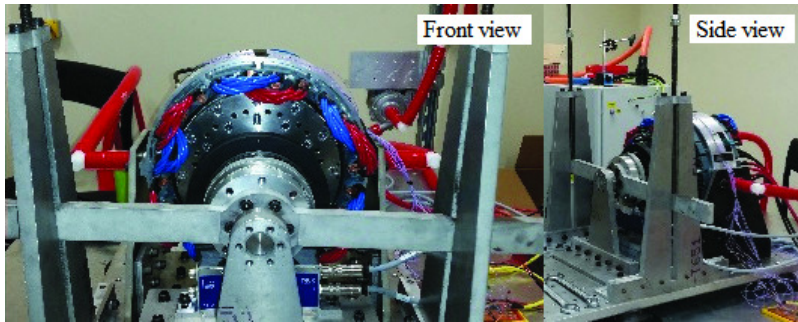


Fig. 12: Experimental SRM on the test bench interfaced with a static adjustment mechanism. Figure based on [5].

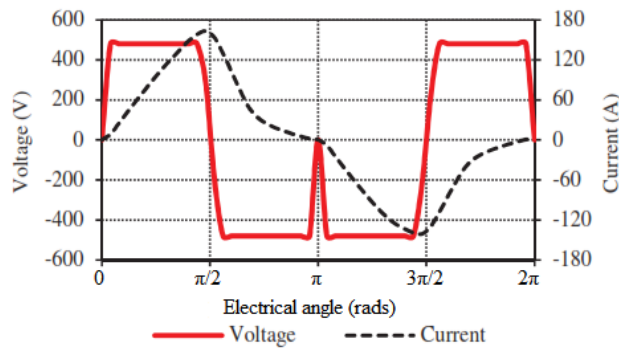


Fig. 13: Voltage and current vs. electrical angle for the SRM prototype (from FE simulations). Figure based on [5].

Fig. 13 to 15 show the FEA results obtained for the prototype SRM. Fig 13 shows the voltage and current of the machine when in operation. Fig. 14 shows the torque vs. electrical angle obtained if the machine is supplied with the voltage and current in Fig. 13. Fig. 15 shows the predicted torque and power as a function of motor speed. Peak speed is defined as 20 000 r/min and base speed as 10 000 r/min.

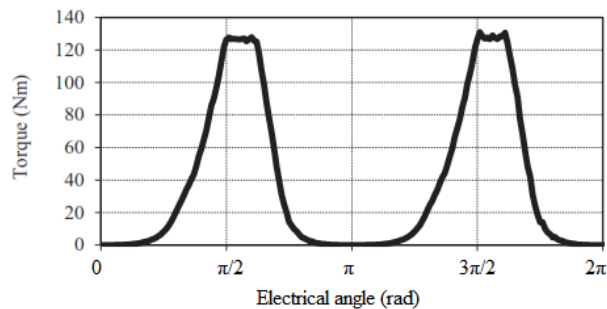


Fig. 14: Torque vs. electrical angle for one electrical period for the SRM prototype (from FE simulations). Figure based on [5].

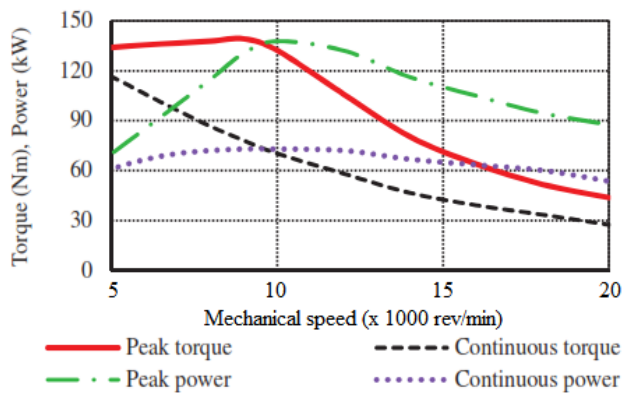


Fig. 15: Peak and continuous torque and power vs. speed for the SRM prototype (from FE simulations). Figure based on [5].

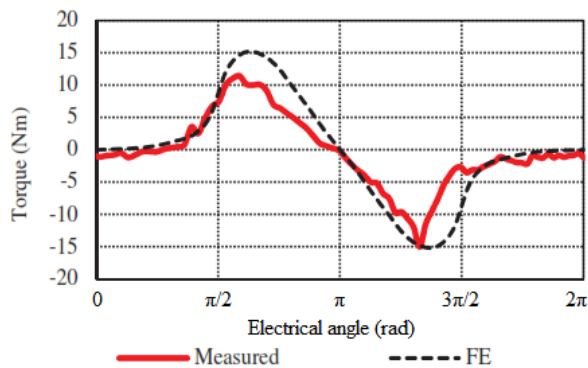


Fig. 16: Measured and predicted static torque waveforms at a fixed current of 30 A. Figure based on [5].

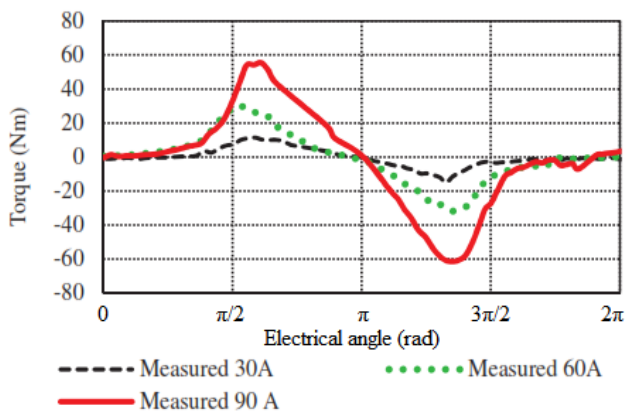


Fig. 17: Measured static torque waveforms at three different current values. Figure based on [5].

Fig. 16 shows the static measured and FE-predicted torque versus position at a constant current of 30 A per inverter leg. Fig. 17 shows the measured static torque versus electrical angle for three different current values. Fig. 18 shows the measured average torque per electrical cycle versus the FE predicted torque. It should be noted that the results shown are not conclusive and more testing is required to provide a more indicative view on the performance of the new concept SRM.

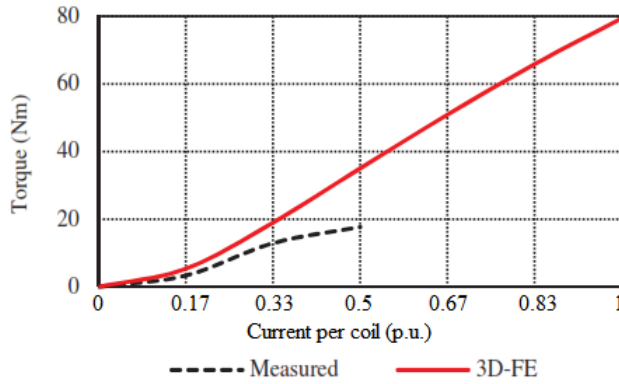


Fig. 18: Measured and FE predicted average torque vs. current per coil of the experimental SRM. Figure based on [5].

## 8.5. Conclusions

This chapter summarizes the work done on a novel SRM concept, featuring a 2-phase axial flux topology, with a segmented stator and twin segmented rotors. The proposed topology is designed for high-speed operation, aiming for power density values in the range of 7 kW/kg. This extreme operation conditions motivate the development of a novel cooling concept, decoupling the temperatures of the winding and the stator poles.

Mechanical and thermal models of the machine have been developed and integrated in an optimization scheme. A prototype has also been built and tested.

The design methodology has proven to be useful, and the optimizer with integrated mechanical and thermal models has provided meaningful results.

The results from the experimental tests on the single-core motorettes show great potential for the cooling solution. However, a number of manufacturing problems in the full machine prototype impossible to solve in the available time for the project limited the number of tests significantly. The static tests conducted show good agreement at low current values, however, further testing would be required to understand the deviations as the current level increases.



## 8.6. References

- [1] Universitat Politècnica de Catalunya. GAECE - Grup d'Accionaments Elèctrics amb Commutació Electrònica. "Workshop SRM Drives an Alternative for E-Traction: Proceedings", 2018. <http://hdl.handle.net/2117/116160>
- [2] J.H.J. Potgieter, F.J. Márquez-Fernández, A. G. Fraser and M.D. McCulloch, "Loss coefficient characterisation for high frequency, high flux density, electrical machine applications", International Electric Machines and Drives Conference IEMDC 2015, Coeur d'Alene, US.
- [3] J.H.J. Potgieter, F.J. Márquez-Fernández, A. G. Fraser and M.D. McCulloch, "Design optimisation methodology of a high-speed switched reluctance motor for automotive traction applications", Conference on Power Electronics Machines and Drives PEMD 2016, Glasgow, UK.
- [4] F.J. Márquez-Fernández, J.H.J. Potgieter, A. G. Fraser and M.D. McCulloch, "Thermal management in a high speed switched reluctance machine for traction applications", Conference on Power Electronics Machines and Drives PEMD 2016, Glasgow, UK.
- [5] J.H.J. Potgieter, F.J. Márquez-Fernández, A. G. Fraser and M.D. McCulloch, "Performance evaluation of a high speed segmented rotor axial flux switched reluctance traction motor", International Conference in Electrical Machines ICEM 2016, Lausanne, Switzerland.
- [6] F.J. Márquez-Fernández, J.H.J. Potgieter, A. G. Fraser and M.D. McCulloch, "Experimental validation of a thermal model for high speed switched reluctance machines for traction applications", International Conference in Electrical Machines ICEM 2016, Lausanne, Switzerland.
- [7] J.H.J. Potgieter, F.J. Márquez-Fernández, A. G. Fraser and M.D. McCulloch, "Effects Observed in the Characterization of Soft Magnetic Composite for High Frequency, High Flux Density Applications", in IEEE Transactions on Industrial Electronics, vol. 64, no. 3, pp. 2486-2493, March 2017.
- [8] F.J. Márquez-Fernández, J.H.J. Potgieter, A. G. Fraser and M.D. McCulloch, "Experimental validation of a thermal model for high speed switched reluctance machines for traction applications", IEEE Transactions on Industrial Applications, vol. 54, no.4, pp.3235-3244, July-August 2018.